

Dinosaur track assemblages from mid-Cretaceous of Fujian Province, southeastern China: ichnotaxonomy and faunal comparison (#109629)

1

First submission

Guidance from your Editor

Please submit by **12 Jan 2025** for the benefit of the authors (and your token reward) .



Structure and Criteria

Please read the 'Structure and Criteria' page for guidance.



Custom checks

Make sure you include the custom checks shown below, in your review.



Author notes

Have you read the author notes on the [guidance page](#)?



Raw data check

Review the raw data.



Image check

Check that figures and images have not been inappropriately manipulated.

If this article is published your review will be made public. You can choose whether to sign your review. If uploading a PDF please remove any identifiable information (if you want to remain anonymous).

Files

Download and review all files from the [materials page](#).

51 Figure file(s)

1 Table file(s)

2 Raw data file(s)

! Custom checks

New species checks



Have you checked our [new species policies](#)?



Do you agree that it is a new species?



Is it correctly described e.g. meets ICZN standard?




Structure and Criteria

Structure your review

The review form is divided into 5 sections. Please consider these when composing your review:

1. BASIC REPORTING
2. EXPERIMENTAL DESIGN
3. VALIDITY OF THE FINDINGS
4. General comments
5. Confidential notes to the editor






 You can also annotate this PDF and upload it as part of your review

When ready [submit online](#).





Editorial Criteria

Use these criteria points to structure your review. The full detailed editorial criteria is on your [guidance page](#).




BASIC REPORTING

-  Clear, unambiguous, professional English language used throughout.
-  Intro & background to show context. Literature well referenced & relevant.
-  Structure conforms to [Peerj standards](#), discipline norm, or improved for clarity.
-  Figures are relevant, high quality, well labelled & described.
-  Raw data supplied (see [Peerj policy](#)).

EXPERIMENTAL DESIGN

-  Original primary research within [Scope of the journal](#).
-  Research question well defined, relevant & meaningful. It is stated how the research fills an identified knowledge gap.
-  Rigorous investigation performed to a high technical & ethical standard.
-  Methods described with sufficient detail & information to replicate.

VALIDITY OF THE FINDINGS

-  **Impact and novelty is not assessed.** Meaningful replication encouraged where rationale & benefit to literature is clearly stated.
-  All underlying data have been provided; they are robust, statistically sound, & controlled.
-  Conclusions are well stated, linked to original research question & limited to supporting results.



The best reviewers use these techniques

Tip

Example

Support criticisms with evidence from the text or from other sources

Smith et al (J of Methodology, 2005, V3, pp 123) have shown that the analysis you use in Lines 241-250 is not the most appropriate for this situation. Please explain why you used this method.

Give specific suggestions on how to improve the manuscript

Your introduction needs more detail. I suggest that you improve the description at lines 57- 86 to provide more justification for your study (specifically, you should expand upon the knowledge gap being filled).

Comment on language and grammar issues

The English language should be improved to ensure that an international audience can clearly understand your text. Some examples where the language could be improved include lines 23, 77, 121, 128 - the current phrasing makes comprehension difficult. I suggest you have a colleague who is proficient in English and familiar with the subject matter review your manuscript, or contact a professional editing service.

Organize by importance of the issues, and number your points

1. Your most important issue
2. The next most important item
3. ...
4. The least important points

Please provide constructive criticism, and avoid personal opinions

I thank you for providing the raw data, however your supplemental files need more descriptive metadata identifiers to be useful to future readers. Although your results are compelling, the data analysis should be improved in the following ways: AA, BB, CC

Comment on strengths (as well as weaknesses) of the manuscript

I commend the authors for their extensive data set, compiled over many years of detailed fieldwork. In addition, the manuscript is clearly written in professional, unambiguous language. If there is a weakness, it is in the statistical analysis (as I have noted above) which should be improved upon before Acceptance.

Dinosaur track assemblages from mid-Cretaceous of Fujian Province, southeastern China: ichnotaxonomy and faunal comparison

Lida Xing ^{Corresp., Equal first author, 1, 2}, **Kecheng Niu** ^{Equal first author, 3, 4}, **Qiyang Chen** ^{Corresp., 2}, **Hendrik Klein** ⁵, **Anthony Romilio** ⁶, **Runsheng Chen** ⁷, **Min Lin** ⁷, **Ke Deng** ⁷, **Jianrong Tang** ⁷

¹ Frontiers Science Center for Deep-time Digital Earth, China University of Geoscience (Beijing), Beijing, China

² School of the Earth Sciences and Resources, China University of Geoscience (Beijing), Beijing, China

³ State Key Laboratory of Cellular Stress Biology, School of Life Sciences, Xiamen University, Xiamen, Fujian, China

⁴ Yingliang Stone Natural History Museum, Nan'an, Fujian, China

⁵ Saurierwelt Paläontologisches Museum, Neumarkt, Bavaria, Germany

⁶ School of the Veterinary Science, University of Queensland, Gatton, Queensland, Australia

⁷ Fujian Institute of Geological Survey, Fuzhou, Fujian, China

Corresponding Authors: Lida Xing, Qiyang Chen

Email address: xinglida@gmail.com, qiyang_chen@163.com

The intermountain basins become the most dominant depositional environment in southeastern China after the tectonic uplift in the 'Mid' to Late Cretaceous, preserving a considerable dinosaur record including fossil skeletons, eggs and tracks, especially in the Maastrichtian. The Shanghang Basin is one of the sporadic red-stratified basins distributed in western Fujian, China, and has previously been discovered as the home of large troodontid *Fujianipus*, and an ichnofauna representing the almost sole record of dinosaur fauna with structural integrity during the mid-Cretaceous in southeastern China. New material of the Longxiang ichnofauna, including possible large didactyl trackways (>50 cm), a new ichnospecies under *Tridentigerpes* and many more ornithopod trackways, has been newly distinguished. This early ornithopod-dominated ichnofauna is unique in southeastern China and can be compared with the contemporaneous dinosaur fauna of Mongolia or the Early Cretaceous fauna of NW China. The influence of various factors, including the timing and extent of short-term cooling and humidifying events across southeastern and northwestern China, the geographical boundaries within the mountainous region of southeastern China, and the possible regional immigration of the fauna from the north, may have shaped the occurrence of this ichnofauna.

1

2 **Dinosaur track assemblages from mid-Cretaceous of** 3 **Fujian Province, southeastern China: ichnotaxonomy** 4 **and faunal comparison**

5

6

7 **Abstract**

8 The intermountain basins become the most dominant depositional environment in southeastern
9 China after the tectonic uplift in the 'Mid' to Late Cretaceous, preserving a considerable
10 dinosaur record including fossil skeletons, eggs and tracks, especially in the Maastrichtian. The
11 Shanghang Basin is one of the sporadic red-stratified basins distributed in western Fujian, China,
12 and has previously been discovered as the home of large troodontid *Fujianipus*, and an
13 ichnofauna representing the almost sole record of dinosaur fauna ~~with structural integrity~~ during
14 the mid-Cretaceous in southeastern China. New material of the Longxiang ichnofauna, including
15 possible large didactyl trackways (>50 cm), a new ichnospecies under *Tridentigerpes* and many
16 more ornithopod trackways, has been newly distinguished. This early ornithopod-dominated
17 ichnofauna is unique in southeastern China and can be compared with the contemporaneous
18 dinosaur fauna of Mongolia or the Early Cretaceous fauna of NW China. The influence of
19 various factors, including the timing and extent of short-term cooling and humidifying events
20 across southeastern and northwestern China, the geographical boundaries within the
21 mountainous region of southeastern China, and the possible regional immigration of the fauna
22 from the north, may have shaped the occurrence of this ichnofauna.

23

24 **Introduction**

25 During the Cretaceous, after the end of the subduction stage on the eastern side of the Cathaysia
26 block, the tectonic stage in southeastern China shifted from a syn-orogenic shortening stage to a
27 post-orogenic stage (Li et al., 2014). This stage was mainly represented by NW-SE extension in
28 the Late Valanginian to Early Aptian. Subsequently, the collision of the South China continental
29 crust and the West Philippine Plate transformed the region into an isotropic compressional event
30 in the Late Aptian to Early Albian (Charvet, 1994; Li et al., 2014). During the compressional
31 phase, tectonic uplift induced by Minchenorogeny (Gu, 2005), the mountains included the area
32 covered by Paleo-Yunmengze Lake and the associated inland river system, i.e. most of Hubei,
33 northern and northwestern Hunan, and part of Henan and southwestern Jiangxi (Chen, 1979,
34 _Compilation Committee of Geological Atlas of China, 2002; Wan et al., 2010). The high and
35 _wide Zhe-Min-Yue Mountains (i.e. Zhejiang, Fujian and Guangdong) made it difficult for the
36 paleo-Pacific moisture flow to reach the above regions, causing these areas to develop into
37 tropical-subtropical hot plains, hills and desert landscapes (Chen, 1979), where gypsum and
38 halite were deposited (Wan et al., 2010). To the east and south of this region are dominated by

39 plains and hills belonging to Zhejiang, Fujian, Jiangxi and Guangdong regions, where dinosaurs
40 lived in these small and sporadic foothill grasslands and intermountain basins (Chen, 2000; Li et
41 al., 2013). The "Mid" to Upper Cretaceous faulted basin deposits in this region are mainly
42 composed of brick-red siltstone and mudstone, also containing gypsum layers, with
43 conglomerates and sandy conglomerates at the base (Zhou, 2007). Considerable dinosaur
44 records, including fossil skeletons, eggs and tracks, are preserved in the Late Cretaceous red-
45 stratified deposits of Zhejiang, Jiangxi and Guangdong, especially in the Jinqu Basin of Zhejiang
46 (Du et al., 2015; Yu, 2013), the Ganzhou Basin of Jiangxi (Lü et al., 2016, 2017; Xing et al.,
47 2020) and the Nanxiong Basin of Guangdong (Xing et al., 2017, 2020).

48 In western Fujian, west of the Zhenghe-Daipu Rift, there are about 36 Cretaceous red-
49 stratified basins spatially distributed in a northeast-trending belt. The Shanghang Basin in
50 western Fujian is dominated by the Chishi Group (Junkou Formation, Shaxian Formation and
51 Chong'an Formation), of which the Shaxian Formation is the most widely distributed (Fujian
52 Institute of Geological Survey, 2016). The Shanghang Basin is one of the small basins in
53 southwestern Fujian Province, where the Cretaceous red beds are a sequence of purplish-red
54 coarse-fine clastic assemblages. In November 2020, the Dinosaur Laboratory of China
55 University of Geosciences, Beijing, in cooperation with the Yingliang Stone Natural History
56 Museum, started to search for dinosaur fossils in the red beds of Fujian Province. This is the first
57 time that dinosaur tracks have been found in Fujian Province (Niu and Xing, 2023). In January
58 2021, the lead author of this paper found a third footprint site at the Kejiayuan Cultural Centre in
59 Longxiang Village (Fig. 1). In April 2021, a detailed investigation of the newly exposed
60 footprint levels of the main tracks was carried out.

61

62 Geological setting

63 Fujian Province in southeastern China is situated on the southeastern margin of the Eurasian
64 Plate. During the Late Jurassic to Early Cretaceous, intense volcanism occurred, leading to the
65 formation of a widely distributed, thick terrestrial volcanic-sedimentary rock system in the
66 eastern part of the province. In the latest Early Cretaceous to Late Cretaceous, the intensity of
67 volcanism decreased, resulting in volcanic or nonvolcanic terrestrial red-bed basin deposits (Li,
68 1997; Xi et al., 2019).

69 In the late Albian to Late Cretaceous, extensive layers of purplish-red sedimentary rocks were
70 developed in west-central Fujian, divided into the lower Shaxian Formation and the upper
71 Chong'an Formation (Li, 1997; Xi et al., 2019). The Shaxian Formation's strata are prone to
72 weathering and erosion, forming gentle hills, while the Chong'an Formation is dominated by
73 coarser-grained conglomerates, which form the basis of Danxia landforms (Lu et al., 2019). The
74 lithology of the Shaxian Formation consists mainly of purplish-red medium-thick bedded
75 calcareous, fine sandstone and muddy siltstone, interspersed with purplish-red sandstone, and
76 complex-composed conglomerate, while regionally interbedded with tuff, tuff lava, and marl,
77 which is composed of terrestrial red clastic rocks. It is exposed in several areas in northern and
78 western Fujian, forming faulted red basins with thicknesses ranging from several hundred meters

79 to over two thousand meters, including a thickness of about 1,913 meters in the Shanghang
80 Basin.

81 According to the 1:200,000 regional geological survey report of Shanghang Area (G-50-27),
82 the dinosaur tracks from Longxiang Village, Shanghang County (Fig. 1), are located at the
83 siltstone layer in the lower part of the Shaxian Formation in the Shanghang Basin (Fig. 2). The
84 sediments in this area generally include thin gypsum layers and calcareous clasts, with local
85 occurrences of Cu-bearing sandstones (Chen, 2008).

86 Hu (1990) suggested that the depositional age of the Shaxian Formation in the red bed of
87 Shanghang is between 80 and 105 Ma, based on magnetic stratigraphy. The $^{206}\text{Pb}/^{238}\text{U}$ dates of
88 the Shaxian Formation in the Shanghang Basin vary from 87 to 101 Ma, with a weighted average
89 of 96.0 ± 4.1 Ma (Chen et al., 2020). Therefore, the Shaxian Formation in the Shanghang Basin
90 can be assigned to the Early Late Cretaceous.

91 Based on palynology (Zheng and Li, 1986; Liang et al., 1992) and paleosoil evidence (Li et
92 al., 2009; Yin and Li, 2014), the Shaxian Formation is a riverine and lacustrine detrital deposit
93 that formed in an inland basin under a dry hot oxidizing environment (Li, 1997). Based on the
94 evidence of stratigraphic magnetic characterization, Li et al (2019) suggested that hematite in the
95 red strata of the Shaxian Formation and Chong'an Formation is indicative of a high-temperature
96 climatic environment.

97


98 **Materials & Methods**

99 **Materials**

100 At least three dinosaur tracksites were discovered in Longxiang Village, which are numbered as
101 Longxiang site I (LXI; GPS: $25^{\circ} 2'15.69''\text{N}$, $116^{\circ}23'58.29''\text{E}$), Longxiang site II (LXII; GPS: 25°
102 $2'38.20''\text{N}$, $116^{\circ}23'35.37''\text{E}$) and Longxiang site III (LXIII; GPS: $25^{\circ} 1'48.36''\text{N}$,
103 $116^{\circ}24'32.25''\text{E}$) (Fig. 1). Among the Longxiang tracks, 274 tracks in LXI has been already
104 reported in Niu and Xing (2023). All the tracks in LXIU, LXID, LXIN, LXII and LXIII are now
105 available *in situ*, except LXIE. The specimen from LXIE (YLSNHM07318) was found at the site
106 of the landslide on the east side of the previously described Longxiang tracksite ($25^{\circ} 2'13.76''\text{N}$
107 $116^{\circ}24'2.70''\text{E}$), with light purple-red silty claystone, and the slab is now preserved in Yingliang
108 Stone Natural History Museum, Nan'an, China.

109 Site LXI is the main tracksite, divided into the upper (LXIU), lower (LXID), northern (LXIN)
110 and eastern (LXIE) parts, with a total area of approximately $1,600 \text{ m}^2$. There are currently more
111 than 700 tracks exposed on the site, including 79 trackways and more than 100 isolated tracks
112 (trackways see Table 1). The LXIU site covers an area of about 320 m^2 , with 17 trackways and
113 eight relatively clear isolated tracks, making a total of about 229 tracks (Fig. 3). Site LXID
114 covers an area of about 170 m^2 , with a large number of planting pits, seven trackways and one
115 relatively clear isolated track, totalling about 81 tracks (Fig. 4). The LXIN tracksite covered an
116 area of about 290 m^2 , with a large number of planting pits, 54 tracks and 31 relatively clear
117 isolated tracks, totaling about 398 tracks (Fig. 5). The LXIE site only including one slab
118 (YLSNHM07318), with one trackway of two tracks (Fig. 6). Site LXII is located approximately

119 950 m northwest of Site I and preserves only three isolated tracks (Fig. 7). Site LXIII is located
120 approximately 1250 m southeast of Site I and preserves only six isolated tracks (Fig. 8). The vast
121 majority of the tracks at these sites are relatively well preserved, with only a small number
122 (<10%) preserved in the form of scattered, structurally ambiguous shallow pits. The tracks in
123 poor preservation condition are not considered in this paper.

124 The electronic version of this article in Portable Document Format (PDF) will represent a
125 published work according to the International Commission on Zoological Nomenclature (ICZN),
126 and hence the new names contained in the electronic version are effectively published under that
127 Code from the electronic edition alone. This published work and the nomenclatural acts it
128 contains have been registered in ZooBank, the online registration system for the ICZN. The
129 ZooBank LSIDs (Life Science Identifiers) can be resolved and the associated information viewed
130 through any standard web browser by appending the LSID to the prefix <http://zoobank.org/>. The
131 LSID for this publication is: urn:lsid:zoobank.org:pub:71833CE3-6955-4C16-BE29-
132 9195236631FD. The online version of this work is archived and available from the following
133 digital repositories: PeerJ, PubMed Central SCIE and CLOCKSS. 

134

135 **Methods**

136 All the exposed footprints were photographed, outlined with chalk, and traced on large sheets of
137 transparent plastics. In addition, a representative area of well-preserved tracks was mapped
138 manually using a simple chalk grid. Latex molds of representative tracks were made. Detailed
139 tracings of selected tracks were made on transparent acetate film. Latex molds, plaster replicas,
140 and most tracings were deposited at China University of Geosciences, Beijing.

141 The whole exposed surface was photographically recorded using a remote controlled four axis
142 quadcopter (DJI Inspire 1: weight: 3400 g; max service ceiling above sea level: 4500 m; max
143 flight time: 15 min; max wind speed resistance: 10 m/s and with DJI GO App, iOS 8.0 or later)
144 with a 12 mega-pixel camera (model X5, with a 15 mm lens). After taking off from the ground,
145 the DJI Inspire 1 was controlled by remote and it provide real-time HD video through a mobile
146 APP (DJI GO version 3.1.23).

147 Digital 3D models were created of the *in situ* track-bearing surface following photogrammetry
148 methods outlined by Romilio (2020). Digital photographs were taken from multiple viewpoints
149 of the *in situ* tracks with an Apple iPhone XS Max (focal length 4.25 mm). Virtual 3D models
150 were created following the step-by-step process outlined by Romilio (2020), which included
151 adding photographs to Agisoft Metashape Professional (v.1.6.3), repositioning and centring
152 models using Meshlab (Cignoni et al., 2008), and visualising the surface topography using
153 Paraview (v. 2020.06; Ahrens et al. 2005) and CloudCompare (v. 2.10.2;
154 <http://www.cloudcompare.org/>) filters.

155 Maximum Length (ML), maximum width (MW), pace length (PL), stride length (SL), pace
156 angulation (PA) and rotation of tracks (R) were measured according to the standard procedures
157 of Leonardi (1987) and Lockley and Hunt (1995). For the trackways of quadrupeds, gauge
158 (trackway width) was quantified for pes and manus tracks using the ratio WAP/PML (Marty et

159 al., 2010). The distance between the pes and manus imprints (MPL) was measured from the
160 proximal margin of the manus to the distal margin of the pes following the method of Xing et al.
161 (2014a). Hip heights and speed estimations of the theropod, sauropod and ornithopods
162 trackmakers were derived from the trackways following the methods of Alexander (1976),
163 Thulborn (1990), and González Riga (2011) respectively (see below).

164

165 **Results**

166 **Sauropod tracks**

167 **Description**

168 The sauropods trackways at the Longxiang tracksite are mainly distributed in the site LXIU and
169 LXIN (Fig. 3, 5).

170 The site LXIU contains medium-large sized sauropod trackway, with a specimen number of
171 LXIU-S1, containing 48 tracks in 24 pairs of manus-pes sets (Fig. 9). The sauropod trackway at
172 the LXIU site is medium-large in size with a specimen number of LXIU-S1 which contains 48
173 tracks in 24 pairs of manus-pes sets, scale of Belvedere and Farlow (2016), with distinguishable
174 manus and pes tracks retaining only general outlines. These tracks can only be assigned to
175 previously defined ichnogenera, rather than forming a new one. Due to the tight spacing between
176 the manus and pes of LXIU-S1, it is more difficult to accurately recognise the boundaries
177 between the two, so only the general morphology of the two was taken into account when
178 making regular measurements. Their total length was 55.4 cm and the width was 33.2 cm for an
179 elliptical impression, with an L/W ratio of 1.7. Judging from some of the tracks with a relatively
180 clear separation between the manus and pes tracks, the pes tracks averaged 40.8 cm in length,
181 ~74% of the total length, and 33.2 cm in width, with an L/W ratio of 1.2; the manus tracks
182 averaged 16.6 cm in length and 25.9 cm in width, with an L/W ratio of 0.7.

183 Almost all of the manus tracks lie anterior to the pes. Taking the best-preserved examples, S1-
184 LP8/RM8 and S1-RP10/RM10, the manus prints are oval-shaped and the marks of the digit
185 II–IV and metacarpophalangeal regions are indistinct. Digit I and V are observable, but without
186 detail. The pes tracks are oval-shaped, and the digits I–IV are indistinct, with the smoothly
187 curved metatarsophalangeal region. The manus and pes impressions are rotated approximately
188 27° and 26° outwards from the trackway axis. The mean pace angulation of the pes is 127°.

189 Poor preservation results in a large variation in the size of the manus and pes tracks in
190 trackway S1. The heteropody (ratio of manus to pes size) ranges from 1.6 to 13.3, with a mean of
191 4.4, a median of 3.0, and only 21% reaches 5. The range of width of S1 pes tracks reaches 62.2%
192 of the width of the smallest (S1-RP5). Given the presence of the aforementioned variations, it is
193 more likely that the cause of the variance in track size within a trackway is as follows:

194 Once the hindlimb of the trackmaker has left the substrate, the previously deformed sediment
195 undergoes reflux to varying degrees, contingent on the dissimilarities in the nature of the local
196 substrate and the forces exerted on the ground during travel. The relatively elongated pes track
197 (e.g., S1-LP2, RP13) may have originated from the closer proximity of its centroid to that of the
198 relevant manus, or from the deeper depth at which the trackmaker stepped into the sediment. In

199 the adjacent deformations, the deformed sediment undergoes gradual recovery at varying
200 velocities in response to both flow and pressure gradients. In instances where the ridge of
201 sediment separating the two is not sufficiently stable, the lesser deformation will tend to be filled
202 in first in order to reduce the surface energy of the entire depression (Cross and Hohenberg,
203 1993; Israelachvili, 2011). In other words, the partially capped manus track undergoes further
204 shrinkage and shallowing during the restoration of deformation. The degree of shrinkage may be
205 related to the level of overlapping of the manus-pes tracks and the initial depth of the pes.

206 Additionally, an isolated left pes track, designated LXIU-SI1, is present on the northernmost
207 side of the LXIU site (Fig. 10). This sauropod track is located on the periphery of the LXIU site
208 and exhibits superior preservation in comparison to S1 at the same site (level 2 in Belvedere and
209 Farlow, 2016). The dimensions of LXIU-SI1 were slightly larger than the mean value of the pes
210 track in LXIU-S1, measuring 50.1 cm in length and 38.0 cm in width. In comparison to the
211 tracks in LXIU-S1, LXIU-SI1 did not retain the associated manus track. However, it did retain
212 four more discernible digit traces (I-IV). The widths of the digit II to digit IV are comparable,
213 and the anteroposterior width of the digit I region is comparable to that of the remaining three
214 visible digits. However, the widths are approximately twice that of the others.

215 Site LXIN also contains a medium to large-sized sauropod trackway, LXIN-S1 (Fig. 11). It
216 contains 16 tracks with seven manus-pes sets and two separate pes tracks. The preservation
217 status of the tracks is level 1 on the Belvedere and Farlow (2016) scale. The manus and pes
218 tracks of LXIN-S1 were separated, with the pes tracks averaging 65.3 cm in length and 51.2 cm
219 in width, and an L/W ratio of 1.3; the manus tracks averaging 36.6 cm in length and 48.8 cm in
220 width, and an L/W ratio of 0.8. Almost all the manus tracks in site LXIN are anteromedial to the
221 pes. In the best preserved examples S1-RP2 and RM2, the manus impressions are oval and the
222 marks of the digits I, II, IV and V are visible but not detailed (Fig. 12). The metacarpophalangeal
223 regions are distinct. The pes prints are oval and the digits I-IV are indistinct. The
224 metatarsophalangeal region is smoothly curved. RM3 has a well-developed digit V. RP3,
225 corresponding to RM3, has distinct digits I and II. These features are not seen in the other manus
226 impressions, probably because the substrate in this region are wetter and softer, leaving the
227 tracks with more detail. The manus and pes impressions are rotated approximately 61° and 43°
228 outwardly. The pace angulation of the pes is 108° .

229 Almost all LXIN-S1 tracks had distinct outer sediment rims. Including these rims, the length
230 of the pes track is approximately 80.1 cm with an L/W ratio of 1.2, and the length of the manus
231 track is 59.7 cm in length with an L/W ratio of 0.9. The area of the track, including the rims, can
232 be up to 1.5 to 2 times the original area for pes and 2 to 2.5 times the original area for manus.
233 The heteropody is 1.8, reduced to 1.5 if the rims are included.

234 Site LXIII preserves an isolated sauropod pes track LXIII-SI1 (Fig. 13). SI1 is surrounded by
235 very distinct sediment displacement rims. The pes prints are oval, with a length of 34.6 cm and
236 an L/W ratio of 1.1. The marks of digits I-IV are indistinct and the metatarsophalangeal region is
237 smoothly curved. Unlike other sauropod pes tracks in the Longxiang area, the heel of SI1 is quite
238 narrow, with a width of about 1/2 of the digit region. In the absence of other related tracks, it is

239 not possible to determine whether this character is a stable morphological feature or an
240 ectomorphic variation.

241 **Comparison and discussion**

242 The pes and manus morphology and trackway configurations of the LXIU-S1 and LXIN-S1
243 quadruped trackways are typical of sauropods (Lockley, 1999, 2001; Lockley and Hunt, 1995).
244 Most sauropod trackways in China are wide- (or medium-) gauge and are, therefore, referred to
245 the ichnogenus *Brontopodus* (Lockley et al., 2002).

246 The average ratio of the WAP (the width of the angulation pattern of the pes) to the length of
247 the pes of the LXIU-S1 and LXIN-S1 is both 1.0. A value of 1.0 separates narrow-gauge from
248 medium-gauge trackways, whereas the value 1.2 is arbitrarily fixed to distinguish between
249 medium-gauge and wide gauge trackways (Marty 2008). Therefore, LXIU-S1 and LXIN-S1 are
250 medium-gauge trackways.

251 The preservation of LXIU-S1 is somewhat limited. For instance, one of its principal
252 identifying characteristics, heteropody, is challenging to ascertain a reliable value for. With
253 regard to the distribution of data and morphology, the mean heteropody is 1.8, and the interval 2-
254 3 encompasses eight tracks, representing one-third of the total number of tracks. This may be
255 considered a relatively stable feature, with the heteropody of LXIU-S1 falling between 1:2 and
256 1:3. This is slightly lower than the 1:1.8 observed in LXIN-S1. Both LXIU-S1 and LXIN-S1
257 tracks are characterised by outer rotation, but the latter is significantly higher than the former.
258 All of them are lesser heteropody than in *Brontopodus birdi* (1:3) and the narrow-gauge
259 ichnotaxa *Breviparopus* (1:3.6) or *ParaBrontopodus* (1:4 or 1:5) (Lockley et al., 1994), but
260 closer to both *Polyonyx gomesi* (Santos et al., 2009) and *Gyeongsangsauropus pentadactylus*
261 with a low heteropody of 1:2 (Kim and Lockley, 2012; Xing et al., 2024a). *Polyonyx* or
262 *Polyonyx*-like trackways are wide-gauge, with pes prints bearing four claw marks and
263 asymmetric manus prints with a large digit I trace (Santos et al., 2009). These are all
264 characteristics not seen in any of the LXIN-S1 sauropod tracks. However, as noted above the
265 similarities to *Gyeongsangsauropus pentadactylus* for LXIN-S1 are much greater.

266 LXIU-S1, however, indeed shows some similar features to *Brontopodus*-type trackways,
267 including: 1) wide/ medium -gauge; 2) pes tracks that are longer than wide, and large and
268 outwardly directed; 3) U-shaped / oval manus traces; and 4) a high degree (1:3 in *Brontopodus*
269 *birdi*; 1:1.86 in *Brontopodus plagnensis*) of heteropody (Farlow et al., 1989; Lockley et al., 1994;
270 Santos et al., 2009; Mazin et al., 2017). Due to the limitations of preservation, we tend to assign
271 LXIU-S1 to the *Brontopodus* -type trackway.

272 In the LXIN-S1 trackways, the most typical features are: 1) medium-gauge; 2) low degree of
273 heteropody (1: 1.8), 3) manus prints rotated approximately 61° outward from the trackway axis,
274 more than 1.4 times the outward angle of the pes prints; 4) individual pes prints with identifiable
275 digit I–II traces; and 5) the distance between the posterior margin of the manus and the anterior
276 margin of the pes (MPL) is 0.6–0.7 times the length of the pes prints. In comparison, the
277 MPL/P'ML in the *Gyeongsangsauropus pentadactylus* type trackway is ~0.6 (based on Kim and
278 Lockley, 2012: Fig. 5), 0.3 in the type of *Brontopodus birdi* (based on Kim and Lockley, 2012:

279 Fig. 6) and 0.8–1.0 in the type of cf. *G. pentadactylus* (Xing et al., 2021a)

280 The diagnosis for *Gyeongsangsauropus pentadactylus* is the following (emended after Kim
281 and Lockley, 2012, Xing et al., 2024a): Medium-gauge sauropod trackway of small to medium-
282 size (pes print length about 40–50 cm), characterized by wide pentadactyl manus tracks, with
283 very wide blunt manus digits. Manus tracks strongly rotated outwards from the midline of
284 trackway (about 30°–60° in holotype, 85°–125° in another trackway). Pentadactyl pes tracks
285 with outwardly rotated digit claws I–III, also rotated outward (about 30°–50°). Manus is wider
286 than long and pes is longer than wide. Moderate heteropody with manus-pes area ratio about 1:
287 2. Among these features, LXIN-S1 is similar to *Gyeongsangsauropus pentadactylus* in terms of
288 gauge, size, manus rotated outwards, and heteropody, but the important features, the morphology
289 of each digit, cannot be compared due to preservation reasons. We temporarily transfer LXIN-S1
290 to cf. *Gyeongsangsauropus*.

291 The question of whether large angles or significant rotation of manus prints is a valid
292 diagnostic feature needs to be treated with caution, as there are quite a few factors that influence
293 this feature. Lallensack et al. (2019) analyzed sauropod trackways from the global record and
294 found that strong lateral or postero-lateral rotation (supination) of the manus is restricted to
295 trackways of small- and medium-sized individuals (pedal impression length <60 cm), this feature
296 is also correlated with low speed and narrow gauge. Lallensack et al. (2019) also conclude that
297 pronation occurs when the forelimb is actively contributing to the progression, at higher speed or
298 when performing a wider gauge with the center of mass (COM) shifted anteriorly. There may
299 also be relationships between the rotation of the pes and manus in trackways (Xing et al., 2021b).

300 **Speed Estimation**

301 For sauropods, Alexander (1976) first suggested that hip height be estimated as $h=4 \times$ foot
302 length, whereas, later, Thulborn (1990) estimated hip height as $h=5.9 \times$ foot length. González
303 Riga (2011) estimated hip height as $h=4.586 \times$ foot length. Relative stride length (SL/h) may be
304 used to determine whether an animal was walking ($SL/h \leq 2.0$), trotting ($2 < SL/h < 2.9$), or
305 running ($SL/h \geq 2.9$) (Alexander, 1976; Thulborn, 1990). Based on the formula of Thulborn and
306 González Riga, the SL/h ratios of the LXIU-S1 and LXIN-S1 sauropod trackway are between
307 0.67–0.87, 0.49–0.63, and accordingly suggest walking. Using the equation to estimate speed
308 from trackways (Alexander, 1976), the locomotion speed of the trackmaker of LXIU-S1 is
309 between 2.27–3.02 km/h, LXIN-S1 is estimated as 1.66–2.23 km/h, and are consistent with most
310 Chinese *Brontopodus*-type trackways (Xing et al., 2016a, b), for which speed estimates are
311 always low.

312 It is notable that the relative stride length values of LXIU-S1 are highly consistent with those
313 of BTY-S1 from the Tuchengzi Formation (across the J-K boundary) in western Liaoning (Xing
314 et al., 2021c). In other words, the LXIU-S1 and LXIN-S1 specimens demonstrate that the
315 outward rotation of the manus and pes tracks, as well as the degree of MPL, can exhibit notable
316 differences in the gait during low-velocity movements.

317 **Trackmaker and the analogy of sauropod quadruped gaits**

318 The gleno-acetabular distance (GAD) has been proposed as an independent trackway parameter

319 for estimating the body size of the sauropod trackmaker (trunk length) by Lallensack et al.
320 (2019). This method is adapted for estimating trunk length when the trackmaker is in a stable
321 gait (limb phase) (Lallensack et al., 2022), without influenced by the limb lengths in the direction
322 of trackway orientation. Furthermore, the actual gait of sauropods has been re-evaluated in order
323 to determine which pair of manus and pes tracks should be selected for GAD measurement
324 (Lallensack and Falkingham, 2022; Stevens et al., 2022).

325 Based on the above study, we selected only the limb phase of 25% and 50% as two plausible
326 gait end members to measure the GAD of the sauropod trackway at sites LXIU and LXIN.
327 Among them, LXIU-S1 has adjacent manus and pes tracks, with strong reduction of the manus
328 track by deformation. Therefore, for LXIU-S1, we only use the more clearly-delimited segment
329 from LXIU-S1-RP9/RM9 to LP13/LM13 in the southwest for estimation. Since the pes tracks of
330 LXIU-S1 cover the correlative manus track, the measured value of this trackway is theoretically
331 smaller than the actual value. It should also be noted that in LXIU-S1 there is a marked change
332 in orientation between RP11 and LP11, so in this case we used two measurement methods for the
333 25% limb phase of LXIU-S1: 1) using RP11 as the boundary, dividing LXIU-S1 into two
334 segments and considering the orientation in each part of the trackway as constant; 2) using the
335 four adjacent manus-pes sets as a cluster to define the orientation of the posterior stride.

336 For LXIU-S1, the interval of its GAD was 1–1.63 m. When estimating the midline of the track
337 using the different methods, the mean of the maximum estimates were all about 1.53 m (limb
338 phase=25%), with a variance of about 0.0080, and the mean of the minimum estimates were all
339 about 1.09 m (limb phase=50%), with a variance of about 0.0035. For the LXIN-S1 trackmaker,
340 the GAD interval was 1.75-3.19 m. The mean of the maximum value was 3.14 m with a variance
341 of about 0.0078- 0.0080, and the mean of the minimum value was 1.83 m with a variance of
342 about 0.0060. The greater variance in the LXIN-S1 data is due to: 1) apparent turning point; 2)
343 increased stride length (RP12/LP13).

344 The wide/medium gauge of the *Brontopodus*/*Gyeongsangsauropus*-type trackways, especially
345 the wide gauged trackways, are commonly attribute to titanosaurian sauropods by their
346 compulsive abducent femur posture (Wilson and Carrano, 1999; Lockley et al., 2002; Henderson,
347 2006; Mannion and Upchurch, 2010). This posture is co-occurred with the ante-displacement
348 with the COM (Henderson, 2006), and is hypothesised to be the consequence of adaptation to
349 gigantism, as opposed to being merely phylogenetic-related in *Macronaria* (Blazquez et al., 2024
350 (preprint)). Furthermore, the discovery of early medium-sized wide-gauge trackways in the
351 Lower-Middle Jurassic can be attributed to the basal Eusauropoda (Xing et al., 2016). However,
352 it is also probable that these trackways could be the consequence of intense orientation-turning in
353 their path (medium-gauge instead).

354 Both Lallensack and Falkingham (2022) and Stevens et al. (2022) demonstrate a tendency for
355 sauropods to utilise a symmetrical, diagonal-supported walking gait. The diagonal-supporting
356 gait is similar to the wide-gauge, classically hypothesised to be correlated with demand for
357 stability maintaining of gigantic trackmakers (Henderson, 2006).

358 The hippopotamus is the most typical of the extant mammals that can use a torting gait

359 (Hildebrand, 1989). They differ from other extant large-sized quadrupeds, and is the only known
360 compulsory diagonal-supporting quadruped (e.g. elephants and giraffes; see Fig. 1 in Lallensack
361 and Falkingham, 2022). With the exception of hippos, rather than graviportal elephants, which
362 are more commonly analogised with sauropods, rhinos are also capable of utilising this gait at
363 low-speed running (Henderson, 2006; Hutchinson, 2021; Lallensack and Falkingham, 2022). The
364 body size, body mass and total track area of rhinoceroses are comparable to that of
365 hippopotamuses (the track size estimation is from Van den Heever et al., 2024), yet the overall
366 gait performance differs markedly (Hutchinson, 2021).

367 We hypothesise that this extreme obligate gait in hippopotamus terrestrial locomotion is likely
368 to be related to its significantly shorter limbs relative to body mass (or possibly trunk length), in
369 addition to the gravitational constraints it faces in common with other giant mammals
370 (Hutchinson, 2021). First, the sub-ellipsoidal, elongated trunk is associated with the presence of
371 its amphibius-adapted habit, with a specialisation logic approximating Sauropterygia (Endo et al,
372 2019; Gutarra et al., 2023). For hippos and rhinos, which have similar other body parameters, the
373 proportion of trunk length relative to the legs clearly distinguishes the two, and this particular
374 proportion for hippos is also rare in the full range of extant large-sized terrestrial quadrupeds
375 (Christiansen, 1999). Second, given that modern giant mammals all use a narrow-gauge, the
376 simultaneous usage of a diagonal-supporting gait during walking may limit the location of the
377 pes drop point in the presence of a large limb length. To illustrate, narrow-gauged trackways for
378 extant mammal trackmakers have been observed to avoid collisions between the front and hind
379 limbs during walking. This has led to the hypothesis that terrestrial mammal trackmakers with
380 longer hindlimbs are more likely to choose a lateral-supporting gait to ensure walking efficiency.
381 However, the need to maintain trunk stability is not as pronounced in extant mammalian clades
382 (Vermeij, 2016), as it is not as extreme as in the case of titanosaurian sauropods, which have
383 undergone a extreme process of gigantism (the phylogenetic relationship of paraceratheriids to
384 extant rhinos see Bai et al., 2020).

385 It can be reasonably deduced that the underlying causes of the disparate tortting gaits observed
386 in sauropods and certain other gigantic mammals are likely to be inconsistent. Sauropods exhibit
387 a distinctive array of intra-clade body plan variations with regard to their mechanical locomotion,
388 when compared to the extant gigantic mammals. For example, large mammals exhibit
389 considerable variation in their relative trunk length (GAD-associated) in comparison to limb
390 length (Hutchinson, 2021), as previously discussed. Conversely, the typical sauropod
391 trackmakers display a notable discrepancy in the relative length of their forelimb and hindlimb
392 along with the antedisplacement of COM (e.g. see the reconstructions of macronarian
393 *Brachiosaurus* and diplodocoids *Diplodocus* by Henderson, 2006). It is similarly conceivable that
394 these factors facilitated the advent of the hypothetical specialised gaits utilised by the makers of
395 wide-gauged trackways via the disparate COM and hindlimb postural adaptations. However, this
396 hypothesis requires further investigation in the future. However, since the GAD's estimation of
397 trunk size is independent of the functional reasons for the generation of tortting gait, it does not
398 affect the possibility of using the aforementioned approach to constrain the trackmaker's trunk

399 size.

400 Besides, handful of questionable trackways of large Paleocene-Eocene mammals are likely
401 wide-gauged as sauropods (e.g., Henderson, 2015; Wroblewski and Gulas-Wroblewski, 2021).
402 Wroblewski and Gulas-Wroblewski (2021) argue that some wide-gauge mammal trackways are
403 possible parallel pairs of narrow-gauge ones. However, the relative size of their tracks suggests
404 that the body width of their makers was probably wider than the width of the inner part of their
405 trackways, and also that if they are treated as parallel trackways, their gait angulation does not
406 seem to match the non-cursorial morphology of their trackmaker's autopods. Therefore, we
407 suggest that the wide-gauged trackways of early mammals should be further considered together
408 with sauropods.

409

410 **Theropod tracks**

411 The theropod tracks at Longxiang Site are distributed in the three main layers of LXI and LXIII
412 (Fig. 3–5, 8), and can be divided into at least five different forms, including *Grallator*
413 morphotype, *Eubrontes* morphotype, *Tridentigerpes* morphotype, and two different morphotypes
414 of didactyl tracks, including one possible large didactyl track. Given the many Given that many
415 of the scattered tracks are not well preserved (e.g. LXIN-TI17 to TI23), only the best preserved
416 tracks were selected for measurement. The rest of the tracks can be found in the distribution map.
417

418 ***Grallator* morphotype**

419 Typical tracks of *Grallator* morphotype is only shown in LXIU-TI7, an isolated footprint at the
420 LXIU site (Fig. 10). LXIU-TI7 is 12.9 cm in length, with a length/width ratio of 1.8. The
421 mesaxony of TI7 is distinct (1.08), and has relatively wide divarication angles between digits II
422 and IV (66°). The metatarsophalangeal pad trace of digit IV is round and blunt, positioned near
423 the axis of digit III. Each digit impression ends in a sharp claw mark, while no clear phalangeal
424 pads can be observed.

425 LXIU-TI7 shows typical *Grallator* morphotype features in elongate tridactyl mesaxonic
426 morphology, similar to *Grallator* type tracks reported from China (Lockley et al., 2013; Xing et
427 al., 2024b). However, it is weaker in length/width ratio and mesaxony, and higher in divarication
428 of the digits II–IV than reported for the typical North American *Grallator* (2.64 and 1.22 in
429 mesaxony, see Lockley, 2009), and seems to be in accordance to the trait of Chinese *Grallator*-
430 type tracks (Xing et al., 2024b). Xing et al. (2024b) believed that a large number of *Grallator*
431 morphotypes from the Late Mesozoic, especially which in Early Cretaceous of China can be
432 classified as *G. ssatoi*. *G. ssatoi* is the first valid species of *Grallator* in China (Yabe et al.,
433 1940), which is distinguished from North American *Grallator* by its lower length/width ratio and
434 mesaxony (1.6 and 0.8), as well as higher divarication angle (~ 57°) (Xing et al. 2024b).

435

436 ***Eubrontes* morphotype**

437 **Description.** Tracks belongs to *Eubrontes* morphotype including three trackways and 13 isolated
438 footprints are from the LXIN site, and four isolated tracks in LXIII (Fig. 5, 8).

439 Three trackways from the LXIN site including LXIN-T1, T3, and T5 (Fig. 14–16). All three
440 trackways preserve three continuous footprints, of which T5 is the best preserved, with the
441 footprint preservation state being level 2 on the scale of Belvedere and Farlow (2016). The digit
442 imprints are quite clear and sharp, and claw marks and some digit pads can be identified.
443 Trackway LXIN-T5 shows functionally tridactyl, digitigrade and mesaxonic pes imprints that
444 have an average length of 32.4 cm and length/width ratio of 1.2. Digit II is the shortest and digit
445 III and digit IV are similar lengths. There is a wide divarication angle (59°) between digit II and
446 digit IV. Each digit impression ends in a sharp claw mark. The tracks are rotated slightly
447 outwards towards the axis of the trackway. The average pace angulation is 127° . The mean
448 mesaxony of LXIN-T5 is 0.49. In the best-preserved T5-R1, it can be observed that digit II has
449 two digit pads. The metatarsophalangeal pads of digit II are fairly well-developed, with a size
450 almost as large as the phalangeal pad of digit IV. However, this feature is not preserved in the
451 other two footprints in the trackway. The metatarsophalangeal area of L1 does not have a two-
452 part demarcation, it is situated in alignment with the track axis. R2 does not preserve the heel, or
453 the heel is quite unclear, and three separate digits are preserved.

454 LXIN-T1 contains three consecutive tracks with an average length of 31.5 cm and a
455 length/width ratio of 1.2 (Fig. 14). Distinct external morphological changes can be found in
456 trackway T1-L1 (Fig. 17), with the curved impression of number IV, possibly signalling its entry
457 and exit. Digits II to IV are sandwiched between the semicircular heel track and have an overall
458 shuttlecock-shape, with a possible large, rounded trace of digit I proximally. The morphologies
459 of T1-R1 and L2 are comparatively conventional, with a mean mesaxony of 0.54, which is
460 overall quite close to the LXIN-T5 traces (Fig. 16). LXIN-T3-L1 and L2 only preserve digit III
461 and IV, while the former is poorly preserved in R1. The overall L/W ratio of T3 is 1.3, similar to
462 that of L1 and T5 (Fig. 15).

463 Of the 17 isolated *Eubrontes*-type tracks from LXIN, those similar to the well-preserved
464 LXIN-T5 include TI2, TI3 and TI12 (Fig. 17), which range in length from 26.4 cm to 36.8 cm,
465 with mesaxony greater than 0.45 and L/W ratios between 1.1 and 1.6. Distinct external
466 morphological changes can be found in isolated tracks TI1 and TI5, reflected in a pronounced
467 curvature of the digit or a deformity of the heel. There was an overlap between TI6 and TI7, with
468 the former destroying the track of the latter.

469 The LXIII site preserves four tridactyl theropod tracks (Fig. 13), of which LXIII-TI1 shows
470 functionally tridactyl, digitigrade and mesaxonic pes imprint that have an average length of 28.9
471 cm and length/width ratio of 1.0. Digit II is the shortest, and digit III is shorter than digit IV.
472 Digit III accounts for 64% of the total length of the footprint. There is a wide divarication angle
473 (76°) between digit II and digit IV. The divarication angle between digits II and III (37°) is
474 almost equal to the one between digits III and IV (39°). Each digit impression ends in a sharp
475 claw mark. The mean mesaxony of LXIII-TI1 is 0.51.

476 The other three tridactyl theropod footprints from site LXIII are all less than 25 cm in length.
477 TI2 lacks the heel, TI4 is 15.8 cm in length, has a length/width ratio of 1.1, and a mesaxony of
478 0.53, and the overall morphology is similar to the *Eubrontes* morphotype.

479 **Comparison and discussion.** The average mesaxony of LXIN-T1, and T5 is about 0.54 and 0.49
 480 (Fig. 14, 15), which is typical for the morphofamily Eubrontidae (Lull, 1953). LXIN-T5-R1 track
 481 shows convergent traits with type *Eubrontes* tracks, such as the presence of a distinct
 482 metatarsophalangeal pad trace posterior to digit II. This characteristic is common in *Eubrontes*
 483 tracks, including type *Eubrontes* AC 151 (Olsen et al. 1998), This feature also distinguishes type
 484 *Eubrontes* from most other *Eubrontes*, from common ichnogenus *Kayentapus* of the Early–
 485 Middle Jurassic (Lockley et al. 2011; Xing et al. 2020), and from such Cretaceous ichnogenera
 486 as *Asianopodus*.

487 Based on the pes length/width ratio of 1.2, medium mesaxony of 0.49, and relatively small
 488 divarication angle (about 59°) between digit II and IV. Digit III is 70% of the total pes length.
 489 Digit II is 76% of the length of digit III. The metatarsophalangeal pads of digit II are fairly well
 490 developed, with a size almost as large as the phalangeal pad of digit IV. LXIN-T1 is relatively
 491 similar to *Eubrontes nobitai* (Xing et al. 2021d), but the mesaxony of LXIN-T5 was significantly
 492 higher than that of *E. nobitai* which was 0.37. Xing et al. (2021d) reviewed most of the records
 493 of *Eubrontes* in China. The Lower Cretaceous of China has yielded a considerable record of
 494 theropod tracks of the generalized *Grallator-Eubrontes* plexus type, which are typical in
 495 Jurassic formations of North America and China (Lockley et al. 2013, Xing et al., 2021d). This
 496 has extended the stratigraphic and palaeobiogeographic range of these generalized theropod
 497 trackmakers into Cretaceous East Asia (Xing et al., 2018a). The records of LXIN-T5 extend this
 498 assembly to the early Late Cretaceous.

499 **Speed estimates.** For large theropods, Thulborn (1990) suggested that hip height $h=4.9 \times$ foot
 500 length. The stride length/hip height ratios of the LXIN-T1 and T5 trackway are 1.34, 1.14,
 501 respectively, indicating a trotting state. The speed of these trackmakers is 5.69 and 4.39 km/h
 502 respectively. The body length of the LXIN-T1 and T5 track maker is approximately 4.1–4.2 m,
 503 further calculated using the average hip height to body length ratio of 1:2.63 (Xing et al. 2009c).

504

505 ***Tridentigerpes morphotype***

506 Theropoda Marsh 1881

507 *Tridentigerpes* Xing et al. 2021e

508 Type ichnospecies *T. huashibanleei* Xing et al. 2021e

509 *Tridentigerpes longyanensis* ichnosp. nov.

510 **Etymology.** Ichnospecies name after the locality of the fossil site in Longyan City, Fujian
 511 Province.

512 **Holotype.** A complete natural mold of four footprint trackway was catalogued as LXIN-T2. The
 513 resin mold is stored in the Yingliang Stone Natural History Museum, Nan'an, Fujian, China.

514 **Type horizon and locality.** Longxiang tracksite IN (LXIN), Shaxian Formation, Longyan City,
 515 Fujian Province, China.

516 **Referred materials.** Trackways LXIU-T2, LXID-T1 and T3, LXIN-T4 from Longxiang LI
 517 tracksites.

518 **Diagnosis.** A relatively medium-sized tridactyl footprint with pes length/width ratio of 0.8, weak

519 mesaxony of 0.35, and large divarication angle (about 91°) between digit II and IV. Digit III is
520 70% of the total pes length. The posterior margin of footprints has a short area connected to form
521 a small heel. Step length is about $5.4 \times$ footprint length, and the mean pace angulation is high
522 (about 166°). *T. longyanensis* is different from the type ichnospecies *T. huashibanleei* by (1)
523 narrower digit II–IV divarication, (2) stronger mesaxony, and (3) higher length/width ratio; and,
524 different from *T. pinuelai*, by (1) noticeably strong digits, and (2) smaller digit II–IV divarication.
525 **Description.** The *Tridentigerpes* morphotype of Longxiang can be clearly divided into two
526 morphotypes. morphotype A includes LXID-T3, LXIN-T2 and T4 (Fig. 4, 5), and morphotype B
527 includes LXIU-T2, LXID-T1 (Fig. 3, 4).

528 **Morphotype A.** The tracks in morphotype A, including LXID-T3, LXIN-T2 (holotype) and T4,
529 characterized by their large divarication angles between digit II and IV of $\sim 90^\circ$ and the primarily
530 absence of metatarsophalangeal pads. These resulting in exceptionally low L/W ratio of ~ 0.8 to
531 0.9, and the concomitant weak mean mesaxony of 0.3 to 0.4 (Fig. 18–20).

532 The LXIN-T2 contains four consecutive tracks, of which R1 and L2 are better preserved (Fig.
533 18). The average length of these tracks is 23.7 cm, with an average width of 28.3 cm. The L/W
534 ratios of LXIN-T2 tracks present a mean value of 0.8, with particularly wide digit divergence
535 angles between digits II and IV (mean 91° , range 82° – 97°). Three of these tracks have been
536 preserved as tridactyl, and the II–III angles of all three tracks are smaller than those of III–IV.
537 The mean mesaxony of LXIN-T2 is 0.35, with digit III occupying between 62% and 74% of the
538 length of the track (N=3). The tracks exhibit a rotation of approximately -15° with respect to the
539 trackway axis.

540 T2-R1 is in the most well-preserved among the LXIN-T2 tracks (Fig. 17), yet no phalangeal
541 pads could be identified. All the digits of R1 are sub-fusiform, with deep claw marks, and
542 occupy 62%–74% of the length of the track (N=3). The digit II and III traces of R1 are notably
543 wider than those of digit IV, which are narrow and connected to the posterior margin at a small
544 heel.

545 The overall morphology of LXIN-T4 is comparable to that of LXIN-T2 (Fig. 19). The LXIN-
546 T4 also comprises four consecutive tracks, with a mean length of 24.3 cm and a mean width of
547 28.7 cm and mean L/W ratio of 0.9. The principal distinction between the two is the presence of
548 a distinctive, very short heel in the posterior margin of the tracks. In LXIN-T4-R1, which lacks
549 the posterior margin of the track, the digit III occupies 80% of the length of the track.

550 Of the other 17 isolated tracks from LXIN, TI14 and TI15 also lack heel traces (Fig. 17), or
551 the heel is rather indistinct as in T4-R1.

552 The LXID-T3 contains three continuous and poorly preserved tridactyl tracks, which
553 demonstrate the possible heel state of type B (Fig. 20). The T3-R2 track in this trackway has
554 digits II to IV, occurs over a track length of 15.4 cm and a width of 26.4 cm, resulting in a L/W
555 ratio of 0.6. The mesaxony of R2 is 0.26, and the divarication angle between digit II and IV is
556 approximately 97° . Additionally, R2 exhibits a distinct sedimentary ridge between digit III and
557 IV. In T3-R1 and L1, the large metatarsophalangeal region is well-preserved, displaying a
558 notable degree of development and bearing a resemblance to the tracks of large ornithopods

559 rather than those of theropods. L1 is in a superior state of preservation, and it can be observed
560 that a distinct median line is present in each digit trace, resulting in a cross-section that is V-
561 shaped. This suggests that the substrate was highly fluid. As the sediment becomes more
562 hydrated, the likelihood of the trackmakers leaving impressions of the metatarsal increases,
563 particularly in birds or bird-footed dinosaurs, such as the extant helmeted guineafowl (*Numida*
564 *meleagris*; see Gatesy et al., 1999).

565 **Morphotype B.** The tracks in Morphotype B, including LXIU-T2 and LXID-T1, are
566 characterized by their large divarication angles of $\sim 100^\circ$ – 110° and the primarily absence of
567 metatarsophalangeal region. These resulting in exceptionally low L/W ratio of ~ 0.5 to 0.6 , and
568 the concomitant weak mean mesaxony of <0.3 (Fig. 21, 22).

569 The LXIU-T2 trackway is representative of the type B from the Longxiang site, comprising
570 seven consecutive tridactyl tracks (Fig. 21). The preservation condition of the LXIU-T2 is
571 classified as level 2 on the scale proposed by Belvedere and Farlow (2016). The mean length of
572 the T2 tracks is 14.7 cm, with a mean width of 29.3 cm. The mean L/W ratio is 0.5, and
573 mesaxony is 0.29. The digit traces are clearly discernible and distinct, and the claw marks are
574 readily apparent. The length of digit III occupies between 87% and 92% of the length of the track,
575 as observed in three specimens. All the tracks exhibit markedly distinct divarication angles
576 between digits II and IV, with a mean value of 107° and a range of 100° to 114° . The trackway is
577 notably broad, with a pace angulation of 133° and a stride length of approximately 6.7 times the
578 track length. The tracks exhibit a rotation of approximately 9° (between -9° and 8°) from the
579 trackway axis.

580 LXIU-T2-R1 is the most well-preserved of the LXIU-T2 tracks (Fig. 23). However, no
581 phalangeal pads can be identified. The trace of digit III is notably broader in comparison to the
582 traces of digits II and IV, and the posterior margin of the footprint is not distinctly delineated.
583 The digit III of R2 is distinctly conical in shape, exhibiting the sharpest claw marks; digit II is
584 subfusiform with the deepest claw marks; digit IV is the smallest and oval in shape, with claw
585 marks only visible at the anterior margin. Comparatively, L1, L2, and R3 in T2 only preserved
586 digit II and III, and digit II of them show claw marks tangent to the median axis of the digit, as
587 an ectomorphological feature as the lifting of digit.

588 Morphologically, almost all the features and dimensions of track LXID-T1 match those of
589 LXIU-T2 (Fig. 22). LXID-T1 consists of seven tridactyl footprints with an average length of 14
590 cm and an average width of 30.7 cm. This gives an average L/W ratio of 0.5. LXID-T1 appears
591 to have a longer stride length, which is approximately 10.3 times the length of the track. The
592 tracks have an outward rotation of approximately 28° (with a range of -45° to 24°) from the track
593 axis.

594 **Comparison and discussion.** Xing et al. (2021e) provided diagnostic features of *Tridentigerpes*
595 including: weakly mesaxonic tridactyl tracks with unusually wide digit divarication, averaging
596 from $\sim 107^\circ$ – 135° in three samples, and short digit III giving pes length width ratios of ~ 0.5 –
597 0.80 . Trackway narrow with step typically 4 time track length. Morphotype A and B generally
598 meet the above characteristics. The detailed characteristics of Morphotype B are almost

599 completely consistent with *Tridentigerpes huashibanleei*, including length/width ratios (both are
600 0.5), wide digit divarication angles (both mean 107°), the mesaxony (both are 0.29), the
601 difference is that Morphotype B tracks seem to have a faster speed, step about 6.7 times footprint
602 length, different from step 4 time track length of *T. huashibanleei*. In addition, *T. huashibanleei*
603 tracks are rotated approximately 25° inward from the trackway axis, Morphotype B tracks
604 rotated inward and outward with small angles. Based on the above comparison, we classified
605 Morphotype B tracks as *T. huashibanleei* ichnospecies.


606 Morphotype A tracks differ from *T. huashibanleei* and Morphotype B tracks in that they have
607 higher length/width ratios (mean 0.8-0.9), a smaller heel, so that the length of digit III occupies
608 less of the total length of the footprint, 87%–92% in Morphotype B tracks vs. 62%–74% in
609 Morphotype A tracks, lower digit divarication angles (mean 91°), and higher mesaxony (mean
610 0.35). Morphotype A tracks have similar length/width ratios (mean 0.79 in *T. pinuelai*), a step
611 about 4.5 x footprint length, and differences in that they have narrow digit traces, higher digit
612 divarication angles (mean 113.5° in *T. pinuelai*), and possibly very short hallux traces in *T.*
613 *pinuelai*.

614 **Speed estimates.** Thulborn (1990) put forth the proposition that hip height (h) = $4.5 \times$ track length
615 (Fl) for small theropods (track length < 25 cm). From this, it is inferred that the relative stride
616 length (SL/h) of the LXIU-T2, LXID-T1, LXID-T3, LXIN-T2 and LXIN-T4 is 2.72 (trotting),
617 4.44 (running), 1.82 (walking), 2.32 (trotting), and 1.9 (walking), with estimated speeds of 12.14,
618 26.93, 7.86, 11.92, and 8.58 km/h respectively. The walking trackway LXIN-T2 are similar in
619 walking gait to trackway HSB-T2 of *T. huashibanleei* (Fig. 17; Xing et al., 2021e). Given the
620 considerable density of tracks at the LXIN site, it seems reasonable to suggest that subsequent
621 trackmakers slowed down when confronted with the rugged substrate in the bustling area. It is
622 important to note, however, the co-existence of the absence of the heel traces, low divarication
623 angle and the low L/W ratio is correlated with an incomplete estimation of foot length, by which
624 the estimated velocity would be relatively large when using the aforementioned methods.

625 **Trackmaker and formation of *Tridentigerpes*.** *Tridentigerpes*, especially *T. pinuelai*, has been
626 hypothesised a bird affinity by its slenderness of digit traces and prominent larger divarication
627 angle than non-avian theropods (Xing et al., 2021e), and the similar morphology can be seen in
628 the tracks of extant shorebirds (Lockley, 2009; Brown et al., 2021). However, the morphology of
629 *T. huashibanleei* can not be found in typical extant bird tracks for the synchronal absence of heel
630 trace and proximal part of the digits, and the insignificant mesaxony (Brown et al., 2021), while
631 it is evident that the slight mesaxony is discernible in at least a heel-included few moa tracks
632 (Lockley et al., 2017; Fleury et al., 2024). It is also possible that the previously interpreted digits
633 II and IV of R2 and L1 may be identified as outward-rotated claw marks if the previously
634 uninterpreted post-digits portion of HSB-T2-R1, as represented by a line drawing, is included in
635 the scope of the footprint. The outward rotation of the anterior claw is a common occurrence in
636 tracks with long, pointed claw marks, as exemplified by those of saurischians (e.g., the well-
637 preserved *Brontopus* and the holotype of *Eubrontes nobitai* (Xing et al., 2021d)). If this is indeed
638 the case, the actual divarication angle of the specimens referred to as *T. huashibanleei* is lower

639 than has been previously described. In combination with the relatively short digit III, this
640 ichnospecies may rather indicate an ornithischian affinity (Lallensack et al., 2019).

641 Additionally, the potential for posterior kick-off signs observed in HSB-T2-R1 (McAllister
642 and Kirby, 1998) and the presence of short, pointed tracks with extremely low mesaxony, which
643 can be seen in buoyancy-related punting tracks (Romilio et al., 2013; Navarro-Lorbés et al.,
644 2023), should be considered. Based on the above, it may be hypothesized that the morphology
645 resembling *T. huashibanleei* may also be formed in a swimming-like state with the pes in a
646 distinctly oblique position to the ground. The specific genesis of this state is not unique and may
647 be behavioural (McAllister and Kirby, 1998) or by substrate condition (Milàn, 2006). Both of
648 these can be manifested as the distal end of digit III moving relatively proximally in the plane.
649 With regard to the large divarication angle, it may be a consequence of the oblique intersection
650 with the ground during footfall (Milàn, 2006). However, in purely substrate-related speculation,
651 the large divarication angle is only observed on the upper surface of muddy substrate that is
652 sufficiently wet and soft to retain plastic deformation at the track (Milàn, 2006). The presence or
653 absence of heel traces on the upper surface of the substrate is indicative of the degree of
654 weathering. In lower surfaces where heel traces are absent, the divarication angle is not
655 significantly larger than that of conventional tracks (Falkingham and Gatesy, 2014; Turner et al.,
656 2017).

657 In conclusion, this suggests that the morphology of *T. huashibanleei* may represent either a
658 type of ornithischian? bipedal trackmaker with a notably shorter digit III, or that there may be a
659 behavioural genesis that approximates swimming, or a combination of the two. Further
660 speculation is contingent upon further observation of the holotype. 

661

662 ***Didactyl tracks***

663 The LXIU-T1 and T3 trackways in the LXIU site are didactyl trackways, which are typically
664 interpreted as deinonychosaurian trackways (Fig. 24, 25). The average length of LXIU-T1 is
665 approximately 11 cm, and it can be classified within the ichnogenus *Velociraptorichnus* (Fig. 24;
666 Niu and Xing, 2023). The T3 tracks are markedly larger, measuring ~36 cm in length. They have
667 been classified as a new ichnotaxon, *Fujianipus*, and represent the largest troodontid
668 deinonychosaurian track documented to date (Fig. 25; Xing et al., 2024c). These two trackways
669 will not be discussed further in this paper.

670

671 ***Possible large didactyl tracks***

672 **Description and comparison.** In the site LXID, the trackway LXID-T2 comprises four
673 consecutive tracks and exhibits a distinctive feature among theropod tracks (Fig. 26). The depth
674 of the T2 tracks is notably shallower than that of the majority of tracks in the same layer. This
675 may indicate that the T2 tracks are likely to be undertracks, yet they still exhibit some discernible
676 morphological and trackway characteristics. The trackway LXID-T2 comprises functionally
677 didactyl, digitigrade pes tracks. The average length of the tracks is 53.4 cm, with an L/W ratio of
678 3.8. The trace of digit II is either absent or present as an oval imprint proximally. In contrast, the

679 traces of digits III and IV are essentially parallel (with a divarication angle of approximately 15°),
680 and their lengths are similar, resulting in low mesaxony. The anterior margin of each digit trace
681 exhibits sharp claw marks. The tracks exhibit minimal rotation from the trackway axis, with an
682 average pace angulation of 179° .

683 In the most well-preserved track in the LXID-T2, T2-R1, can be observed that digit III has
684 four phalangeal pads, or three phalangeal pads and one rounded claw mark. The length of digit
685 III is 51.9 cm, while which of digit IV measures 52.1 cm. The proximal ends of digits III and IV
686 exhibit a minimal metatarsophalangeal area. The L1 only preserves the impressions of digit III
687 and digit IV, which have a length of 50.8 and 53.6 cm, respectively. It is possible that the R2
688 may preserve the impression of digit II, which is ~ 17.6 cm in length, and the impressions of digit
689 III and digit IV are ~ 50.3 and 45.5 cm in length, respectively. The digit II trace is isolated, with
690 the digit II depression situated posteromedial to the margin of digit III. The L2 has only one
691 overall oval impression.

692 LXID-T2 is comparable to typical deinonychosaur tracks, which are currently classified into
693 six ichnogenera (*Velociraptorichnus*, *Dromaeopodus*, *Dromaeosauripus*, *Menglongipus*,
694 *Sarmientichnus* and *Fujianipus*) (Xing et al., 2024c). The length of 53.4 cm in LXID-T2 is
695 undoubtedly significantly larger than all current ichnogenera and unclassified species. In a recent
696 review, the largest and most conclusive didactyl track was identified as *Fujianipus* (36.4 cm),
697 while the probable isolated didactyl troodontid track from Nanxiong (Guangdong, China) was
698 found to be 39 cm in length. It is noteworthy that both the *Fujianipus* and Nanxiong tracks
699 exhibit clear troodontid affinities. In contrast, the largest record of typical dromaeosaur-type
700 tracks is that of cf. *Dromaeopodus* (29.8 cm) from the Mid Cretaceous, Gulin (Sichuan, China;
701 Xing et al., 2016). The R1 and L1 tracks of LXID-T2 exhibit morphological similarities to digit-
702 only *Dromaeosauripus hamanensis* (Kim et al., 2008) and *D. jinjuensis* from Korea (Kim et al.,
703 2012), with strong, elongated, parallel, and almost equal lengths of digit III and IV.

704 The insufficiency in the details of LXID-T2 is somewhat reminiscent of specially preserved
705 tracks, such as the possibility as flattened tracks of large cf. *Dromaeopodus* (Xing et al., 2013;
706 Lockley and Xing, 2015). It is also possible that the vague margins indicate that the tracks may be
707 undertracks. Furthermore, while the LXID-T2 tracks lack sufficient detail to provide definitive
708 morphological traits, their large size is also reminiscent of bipedal ornithomimid tracks from the
709 same site. Nevertheless, the LXID-O1 tracks, which are approximately 40 cm in length, do not
710 exhibit the parallel and nearly equal lengths of the digits observed in the LXID-T2 tracks; the
711 almost straight trackway of LXID-T2 tracks (pace angulation= 179°) is also larger than that of the
712 aforementioned LXID-O1 (pace angulation= 161°), which is more akin to a theropod-type
713 trackway.

714 It is notable that, though lacking the signs of kick-off scours in classic swimming tracks
715 (McAllister and Kirby, 1998), the feature of low divarication angle, the lack of heel, and the
716 combination of rounded posterior region and awl-shaped anterior part could also be referred to
717 non-pointed punting-related swimming tracks (Romilo et al., 2013; Navarro-Lorbés et al., 2023).
718 The absence of digit II and the proximal linkage of digit III and IV may related to the lateral

719 rotation of the hip/pelvic girdle (Milàn, 2006; Tanaka, 2021). However, like previously discussed
720 in 4.2.3, the complete absence of heel traces (including the posteriorly supporting digit I in the
721 bird-like tracks, see Tanaka (2021)) can be hardly interpreted by certain origin, so we merely
722 retain the possibility of a cf. *Dromaeopodus* affinity of LXID-T2.

723 **Speed Estimates.** Under the assumption that LXID-T2 is of deinonychosaurian trackmaker
724 origin, the ratio based on hip-height/foot-length (h/Fl) ratio is 4.32 for dromaeosaurids as
725 proposed by Tsukiji et al. (2021). In contrast, the standard equation for estimating hip height in
726 small/medium theropods is $h = 3.06 FL^{1.14}$ (Weems, 2006). In the case of the LXID-T2 tracks,
727 the estimated average hip height could be 2.3 m or 2.85 m, depending on the equation used. Xing
728 et al. (2024c) proposed that the length of digit III and deinonychosaurian body length is 5.11%
729 on average, and the body length of LXID-T2 track maker would be estimated as at least 9.98 m.

730 **Trackmaker.** The estimated size of LXID-T2 trackmaker is not only dramatically larger than
731 which of the troodontid *Fujianipus* (~5 m), but also than the skeletal records of large members
732 from Dromaeosauridae, including *Utahraptor ostrommaysorum* from Utah (Molina-Pérez and
733 Larramendi, 2016), measuring 4.65 to 6 m in length and 1.5 m in hip height; *Dakotaraptor steini*
734 from Dakota (DePalma et al., 2015), measuring 4.35 to 6 m in length and 1.4 m in hip height;
735 *Austroraptor cabazai* from Argentina (Novas et al., 2008), measuring up to ~6 m and 1.5 m in
736 hip height; and the asian *Achillobator giganticus* from Mongolia (Perle, 1999), measuring 3.9 to
737 5 m in length and 1.25 m in hip height. All the end-members of estimated size are from Molina-
738 Pérez et al. (2019) and Paul (2024), the smaller records are from the former; the hip height
739 estimations are from Molina-Pérez et al. (2019). Among them, the overlapping of the temporal
740 range of the Shaxian Formation (*Fujianipus*) and Bayan Shireh Formation (*A. giganticus*)
741 thereby rendering a biogeographic distribution from Mongolia to southeastern China entirely
742 feasible for different clades within deinonychosaurians to become such considerable size (Xing
743 et al., 2024c).

744 The morphological characteristics of LXID-T2 and *Fujianipus* trackmaker are entirely distinct,
745 with the former displaying clear dromaeosaur-like traits. The discovery of additional specimens
746 of the LXID-T2 morphological type would constitute significant evidence of the gigantism of
747 dromaeosaurid deinonychosaurians, whose body size is undoubtedly at the top of the local food
748 chain.

749 It is important to note that, however, the digit III-body length proportion provided by Xing et
750 al. (2024c) does not encompass the length of the drag mark in the average-preserved footprints,
751 which occurs in LXID-T2. However, it should be noted that this is not necessarily representative
752 of the true length of digit III. With regard to track width, LXID-T2 is marginally shorter than that
753 of *Fujianipus* (Xing et al., 2024c), and longer than those of large *Dromaeopodus*, which measure
754 ~30 cm in length (Xing et al., 2016). Furthermore, the estimation exclusively considered well-
755 preserved small deinonychosaurians (Xing et al., 2024c) and lacked a sufficient number of large,
756 complete, and referable deinonychosaurian specimens. In conclusion, when considered as a
757 deinonychosaurian, the LXID-T2 trackmakers are likely to be smaller than the aforementioned
758 estimation, but still fall within the range of large deinonychosaurian, which may reach 5 to 6 m.

759 Besides, for the speed of the trackmaker, the relatively short stride lengths of LXID-T2
760 trackway is indicative of a trotting gait, with SL/h ratios between 1.9 and 2.35, which is
761 consistent with the trackways of *Velociraptorichnus* isp. and *Fujianipus* from the Longxiang site.
762 According to the formula proposed by Alexander, the estimated speeds of the trackways are
763 13.93 km/h and 17.86 km/h, respectively.

764

765 **Ornithopods tracks**

766 **Description**

767 The ornithopods left the most abundant footprints in the Longxiang area, which spreading
768 through all the LXI, LXIII sites (Fig. 3–6, 8), and the size of the tracks exhibited considerable
769 variation. The size variation in LXI sites can be divided into five intervals: less than 10 cm, 10–
770 20 cm (20 cm excluded), 20–30 cm (30 cm excluded), 30–40 cm (30 cm excluded), and ≥ 40 cm.
771 The number of preserved tracks within each interval is as follows: 2, 31, 21, 6, and 6,
772 respectively. Although the length appears to be continuous, a relatively clustered area of track
773 lengths between 12 and 26 cm can be observed in the box plots (Fig. 27). However, the
774 preservation condition of ornithopod tracks in this area is quite limited, with the majority being
775 at level 1. These tracks are shallow, blurred, or deformed, yet still recognisable as digit traces.
776 Some claw traces were also present; the manus and pes tracks are distinguishable, with the
777 former retaining only a rough outline. Of the 66 ornithopod trackways, 14 (21%) preserved
778 manus tracks.

779 Four ornithopod trackways are preserved in LXID site (Fig. 4), numbered LXID-O1–O4, with
780 track lengths ranging from 20.8 cm to 33.1 cm (Fig. 28–31). Eight pes tracks are preserved in
781 LXID-O1 (Fig. 28). The pes tracks of LXID-O1 are mesaxonic and functionally tridactyl, with a
782 mean length of 33.1 cm and an average length/width ratio of 1.2. The mean mesaxony is 0.32. In
783 the better-preserved O1-R3 and L5, digit III is observed to project the farthest anteriorly,
784 followed by digits IV and II. Each digit trace exhibits a pronounced ungual or claw mark. A
785 distinct border is absent between the heel and the three digits. The O1-R2 and L3 specimens
786 exhibit an extended heel, which may be part of the metatarsal impression. This is potentially
787 caused by the deeper deposition of the metatarsal. The mean interdigital divarication II–IV is 49° .
788 The average pace angulation of LXID-O1 trackway is 161° . The pes traces show outward and
789 inward rotation mean 7° from the trackway axis.

790 The LXID-O2, 3 and 4 trackways preserved approximately 15, 10 and 14 tracks respectively.
791 All tracks were very similar in length, ranging from 20.8 cm to 22.8 cm. Out of a total of 39
792 tracks, only about 4 had better preserved morphological characteristics. For example, of the 10
793 tracks in O3 (Fig. 30), only L4 shows a distinct tridactyl pattern, the length is 19.4 cm, the
794 length/width ratio is 1.2 and the mesaxony is 0.44. The other tracks in O3 are irregularly
795 elliptical, but the L/W ratios are essentially in the range of 1.1 to 1.4. O2 preserves two possible
796 manus tracks (Fig. 29): R9m and R10m are located in the outer part of digit IV of the pes, with
797 an average length of 5.2 cm and an L/W ratio of 0.7. Due to the poor preservation of the
798 individual tracks, the information on the trackways is remarkable. LXID-O2, 3 and 4 trackways

799 average 154° , 144° and 146° angulation, respectively. The tracks are predominantly outwardly
800 rotated, being 10° , 11° and 12° from the track axis in the three trackways respectively.

801 LXIU site preserves 13 ornithopod trackways and a number of isolated tracks (Fig. 3;
802 Supplementary Information 2), the former numbered LXIU-O1-O13, with tracks ranging from
803 10 cm to 44.5 cm in length. LXIU-O3, O6, O9 and O13 represent the smallest ornithopod
804 trackways (10 cm to 12.2 cm in length) at the LXIU site (Fig. 32–35).

805 LXIU-O3 preserved nine pes tracks that are mesaxonic (Fig. 32), functionally tridactyl with an
806 average length of 10 cm, an average length/width ratio of 1.2 and an average mesaxony of 0.25.
807 In the better preserved O3-R4, digit III projects most anteriorly, followed by digits IV and II.
808 The digits II and IV are almost equal in length. Each digit trace has a strong and blunt claw or
809 unguis mark. There is no distinct border between the heel and the three digits. The average
810 interdigital divarication II-IV is 55° . The average interdigital divarication II-IV is 55° . The
811 average toe angulation of the LXIU-O3 trace is 153° . The pes traces show an average outward
812 rotation of 6° from the trackway axis.

813 LXIU-O6, O9 preserved five and four pes traces respectively (Fig. 33, 34). Both trackways
814 had limited preservation, with tridactyl morphology discernible in O6-L3, and numbers II and IV
815 discernible in O9, the other tracks representing oval pits.

816 LXIU-O13 has preserved five pes tracks (Fig. 35). All except O13-L1 have very pronounced
817 ectomorphological distortions, most likely due to highly fluid sediments. O13-L1 is mesaxonic,
818 functionally tridactyl with a length of 8.2 cm, and the mean length/width ratio is 0.6, the mean
819 mesaxony is 0.18, representing very broad contours and extremely low mesaxony.

820 LXIU-O1, O4, O5 and O7 represent medium sized ornithopod tracks ranging from 18 cm to
821 27.5 cm from the LXIU site (Fig. 36–39). LXIU-O1 has only a single step (Fig. 36), R1 is well
822 preserved, functionally tridactyl with a mean length of 31.6 cm, with a mean length/width ratio
823 of 0.9 and a mean mesaxony of 0.31. The interdigital divarication of digits II-IV is 69° . The three
824 digits are almost equal in width and length from the hypex, while the claws of digit III are more
825 acute than those of digits II and IV.

826 LXIU-O4 is probably the best preserved ornithopod trackway on the LXIU site (Fig. 37). It
827 contains 5 tracks. All tracks are functionally tridactyl with an average length of 26 cm, the
828 average length/width ratio is 0.8, the average mesaxony is 0.14, the interdigital divarication of
829 digit II-IV is 51° . There is a distinct border between the heel and the three digits. The digits II
830 and IV are almost the same length. Each digit has a strong and blunt claw or unguis mark. The
831 average pace angulation of LXIU-O4 trackway is 141° . The pes traces show inward rotation, on
832 average 12° from the trackway axis. LXIU-O4-R1 has a slightly smaller digit III than II and IV,
833 and its heel is quite large, almost twice the size of the individual digits. This feature is not
834 present on the other tracks. The mesaxony of O4-L1 is significantly above average at 0.35. The
835 heel of R3 has a drag mark and preserves a large manus track located between digits III and IV,
836 the track is wider than long, measuring 8.6 cm in length, with a L/W ratio of 0.7, and the track is
837 rotated outwardly by 43° , relative to the axis of the pes. The ratio between the area of the manus
838 track and the pes track is 0.22. Overall, the average length of the right track is 24.1 cm, which is

839 less than that of the left track at 28.7 cm, and may be the result of a large difference between the
840 left and right foot sizes of this trackmaker. Even when well preserved, where each track is clearly
841 quartered, the features of LXIU-O4 are unstable, which is an ectomorphological distortion
842 caused by slippery substrates.

843 LXIU-O5 preserved nine tracks of which three were incomplete (Fig. 38). The mean length of
844 the tridactyl tracks is 27 cm, with an average length/width ratio of 0.8 and a mean mesaxony of
845 0.21. The interdigital divarication of digit II–IV is 51° . A clear delineation between the heel and
846 the three digits is absent. The length of digits II and IV is approximately equal. Each digit trace
847 has a strong and blunt claw or unguis mark. The mean pace angulation of the LXIU-O5 trackway
848 is 160° . The pes traces exhibit outward and inward rotation, with a mean deviation of 5° from the
849 trackway axis. O5-L2, R2, L3 and R3 are particularly well-preserved, with clear claw marks
850 visible on digit IV of L2 and on digits II–IV of R3 (Fig. 23). The claw marks on R3 are the most
851 well-preserved, with a clearly defined boundary. However, other areas of the internal deposition
852 have not been completely removed, which impedes further observation. O5-L1 has a large heel
853 that is twice the length of the other tracks in the same trackway, which may be the result of
854 metatarsals being involved in the formation of the impression, or it may have been formed by the
855 fragmentation of the track layer.

856 LXIU-O7 is the longest ornithopod trackway at the Longxiang site, with a length of 23 m and
857 preserving about 43 tracks, which is probably the longest ornithopod trackway in China (Fig. 38).
858 It commences with an orientation to the northwest and then turns 90° to the southwest after ~ 13
859 metres, subsequently extending progressively in a southward direction. The pes tracks of LXIU-
860 O7 are mesaxonic and functionally tridactyl, with a mean length of 18.3 cm (Fig. 23). The
861 average length/width ratio is 1.1, and the mean mesaxony is 0.24. In the well-preserved R6 and
862 R13, it can be clearly observed that Digit III projects the farthest anteriorly, followed by digits II
863 and IV. Each digit trace has a strong and blunt claw or unguis mark. A clear border between the
864 heel and the three digits is absent; however, at times, the boundaries between digits or between
865 digits and the heel area can be discerned. The mean interdigital divarication II–IV is 55° . The
866 mean pace angulation of the LXIU-O7 trackway is 161° . The pes tracks predominantly exhibit
867 outward rotation, with an average deviation of 23° from the trackway axis. Within the trackway,
868 O7-R11, L12, R12, and L13 represent the location of the change of direction, and the outward
869 rotation angles of them were 17° , -58° , 25° , and -8° separately. From R11, there is a notable
870 decrease in stride length from 114.8 cm to 86.8 cm, followed by a further decrease to 66.8 cm,
871 after which it gradually recovers. From L12, pace angulation decreases from 154° to 102° , before
872 recovering to 166° . In the aforementioned process, the trends of the track rotation angle and pace
873 angulation were found to be largely consistent. These observations indicate a reduction in the
874 speed of the trackmaker during changes in direction.

875 The trackways LXIU-O2, O8, O10, O11, and O12 comprise the largest tracks observed on the
876 same track layer (Fig. 40–44). Of these, O8 is the largest, with an average track length of 44.5
877 cm, while the other trackways range from 31.1 to 39.5 cm in length. The LXIU-O2 trackway
878 preserves only two tracks, forming a single step (Fig. 40). The mean length of these tracks is

879 31.1 cm, with an average length/width ratio of 0.9 and a mean mesaxony of 0.24. The interdigital
880 divarication of digit II-IV is 59°. Among them, L1 contains a manus track on the lateral side of
881 digits III and IV, which represents about 6 cm in length, with a L/W ratio of 0.4. However, as the
882 sediment filled L1, forming a unweathered natural cast, the true morphology of the specimen
883 remains uncertain.

884 The preservation of LXIU-O8 is rather limited (Fig. 41). Although the average length is
885 known to be 44.5 cm, a considerable number of ectomorphic distortions affect this measurement.
886 The average pace angulation of the LXIU-O8 trackway is 160°. The best preserved track in O8 is
887 O8-L3, with a length of 36.9 cm, which can be assumed to represent the true size of LXIU-O8.
888 The length/width ratio of L3 is 1.2, and the mean mesaxony is ~0.3. O8-L1 preserves a manus
889 track on the lateral side of digits III and IV, which is ~7.6 cm in length, with the L/W ratio of 0.6.
890 Given the similarity of the pace angulation to that observed in other ornithopod trackways and
891 the presence of a manus track, it can be posited that this rather limited preserved trackway still
892 has strong ornithopod affinities. The L/W ratio of R7 and R8 reaches 1.8-1.9, which is a
893 relatively uncommon elongation-related distortion observed in ornithopod tracks. This may have
894 resulted from either sliding due to slippery sediments or as partial metatarsal impressions.

895 The large heel traces are also evident in LXIU-O11 and can be classified into two categories:
896 wide and narrow (Fig. 42). The type with wider heels is exemplified by O11-L1 and L7, both of
897 which exhibit a L/W ratio of 2.1. The elongated heel of L7 is approximately three times as long
898 as the anterior part of the track, and the proximal section is similar in width to the distal end. The
899 distal end preserves recognisable tridactyls. The presence of triple elongated digit traces with
900 identifiable claw traces anteriorly is indicative of a substrate that is slippery. This can be
901 observed in the case of the theropod track from the Middle Jurassic of the Turpan Basin,
902 Xinjiang (Xing et al., 2014b). Nevertheless, the digits of LXIU-O11-L7 have not been separated
903 as in theropod tracks. The type with narrower heels includes O11-R1, L2 and R6. These tracks
904 exhibit a markedly constricted heel, with the proximal end measuring between one-half to one-
905 third the width of the distal end. These morphologies are comparable to those observed in
906 metatarsal impressions commonly associated with tridactyl theropod tracks or basal ornithischian
907 tracks.

908 LXIU-O10 trackway preserved 20 footprints, and tridactyl morphology was observed in 90%
909 of the footprints (Fig. 23, 43). These tracks are functionally tridactyl, with a mean length of 35.9
910 cm and an average length/width ratio of 1.1. The mean mesaxony is 0.28, and interdigital
911 divarication II-IV is 53°. There is no clear boundary between the heel and the three digits. The
912 digits II and IV are almost equal in length. Each digit trace features a prominent and blunt claw
913 or ungual mark. The average pace angulation of the LXIU-O10 trackway is 155°. The pes traces
914 demonstrate outward and inward rotation, with an average deviation of 8° from the trackway axis.
915

916 The LXIN site preserves 48 ornithopod tracks and a number of isolated tracks (Fig. 5;
917 Supplementary Information 2), the former including LXIN-O1-O48, ranging in length from 9 cm
918 to 48.8 cm. The preservation of the ~296 tracks is rather limited, and most of them can only be

919 identified by trackway features. Only a few tracks have clear diagnostic features. Some of the
920 better preserved tracks and specific trackways are described below (Fig. 45–50; Supplementary
921 Information 2).

922 LXIN-O1 consists of six tracks, and only LXIN-O1-R3 has identifying features (Fig. 45). R3
923 has a length of 33.9 cm, with an L/W ratio of 1.2 and a mesaxony of 0.42. The interdigital
924 divarication of digits II-IV is 50° , and there is a distinct border between the heel and the three
925 digits. The digits II-IV are almost equal in length. Each digit has a strong and blunt claw or
926 unguinal mark. The average angulation of the LXIN-O1 tracks is 167° .

927 LXIN-O2 consists of nine tracks and only LXIN-O2-R7 has the diagnostic characteristics (Fig.
928 46). O2-R7 is 18.7 cm long, with an L/W ratio of 0.8 and a mesaxony of 0.23. The interdigital
929 divarication of digits II-IV is 67° and there is a very clear border between the heel and the three
930 digits. Digits II and IV are almost equal in length, digit III is about 1/2 the length of the two
931 lateral digits. Each digit has a strong and blunt claw or unguinal mark. The average pace
932 angulation of LXIN-O2 is 131° , which is the lowest for that track point, which may represent a
933 very slow walking gait.

934 LXIN-O11 and O48 are very close together and intersect to form a single very short pseudo-
935 trackway (Fig. 47). Only O11-L2 has some valid features, such as the presence of three relatively
936 well defined toes with a heel. This interlaced trackway requires special care in identification.
937 Overall, the group activity trackways are relatively consistent in their track lengths and
938 step/stride length ratios.

939 LXIN-O12 is a poorly preserved turning trackway (Fig. 48), and the trackmaker of this
940 trackway was probably influenced by the large ornithopod LXIN-O13, which began to turn as it
941 approached O13-L1 (detailed figure see Supplementary Information 2). From O12-L3 the
942 trackway turns about 90° . In contrast to the usual decrease in stride length during the change of
943 direction, the stride length of LXIN-O12 shows an increasing trend, gradually increasing from
944 53.7 cm at L1 to 83.6 cm at L3 and decreasing to 68.8 cm at the end of the turn. Due to poor
945 preservation of the tracks, the rotation angles could not be confirmed.

946 LXIN-O28 contains six tracks forming a discontinuous trackway with one missing in the
947 middle (Fig. 49). R2 and L2 are fairly well preserved with typical tridactyl morphology (Fig. 51).
948 These two functionally tridactyl tracks with a mean length at 19.3 cm, with the average
949 length/width ratio of 1.0 and the mean mesaxony of 0.30. The interdigital divarication of digits
950 II–IV is 50° . There is a clear boundary between the digits, whereas the boundary between the
951 digits and the heel is blurred. The digits II and IV are almost the same length. Each digit has a
952 strong and blunt claw or unguinal mark. The average pace angulation of LXIN-O28 trackway is
953 149° . The pes traces show an average outward rotation of 16° from the trackway axis.

954 LXIN-O41 contains eight tracks with an average length of 25 cm, an L/W ratio of 1.2 and a
955 mesaxony of 0.42, with no clear boundary between the heel and the three digits (Fig. 50). The
956 average pace angulation of LXIN-O41 trackway is 164° . Superimposed tracks are probably
957 present in both the manus track of L1 and the pes tracks of R1 and R2. The superimposed manus
958 tracks were displaced laterally, while the superimposed pes tracks moved towards the centre of

959 the trackway. Tracks of almost equal size appeared over a distance considerably smaller than the
960 track width. This indicates a high frequency of trampling and may suggest that the trackmaker
961 may have been injured. The latter possibility is more likely than the slipperiness of the ground, as
962 neither LXIN-O41 nor the other nearby trackways showed sliding tracks or metatarsal marks.

963 Only two well-preserved tracks can be found on the slab from LXIE site (Fig. 6, 13), which
964 are in the similar orientation and forming a short trackway LXIE-O1. In which only O1-R1 is
965 complete, with 21.5 cm in length, 14.7 cm in length, and forming L/W ratio of 1.5. The
966 divarication angle of digit II–IV is 46° , with a mesaxony of 0.27. The incomplete L1 with only
967 the anterior part can compare to R1 in width and mesaxony.

968 **Comparison and discussion**

969 After the revisions by Lockley et al. (2014) and Díaz-Martínez et al. (2015) and Xing et al.
970 (2024a), the number of ichnogenera belonging to Iguanodontipodidae is quite reduced. The most
971 controversial is *Ornithopodichnus* (Kim et al., 2009), which was originally discovered in Korea
972 and has been used many times. The latest view considered that *Ornithopodichnus* is a *nomen*
973 *dubium* (Xing et al. 2024a), but this does not rule out the possibility that its ichnospecies can be
974 placed in *Caririchnium* and become a valid ichnospecies.

975 *Caririchnium* (Leonardi, 1984) is widely distributed in Berriasian–Albian sediments in Brazil,
976 Portugal, Spain, England, Switzerland, South Korea, Canada, Japan, China, and the USA, with
977 the upper limit of this geological period slightly earlier than the Longxiang age (Cenomanian).
978 The Longxiang specimens fit the diagnosis of *Caririchnium*: pes tracks belonging to
979 Iguanodontipodidae, with a large heel impression that is rounded, centred and wide (wider than
980 the width of the proximal part of the digit III impression); short, wide digit impressions (Díaz-
981 Martínez et al., 2015). Longxiang specimens have a wide range of sizes, which is common in the
982 *Caririchnium*. The ratio between the length and width of the "heel" pad varies between
983 ichnospecies. In general, pes tracks are as wide as or wider than long. The size is highly variable,
984 with common pes tracks between 30 and 60 cm long (Leonardi, 1987; Meyer and Thuring, 2003;
985 Xing et al., 2007; Razzolini et al., 2016), but there may be smaller or larger examples (e.g.
986 Lockwood et al., 2014; Xing et al., 2016, 2018b; Lee et al., 2023).

987 *Caririchnium* currently includes *C. magnificum* (Leonardi, 1984), *C. kortmeyeri* (Currie and
988 Sarjeant, 1979), *C. billsarjeanti* (Meyer and Thuring, 2003), *C. lotus* (Xing et al., 2007, 2015),
989 and *C. yeongdongensis* (Kim et al., 2016), a total of five ichnospecies. Among these
990 ichnospecies, the morphology of the manus tracks is very distinctive and useful to differentiate
991 between ichnospecies: elliptical, rectangular, and cloverleaf-like subtriangular (Leonardi, 1987;
992 Meyer and Thuring, 2003; Xing et al., 2007; Kim et al., 2016). There is limited information on
993 the morphology of the manus tracks in the Longxiang specimens, but they are essentially
994 elliptical, making them similar to *C. lotus* as a whole (Xing et al., 2007, 2015).

995 The *Caririchnium* lotus in the Longxiang tracksite extends the chronological range of this
996 ichnogenus into the early Late Cretaceous.

997 The abundance of Longxiang *Caririchnium* illustrates a diverse range of extramorphological
998 distortion, which is likely caused by the presence of muddy or watery sediments. In this case,

999 only a small proportion of tracks result in distinctly quartered tracks when the substrate is
1000 moderately strengthened. Such slippery substrate condition also causes the aforementioned
1001 elongated ‘heels’ in the tracks, and these additional traces can be divided into both wide and
1002 narrow patterns, possibly caused by sliding or as metatarsal impressions, as in LXIU-O11 (Fig.
1003 43). Additionally, some manus tracks are situated medially to the pes track, rather than laterally
1004 to the midpoint of digits III-IV (e.g., LXIN-O33-R2), which may also be indicative of the
1005 influence of a slippery substrate.

1006 It is also noteworthy that some specific behaviour-related features are present, including the
1007 occurrence of a large number of tracks in a limited area, forming a pattern similar to that of the
1008 manus pes-sets of quadruped trackways (e.g. LXIN-O17-L2 and O18-L1 in Fig. 51; Stevens et
1009 al., 2016). Some special trackways can also be observed, including LXIU-O4 (Fig. 37), which
1010 features a difference in the size of the right and left pes tracks; LXIU-O7 and LXIN-O12, which
1011 exhibit directional changes in the midst (Fig. 39, 48); and LXIN-O41, which contains
1012 overlapping tracks that may have been left by injured individuals (Fig. 50). Meanwhile, in the
1013 northwestern part of the LXIN site, the orientation of the small *Caririchnium* trackways is
1014 notably distinct, forming an assemblage that extends in an east-west direction. This observation
1015 aligns with the commonly documented hypothesis that the smaller trackmakers within this
1016 ichnogenus exhibit gregarious behaviour (e.g. Xing et al., 2015).

1017 **Speed Estimates and trackmaker**

1018 The trackmaker of *Caririchnium* is typically referred to the basal ankylopollexian or
1019 styracosternan, especially which are comparable in sizes, and shares comparable temporal and
1020 spatial interval locally (Díaz-Martínez et al., 2015). For example, the early large *Caririchnium*
1021 from Upper Jurassic of Iberian Peninsula can be linked to *Oblitosaurus* with 6–7 m in length
1022 (Sánchez-Fenollosa et al., 2023). However, the distribution of ornithopod tracks is much more
1023 extensive than their trackmakers (Noè et al., 2020; Sánchez-Fenollosa et al., 2023). For example,
1024 there is a paucity of large quadrupedal ornithopod skeletal remains, while large *C. magnificentum*
1025 have been defined in South America (Bandeira et al., 2024). Although southeastern China also
1026 lacks contemporaneous ankylopollexian trackmakers (Xu et al., 2018), however, complete
1027 geographic barriers did not exist between South and North China during the Cretaceous
1028 theoretically (Cao, 2009; Ke and Meng, 2009). There are large basal ankylopollexian in China
1029 that are contemporaneous with or earlier than the Longxiang *Caririchnium*, including
1030 *Lanzhousaurus* from Gansu (NW; You et al., 2005), and *Bayannurosaurus* from Inner Mongolia
1031 (NW; Xu et al., 2018); basal hadrosaurids including *Bolong* from Liaoning (NE; Wu and
1032 Godefroit, 2012) and *Equijubus* from Gansu, etc. (You et al., 2003). At the same time, given that
1033 the pes track compared in size to *Camptosaurus* (~5 m) pes is more than 20 cm (~25 cm in
1034 estimation) in length, and which to *Brachylophosaurus* (~10 m) pes may reach 60 cm in length
1035 (Gierliński and Karol, 2008; Paul, 2024), it can thus be postulated that the large trackmaker of
1036 Longxiang *Caririchnium* may be similar in size to the above taxa from lower Cretaceous in
1037 China, especially the basal ankylopollexians among them.

1038 For estimating hip height (h), Thulborn (1990) suggests that for large ornithopods (track

1039 length >25 cm) $h=5.9 \times$ foot length, and for small ornithopods (track length <25 cm) $h=4.8 \times$
1040 foot length. The velocity of the trackmakers are estimated by the formula of Alexander (1976),
1041 and the relative speed (gait) are represented by stride length (SL)/h. For the large Longxiang
1042 ornithopods, the relative speed range from 0.67 to 1.48, suggesting a walking gait, and the speed
1043 of the trackmakers is estimated to be between 2.12 and 6.73 km/h. For the smaller trackmakers,
1044 the relative speed range from 0.6 to 2.17, suggesting a walking to slow-running gait, and the
1045 speed of the trackmakers is estimated to be between 1.26-10.44 km/h. The evidence suggests that
1046 smaller ornithopods display a greater degree of bipedalism in their locomotory behaviour, which
1047 is relatively independent of factors such as body weight and limb proportions. This allows them
1048 to achieve higher speeds, as evidenced by the skeletal records (Maidment et al., 2014; Barrett
1049 and Maidment, 2017).

1050 Furthermore, among the Longxiang large *Caririchnium* trackways, three of them indicate a
1051 relatively greater speed of slightly over 2 (2.06-2.17), including LXIU-O9, LXIN-O6 and LXIN-
1052 O22 (Supplementary Information 2). These constitute 7% of the total 45 large ornithopod
1053 trackways. This particular slow-running gait is uncommon among *Caririchnium* and other large
1054 ornithopod ichnogenera. On the contrary, two other tracksites that also preserve a substantial
1055 number of *Caririchnium* tracks in China, including the Lower Cretaceous Zhaojue site (Xing et
1056 al., 2014a) and the Mid-Cretaceous Lotus site from Sichuan (Xing et al., 2015). In these cases,
1057 the related trackways all exhibit a walking gait.

1058 With regard to the track layer of the LXIU site, it can be posited that the relative speed of the
1059 trackways with clearly quartered tracks would have been slightly higher than that of the other
1060 poorly preserved trackways. This may indicate that substrate condition (e.g. water content)
1061 affected the speed of the trackmakers, as previously mentioned. However, on the track layer of
1062 the LXIU site, the majority of tracks are poorly preserved, and the trackmakers can still reach
1063 slow-running gait, thereby indicating that there is no prominent positive correlation between the
1064 speed of the trackmakers and the moderately featured or hardened substrate.

1065

1066 **Dinosaur tracks indent.**

1067 The LXII site contains three isolated tracks with fairly limited preservation (Fig. 7), with a
1068 preservation status of level 0 on the Belvedere and Farlow (2016) scale. Of the three isolated
1069 tracks, LXII-TI1 is 21.6 cm long with an L/W ratio of 1.4, while the other two tracks are 28.8
1070 and 26.1 cm long with fairly high L/W ratios of 2.0 and 2.3. LXII-TI1 is the first track found in
1071 the Longxiang area, and the edge of the track has a distinctive displacement rim. It is
1072 morphologically a possible tridactyl track, although only one lateral and one median digit have
1073 been preserved. Because of the relatively high L/W ratio, these tracks may have a stronger
1074 affinity to theropod tracks.

1075

1076 **Discussion**

1077 **The comparison of mid-Cretaceous dinosaur fauna in Fujian**

1078 In southeastern China, northern Guangdong and southern Jiangxi, which experienced a near-

1079 simultaneous cooling event with the Fujian region, also developed late Lower to Upper
1080 Cretaceous deposits. However, only Fujian and Jiangxi have dinosaur records in the 'Mid-'
1081 Cretaceous period, specifically in the Shanghang and Ganzhou basins, respectively (Xing et al.,
1082 2019, 2024c; Niu and Xing, 2023). The Guangdong region initially developed its stratigraphy
1083 from the Cenomanian in the Nanxiong basin (Xi et al., 2019), yet it was not until the
1084 Maastrichtian that skeletal, track and abundant egg fossil records appeared in the Nanxiong,
1085 Sanshui, and Heyuan basins, which represents oviraptorosaurian-dominated fauna including
1086 titanosauriformes, tyrannosaurids, therizinosaurian, hadrosaurids, ankylosaurian and possible
1087 deinonychosaurian .etc, and records of non-dinosaurian pterosaurs and crocodylomorphs (Dong,
1088 1979; Xing et al., 2017, 2023a, 2024c), and the tracksite there in is dominated by ornithopods
1089 (Xing et al., 2017). For the Ganzhou basin and the surrounding area, however, the mid-
1090 Cretaceous record is also limited to one possible medium-sized tyrannosaurid track (~7.5 m for
1091 the trackmaker; Xing et al., 2019), and some small-sized tridactyl theropod (oviraptorosaur?)
1092 tracks (unpublished data, LX personal observation). The fossil record of Jiangxi is largely
1093 comparable to that of the aforementioned Nanxiong basin in terms of age and member included
1094 (Xing et al., 2020, 2023b; Zhu et al., 2024). Thus, the Longxiang tracksite in Fujian is an
1095 important mid-Cretaceous fossil locality in southeastern China.

1096 Among the aforementioned morphotypes, small (<40 cm) *Brontopodus*-like tracks from
1097 sauropods; *Grallator* from small tridactyle theropods, *Tridentigerpes* from medium- to large-
1098 sized tridactyle theropods?, and cf. *Dromaeosauripus* and *Velociraptorichnus* from large/small
1099 deinonychosaurian; two types of *Caririchnium* isp. from the medium- to large-sized/small-sized
1100 ("*Ornithopodichnus*"-like) ornithopods respectively the has been reported by Niu and Xing
1101 (2023), while medial- to large sized *Eubrontes* tracks from LXIN, large (>60 cm)
1102 *Brontopodus*-like trackway from LXIN, and a possible large didactyl trackway from LXID has
1103 been newly distinguished in this paper. Furthermore, additional specimens belong to
1104 *Tridentigerpes* type A from LXIN, *Caririchnium* isp. from LXID and LXIN has been discovered
1105 on the basis of Niu and Xing (2023) (The distribution of size and morphotype see Supplementary
1106 Information 3).

1107 Among these tracksites, ornithopod, sauropod and theropod tracks can be identified in LXIII
1108 sites, but only LXI sites have recognisable trackways. The tracks of all major dinosaur clades
1109 have been found in LXI and LXIII sites, except for the sauropod tracks in LXID. Certain
1110 ornithopod tracks classified in *Caririchnium* are the most prevalent in all LXI sites, representing
1111 84% of all trackways and 89%, 57% and 76% of the tracks from LXIN, LXID and LXIU,
1112 respectively. Large trackways (≥ 25 cm) account for 19%, 25% and 62% of the trackways from
1113 the above three sites within *Caririchnium* morphotype respectively, and very large ones reaching
1114 ~40 cm occurs in LXIN (5) and LXIU (3) (Table 1). The largest ornithopod trackway in LXIU is
1115 even comparable in size to the sauropod trackway in terms of pes length. This suggests that
1116 contemporaneous large consumers in the region were probably concentrated in ornithopods, i.e.,
1117 that the hot, at least seasonally dry, coastal plateau with mountain ranges acting as barriers
1118 during the mid-Cretaceous period in southeast China was suitable for these ankylopollexian

1119 survival (Chen, 2000; Li et al., 2009; Lü et al., 2019; Zhang et al., 2021). Besides, It should be
1120 noted that for the three tracksites in LXI, particularly LXIN and LXIU, there is a difference in
1121 the size at which the mutation occurs in the ornithopod trackmaker. For the LXIN site, there is a
1122 clear gap between 32 and 41 cm, whereas for the LXIU site, this gap occurs between 19 and 26
1123 cm. for the LXIN site, there is a clear gap between 32 and 41 cm, whereas for the LXIU site, this
1124 gap occurs between 19 and 26 cm. Given that juveniles of large animals can occupy the niche of
1125 smaller ones (Lockley and Xing, 2021; Schroeder et al., 2021; Wyenberg-Henzler et al., 2022), it
1126 can be posited that the discrepancy of the two track layers may be due to differences in the
1127 ontogenetic stage, rather than the variation in clade.

1128 Apart from differences in palaeolatitude and the presence of a coastal location, the
1129 environmental characteristics of southeastern China bear resemblance to those of
1130 contemporaneous or earlier (late Early Cretaceous) regions in northwestern China, particularly
1131 Gansu, Shaanxi, and western Inner Mongolia (Li et al., 2013; Cao et al., 2013; Zhang et al.,
1132 2021). The latter also contains faunas rich in ankylopollexian and large phytophagous theropods,
1133 such as Mazongshan dinosaur fauna from western Gansu (You et al., 2018), Yanguoxia
1134 tracksites in Hekou Group from eastern Gansu (Xing et al., 2021f). However, northwestern
1135 China continues to be characterised by the presence of a large number of saurischian, especially
1136 large sauropods, and an abundance of small theropods, both in the sense of skeletal and track
1137 record (Wang et al., 2015; You et al., 2018; Xing et al., 2018, 2021f); whereas the Shaxian
1138 Formation in Fujian is characterised by greater ornithopods, as well as large deinonychosaurian
1139 record.

1140 During the same period in which these dinosaur faunal remains were discovered, i.e., around
1141 the 'Mid-' Cretaceous, cooling and humidifying episodes occurred across an expanse extending
1142 from southeastern China to northwestern China; however, the intervals between these episodes
1143 spanned a range of timescales. The phytosporic and isotopic evidence indicates that the Zhejiang
1144 region (middle SE) and the western Gansu region (western NW) were the first to experience the
1145 event from the early Aptian onwards. At the Aptian/Albian boundary, the western Gansu and
1146 Ordos Basin (eastern NW) and the Hubei and Jiangsu regions (northern SE) initially experienced
1147 the event, when the impacts in western Gansu began to subside. In the middle to late Albian, the
1148 Guangdong, Jiangxi and Fujian region (southern SE) experienced a cooling trend until the early
1149 Late Cretaceous (Li et al., 2013; Wang et al., 2022); during the same period, the most significant
1150 phase of the event has been largely removed in the region of NW China and Jiangsu (Li et al.,
1151 2013; Wang et al., 2022), and NW China no longer develops significant terrestrial deposits (Cao,
1152 2018). Concurrently, the short-term maximum impacts of cooling events in the Guangdong and
1153 Fujian regions are considerably less significant than those observed in Jiangsu and NW China (Li
1154 et al., 2013; Wang et al., 2022).

1155 The richest dinosaur fauna record during the 'Mid-' Cretaceous in China is found in Zhejiang,
1156 which essentially represents the fauna of the region at the end of the period affected by the
1157 cooling-humidifying event (late Albian-earliest Coniacian) (Xi et al., 2019; Xing et al., 2021). The
1158 fossil record of sauropods and small theropods (and potentially ankylosaurians) persists

1159 throughout this stage (Yu, 2013; Wu et al., 2018)., with large theropods as therizinosaurian
1160 appearing at least in the early part of the period. In contrast, in the more definitive
1161 contemporaneous records of ornithopods from Zhejiang, their body sizes remain in the small- to
1162 medium-sized range (Zhang et al., 2012; Yu, 2013; Du et al., 2015; Wu et al., 2018), with only
1163 two suspected large ornithopod trackways (~40 cm; see Wu et al., 2018) occur in the Jinhua
1164 Formation. These features, particularly the significance of the ornithopod trackmaker in the
1165 fauna, are distinct from those observed in the contemporaneous Fujian.

1166 In comparison to other dinosaurs, including other ornithischians, ornithopods demonstrate a
1167 more pronounced and efficient high-fibre herbivory (Button et al., 2023). Additionally, the dental
1168 texture of this clade has been found to be significantly rougher in the Late Cretaceous period
1169 (Kubo et al., 2023). In the case of hadrosaurids, representatives of the ankylopollexia clade,
1170 which underwent distinct gigantism, the auxiliary abrasive capacity of their teeth has been
1171 further enhanced (Kubo et al., 2023). Concurrently, a comparable herbivorous homogenisation is
1172 observed in the latest Cretaceous global cooling process. During this process, hadrosaurids with
1173 more advantageous border herbivorous diets and larger feeding ranges occupied at least the
1174 ecological space of ankylosaurs and ceratopsians (Condamine et al., 2021). These may be
1175 contributing factors to the distinctive domination of large-sized ornithopod tracks at Longxiang
1176 sites in the Fujian region relative to NW China, during mid-Cretaceous cooling in NW-SE China.

1177 Another noteworthy feature of the Longxiang tracksite in southeastern China is its distinctive
1178 large didactyl track, which includes the *Fujianipus*. For the large deinonychosaurians record to
1179 date, with the exception of *Utahraptor* from the Hell Creek Formation (Pearson et al., 2002;
1180 DePalma et al., 2005), the remaining fauna lacks large tyrannosaurid or abelisaurid predators,
1181 which large deinonychosaurian all occur as currently discovered apex predators of contemporary
1182 terrestrial fauna (Novas et al., 2009; Tsuihiji et al., 2012; Kirkland et al., 2016; Rolando et al.,
1183 2021; Paul, 2024). Concurrently, the associated fauna also exhibits a paucity of large
1184 marginocephalians and giant (>15 m) macronarians (Paul, 2024).

1185 In terms of chronology and palaeogeography, the ichnofauna from Fujian is more closely
1186 related to the contemporaneous Bayan Shireh skeletal fauna from Mongolia. However, it does
1187 not contain definitive theropod tracks as large as the tridactyl tracks from the earlier Yanguoxia
1188 tracksite, which lies between the two aforementioned sites (>40 cm; Xing et al., 2018b,
1189 unpublished manuscript). This may indicate that large deinonychosaurians dispersed in East Asia
1190 during the latest Early Cretaceous period, or that there was convergence in response to similar
1191 environments, including natural conditions and the lack of pre-existing large tyrannosaurids
1192 (Brusatte et al., 2010; Xing et al., 2024c). The paucity of large tyrannosaurids in the current
1193 record from the 'Mid-' Cretaceous of Fujian, and the replacement of large deinonychosaurians,
1194 may be attributed to similar factors to those which led to the domination of ornithopods. Such
1195 factors include differences in the tolerance of the two types of predator to cooling processes
1196 (Condamine et al., 2021).

1197 Given that the degree of floristic change in the Fujian region is not as pronounced as in
1198 neighbouring regions (Wang et al., 2022), the earlier dominance of ornithopods and the

1199 distinctive enlargement of deinonychosaurs observed in the current dinosaur ichnofauna may
1200 also be attributed to biases in preservation, or differences between the specific environment
1201 within the mountainous region in SE China proximate to the track layer (Shu et al., 2009), which
1202 creates significant faunal variation over a limited geographic range (Antonelli et al., 2018).
1203

1204 Conclusions

1205 New material of dinosaur tracks and trackways from Longxing (LX) tracksites in mid-
1206 Cretaceous of Shanghang Basin, Fujian, China are reported in this paper on the basis of Niu and
1207 Xing (2023) and Xing et al. (2024). A few ichnospecies *Tridentigerpes longyanensis*, new
1208 morphotype of medial- to large-sized *Eubrontes* from LXIN site, large (>60 cm)
1209 *Brontopodus*-like trackway from LXIN site, and a possible large didactyl trackway from LXID
1210 site has been newly distinguished, additional specimens belong to *Tridentigerpes* type A from
1211 LXIN, and *Caririchnium* isp. from LXID, LXIN and LXIE has been newly discovered.

1212 The Longxing tracksite is now confirmed to be dominated by ankylopollexian ornithopod
1213 trackways (> 84%), with a proportion of large members within ornithopod (>25 cm, > 27%) ,
1214 and indicates the flourishing of large ornithopods and the relative homogeneity of herbivores
1215 occurring within this period. The Longxiang sites also demonstrate the presence of concurrent,
1216 distinct, large didactyl tracks, which diverge from the composition of the apex predators in the
1217 representative Late Cretaceous fauna, whereby tyrannosaurids and abelisaurids are dominant.

1218 The Longxiang tracksite represents the sole extensive mid-Cretaceous dinosaur tracksite in
1219 the SE China, which can be compared to the dinosaur records in contemporaneous Zhejiang in SE
1220 China and Mongolia, and also similar to earlier Gansu, Shaanxi and Inner Mongolia in NW
1221 China. However, with the exception of Fujian, none of the above records in SE China show
1222 significant large ornithopods in the earliest Late Cretaceous deposits and earlier, whereas
1223 ornithopod records in NW China and Mongolia were widespread during the Lower to Upper
1224 Cretaceous. The discrepancies observed in faunal distributions, particularly within the SE China,
1225 may be attributed to a combination of factors, including the timing and relatively small
1226 magnitude of the short-term cooling- humidifying events that occurred in the Fujian region
1227 during the Late Early Cretaceous; the Longxiang site as a manifestation of the southward
1228 migration of faunas from contemporaneous North China or North Asia; the geographical
1229 isolation of the mountainous region resulting in significant differences in the faunas of the
1230 different regions in between, influenced by migrating taxa.
1231

1232 Acknowledgements

1233 We thank anonymous reviewers and XXXX for their constructive comments and proposals for
1234 improvements.
1235

1236 References

1237 Ahrens, J., Geveci, E., Law, C., Hansen, C., Johnson, C., 2005. 36-paraview: An end-user tool
1238 for large-data visualization. The visualization handbook, 717, pp.50038-1.

- 1239 Antonelli, A., Kissling, W.D., Flantua, S.G., Bermúdez, M.A., Mulch, A., Muellner-Riehl, A.N.,
1240 Kreft, H., Linder, H.P., Badgley, C., Fjeldså, J., Fritz, S.A., 2018. Geological and climatic
1241 influences on mountain biodiversity. *Nature Geoscience*, 11(10), pp.718-725.
- 1242 Bai, B., Meng, J., Zhang, C., Gong, Y.X., Wang, Y.Q., 2020. The origin of Rhinocerotidae.,
1243 phylogeny of Ceratomorpha (Mammalia, Perissodactyla). *Communications Biology*, 3(1),
1244 p.509.
- 1245 Bandeira, K.L., Navarro, B.A., Pêgas, R.V., Brilhante, N.S., Brum, A.S., de Souza, L.G., da
1246 Silva, R.C., Gallo, V., 2024. A reassessment of the historical fossil findings from Bahia
1247 State (Northeast Brazil) reveals a diversified dinosaur fauna in the Lower Cretaceous of
1248 South America. *Historical Biology*, pp.1-42.
- 1249 Barrett, P.M., Maidment, S.C., 2017. The evolution of ornithischian quadrupedality. *Journal of*
1250 *Iberian Geology*, 43(3), pp.363-377.
- 1251 Belvedere, M, Farlow, J.O. 2016. A numerical scale for quantifying the quality of preservation of
1252 vertebrate tracks. In: Falkingham PL, Marty D, Richter A, editors. *Dinosaur tracks—the*
1253 *next steps*. Bloomington and Indianapolis: Indiana University Press; p. 92–98.
- 1254 Blazquez, A.P., Mocho, P., Escaso, F., Ortega, F., 2024. Evolution of hind limb morphology of
1255 Titanosauriformes (Dinosauria, Sauropoda) analyzed via 3D Geometric Morphometrics
1256 reveals wide-gauge posture as an exaptation for gigantism. *eLife*, 13.
- 1257 Brown, R., Lawrence, M., Ferguson, J., Lees, D., 2021. Tracks., signs of the birds of Britain and
1258 Europe.
- 1259 Brusatte, S.L., Benson, R.B., Xu, X., 2010. The evolution of large-bodied theropod dinosaurs
1260 during the Mesozoic in Asia. *Journal of Iberian Geology*, 36(2), pp.275-296.
- 1261 Button, D.J., Porro, L.B., Lautenschlager, S., Jones, M.E., Barrett, P.M., 2023. Multiple
1262 pathways to herbivory underpinned deep divergences in ornithischian evolution. *Current*
1263 *Biology*, 33(3), pp.557-565.
- 1264 Cao, K., 2018. Cretaceous terrestrial deposits in China. *China Geology*, 1(3), pp.402-414.
- 1265 Charvet, J., Lapierre, H., Yu, Y., 1994. Geodynamic significance of the Mesozoic volcanism of
1266 southeastern China. *Journal of Southeast Asian Earth Sciences*, 9(4), pp.387-396.
- 1267 Chen, P.J., 1979. An outline of Palaeogeography during the Jurassic and Cretaceous periods of
1268 China—with a discussion on the origin of Yantze River. *Acta Scientiarum Naturalium*
1269 *Universitatis Pekinensis*, 3(9), 90-109.
- 1270 Chen, P.J., 2000. Paleoenvironmental changes during the Cretaceous in eastern China. In
1271 *Developments in palaeontology., stratigraphy (Vol. 17, pp. 81-90)*. Elsevier.
- 1272 Chen, S., Lin, C., Xu, W., Zhao, J. 2020. Age and Tectonic Significance of Volcanic Rocks in
1273 Cretaceous Red Beds in Fujian. *Editorial Committee of Earth Science-Journal of China*
1274 *University of Geosciences*, 45(7):2508-2523
- 1275 Chen, Y., 2008. Late Cretaceous sedimentary responses to the "Coast Range" and
1276 Paleoclimate changes in Southeast China. Chengdu University of Technology. Master
1277 Thesis. 59pp
- 1278 Chiarenza, A. A., Mannion, P. D., Lunt, D. J., Farnsworth, A., Jones, L. A., Kelland, S.-J.,

- 1279 Allison, P. A. 2019. Ecological niche modelling does not support climatically driven
1280 dinosaur diversity decline before the Cretaceous/Paleogene mass extinction. *Nature*
1281 *Communications*, 10, 1091.
- 1282 Christiansen, P., 1999. Scaling of the limb long bones to body mass in terrestrial mammals.
1283 *Journal of morphology*, 239(2), pp.167-190.
- 1284 Cignoni P., Callieri, M., Corsini, M., Dellepiane, M., Ganovelli, F., Ranzuglia, G., 2008.
1285 MeshLab: an Open-Source Mesh Processing Tool. Sixth Eurographics Italian Chapter
1286 Conference; Eds V. Scarano, R. De Chiara, U. Erra. Salerno, Italy; p. 129–136.
- 1287 Compilation Committee of Geological Atlas of China, 2002. Geological Atlas of China.
1288 Geological publishing house, Beijing, p. 348.
- 1289 Condamine, F.L., Guinot, G., Benton, M.J., Currie, P.J., 2021. Dinosaur biodiversity declined
1290 well before the asteroid impact, influenced by ecological., environmental pressures. *Nature*
1291 *Communications*, 12(1), p.3833.
- 1292 Cross, M.C., Hohenberg, P.C., 1993. Pattern formation outside of equilibrium. *Reviews of*
1293 *modern physics*, 65(3), p.851.
- 1294 DePalma, R.A., Burnham, D.A., Martin, L.D., Larson, P.L., Bakker, R.T., 2015. The first giant
1295 raptor (Theropoda: Dromaeosauridae) from the hell creek formation. *Paleontological*
1296 *Contributions*, 2015(14), pp.1-16.
- 1297 Diaz-Martinez, I., Pereda-Suberbiola, X., Perez-Lorente, F., Canudo, J.I., 2015. Ichnotaxonomic
1298 review of large ornithopod dinosaur tracks: temporal and geographic implications. *PloS one*,
1299 10(2), p.e0115477.
- 1300 Dong, Z.M. 1979. The Cretaceous dinosaur fossils in southern China. In: Institute of Vertebrate
1301 Paleontology., Paleoanthropology., Nanjing Institute of Paleontology, editor. Mesozoic and
1302 Cenozoic Red Beds of South China (in Chinese). Nanxiong: Science Press; p. 342–350.
- 1303 Du, T.M., H. Wu, X.S. Jin, G.Z. Jin, Y.M. Sheng. 2015. The features of footprint fossils from
1304 Guanyintang Village, Yiwu City, Zhejiang Province., the suggestions for protection.
1305 *Research of Natural History and Museum* 2: 54–60.
- 1306 Du, T.M., H. Wu, X.S. Jin, G.Z. Jin, Y.M. Sheng. 2015. The features of footprint fossils from
1307 Guanyintang Village, Yiwu City, Zhejiang Province and the suggestions for protection.
1308 *Research of Natural History and Museum* 2: 54–60.
- 1309 Endo, H., Yoshida, M., Nguyen, T.S., Akiba, Y., Takeda, M., Kudo, K., 2019.
1310 Three-dimensional CT examination of the forefoot and hindfoot of the hippopotamus and
1311 tapir during a semiaquatic walking. *Anatomia, histologia, embryologia*, 48(1), pp.3-11.
- 1312 Falkingham, P.L., Gatesy, S.M. 2014. The birth of a dinosaur footprint: Subsurface 3D motion
1313 reconstruction and discrete element simulation reveal track ontogeny. *PNAS* 111(51):
1314 18279–18284
- 1315 Farlow, J.O., 1989. *Protopedus birdi* Lower Cretaceous sauropod footprints from the US Gulf
1316 coastal plain. *Dinosaur tracks and traces*.
- 1317 Fleury, K., Burns, E., Richards, M.D., Norton, K., Read, S., Wesley, R., Ewan Fordyce, R.,
1318 Wilcken, K., 2024. The moa footprints from the Pliocene–early Pleistocene of Kyeburn,

- 1319 Otago, New Zealand. *Journal of the Royal Society of New Zealand*, 54(5), pp.620-642.
- 1320 Fujian Institute of Geological Survey, 2016. *The Regional Geology of China, Fujian Province.*
- 1321 Geological Publishing House, Beijing (in Chinese). 976pp
- 1322 García-Ramos, J.C.M., Lires, J., Piñuela, L., 2003. *Dinosaurios: rutas por el Jurásico de Asturias.*
- 1323 *La voz de Asturias.*
- 1324 Gatesy, S.M., Middleton, M.K., Jenkins, Jr.F.A., Shubin, N.H. 1999. Three-dimensional
- 1325 preservation of foot movements in Triassic theropod dinosaurs. *Nature*, 399: 141–144.
- 1326 Gierliński, G., Karol, S., 2008. Stegosaurian footprints from the Morrison Formation of Utah and
- 1327 their implications for interpreting other ornithischian tracks. *Oryctos*, 8, p.29.
- 1328 Gu, Z., 2005. Conventions of Language. *J. Stratigr.* 29 (1), 1–48.
- 1329 Gutarra, S., Stubbs, T.L., Moon, B.C., Heighton, B.H., Benton, M.J., 2023. The locomotor
- 1330 ecomorphology of Mesozoic marine reptiles. *Palaeontology*, 66(2), p.e12645.
- 1331 Henderson, D.M., 2006. Burly gaits: centers of mass, stability, the trackways of sauropod
- 1332 dinosaurs. *Journal of Vertebrate Paleontology*, 26(4), pp.907-921.
- 1333 Henderson, D.M., 2015. A wide-gauge, large-mammal trackway from the upper Paleocene of
- 1334 Alberta, Canada. *Canadian Journal of Earth Sciences*, 52(8), pp.696-700.
- 1335 Hildebrand, M., 1989. The quadrupedal gaits of vertebrates. *BioScience*, 39(11), p.766.
- 1336 Hu, L. H., 1990. A Magnetostratigraphic Study of Cretaceous Red Beds From Shanghang,
- 1337 Western Fujian. *Geology of Fujian*, 1: 33-42 (in Chinese with English abstract).
- 1338 Hutchinson, J.R., 2021. The evolutionary biomechanics of locomotor function in giant land
- 1339 animals. *Journal of Experimental Biology*, 224(11), p.jeb217463.
- 1340 Israelachvili, J.N., 2011. *Intermolecular and surface forces.* Academic press.
- 1341 Ke, C., Meng, W., 2009. Constraints of sedimentary records on Cretaceous paleoclimate
- 1342 simulation in China mainland. *Earth Science Frontiers*, 16(5), pp.29-36.
- 1343 Kirkland, J., Suarez, M., Suarez, C., Hunt-Foster, R., 2016. The Lower Cretaceous in east-central
- 1344 Utah—the Cedar Mountain Formation., its bounding strata. *Geology of the Intermountain*
- 1345 *West*, 3, pp.101-228.
- 1346 Kubo, T., Kubo, M.O., Sakamoto, M., Winkler, D.E., Shibata, M., Zheng, W., Jin, X., You, H.L.,
- 1347 2023. Dental microwear texture analysis reveals a likely dietary shift within Late
- 1348 Cretaceous ornithopod dinosaurs. *Palaeontology*, 66(6), p.e12681.
- 1349 Lallensack, J.N., Engler, T., Barthel, H.J., 2020. Shape variability in tridactyl dinosaur footprints:
- 1350 the significance of size and function. *Palaeontology*, 63(2), pp.203-228.
- 1351 Lallensack, J.N., Falkingham, P.L., 2022. A new method to calculate limb phase from trackways
- 1352 reveals gaits of sauropod dinosaurs. *Current Biology*, 32(7), pp.1635-1640.
- 1353 Lallensack, J.N., Ishigaki, S., Lagnaoui, A., Buchwitz, M., Wings, O., 2018. Forelimb
- 1354 orientation., locomotion of sauropod dinosaurs: insights from the? Middle Jurassic
- 1355 Tafaytour tracksites (Argana Basin, Morocco). *Journal of Vertebrate Paleontology*, 38(5),
- 1356 p.e1512501.
- 1357 Li, J., 1997. *Stratigraphy (Lithostratic) of Fujian province.* Wuhan: China University of
- 1358 *Geosciences Press*, 216.

- 1359 Li, J., Zhang, Y., Dong, S., Johnston, S.T., 2014. Cretaceous tectonic evolution of South China:
1360 A preliminary synthesis. *Earth-Science Reviews*, 134, pp.98-136.
- 1361 Li, X., Chen, S., Cao, K., Chen, Y., Xu, B., Ji, Y., 2009. Paleosols of the mid-cretaceous: a
1362 report from Zhejiang., Fujian, SE China. *Earth Science Frontiers*, 16(5), pp.63-70.
- 1363 Li, X., Xu, W., Liu, W., Zhou, Y., Wang, Y., Sun, Y., Liu, L., 2013. Climatic and environmental
1364 indications of carbon and oxygen isotopes from the Lower Cretaceous calcrete and
1365 lacustrine carbonates in Southeast and Northwest China. *Palaeogeography,
1366 Palaeoclimatology, Palaeoecology*, 385, pp.171-189.
- 1367 Liang, S., Cao, B., Ma, A. On the chronogenesis and correlation of Cretaceous red beds in Fujian
1368 province. *Geology of Fujian*, 1992, 11(4), 263-282.
- 1369 Lockley, M.G. and Xing, L., 2021. A review of the non-avian theropod track record and the
1370 implications for the Ontogenetic Niche Shift model. *Earth-Science Reviews*, 220, p.103715.
- 1371 Lockley, M.G., 1986. The Paleobiological and Paleoenvironmental Importance of Dinosaur
1372 Footprints. *Palaios*. 37–47
- 1373 Lockley, M.G., 2009. New perspectives on morphological variation in tridactyl footprints: clues
1374 to widespread convergence in developmental dynamics. *Geological Quarterly*, 53(4),
1375 pp.415-432.
- 1376 Lockley, M.G., Farlow, J.O., Meyer, C.A., 1994. *Brontopodus* and *Parabrontopodus* ichnogen.
1377 nov., the significance of wide-and narrow-gauge sauropod trackways. *Gaia*, 10, 135–145.
- 1378 Lockley, M.G., Gregory, M.R., Gill, B., 2007. The Ichnological record of New Zealand's Moas:
1379 a preliminary summary. *New Mexico Museum of Natural History and Science Bulletin*, 42,
1380 p.73e78.
- 1381 Lü, B., Liu, X., Guo, H., Zheng, X., Chen, Z., He, M., Zhao, G., 2014. The cretaceous strata in
1382 Danxia of Yong'an in Fujian province. *Journal of Shandong Normal University (Natural
1383 Science)*, 29(4), 78-84.
- 1384 Lü, B., Liu, X.M., Guo, H., 2019. Magnetic properties of the cretaceous Shaxian formation
1385 stratum in Fujian province and their environmental significance. *Acta Sedimentologica
1386 Sinica*, 37(03), pp.519-531.
- 1387 Maidment, S.C., Bates, K.T., Falkingham, P.L., VanBuren, C., Arbour, V., Barrett, P.M., 2014.
1388 Locomotion in ornithischian dinosaurs: an assessment using three-dimensional
1389 computational modelling. *Biological Reviews*, 89(3), pp.588-617.
- 1390 Mannion, P.D., Upchurch, P., 2010. A quantitative analysis of environmental associations in
1391 sauropod dinosaurs. *Paleobiology*, 36(2), pp.253-282.
- 1392 Matsukawa, M., Shibata, K., Sato, K., Xu, X., Lockley, M.G 2014. The Early Cretaceous
1393 terrestrial ecosystems of the Jehol Biota based on food-web and energy-flow models.
1394 *Biological Journal of the Linnean Society*. 113; 836-853
- 1395 McAllister, J.A., Kirby, J., 1998. An occurrence of reptile subaqueous traces in the Moenkopi
1396 Formation (Triassic) of Capitol Reef National Park, south central Utah, USA. *National Park
1397 Service, Technical Report*, 98(1), pp.45-49.
- 1398 Milàn, J., 2006. Variations in the morphology of emu (*Dromaius novaehollandiae*) tracks

- 1399 reflecting differences in walking pattern and substrate consistency: ichnotaxonomic
1400 implications. *Palaeontology*, 49(2), pp.405-420.
- 1401 Molina-Pérez, R., Larramendi, A., 2016. Récords y curiosidades de los dinosaurios: terópodos y
1402 otros dinosauriomorfos. Larousse.
- 1403 Molina-Pérez, R., Larramendi, A., Connolly, D., Cruz, G.Á.R., 2019. *Dinosaur facts., figures:*
1404 *The theropods and other dinosauriformes.* Princeton University Press.
- 1405 Navarro-Lorbés, P., Díaz-Martínez, I., Valle-Melón, J.M., Rodríguez-Miranda, A., Moratalla,
1406 J.J., Ferrer-Ventura, M., San Juan-Palacios, R., Torices, A., 2023. Dinosaur swim tracks
1407 from the Lower Cretaceous of La Rioja, Spain: An ichnological approach to non-common
1408 behaviours. *Cretaceous Research*, 147, p.105516.
- 1409 Niu, K., Xing, L., 2023. The first dinosaur track assemblages from the Upper Cretaceous
1410 Shaxian Formation, Fujian Province, southeastern China. *Cretaceous Research*, 146,
1411 p.105486.
- 1412 Noè, L.F., Gómez-Pérez, M., Rodríguez, J.V., Corrales-García, A., Caranton-Mateus, W.G.,
1413 2020. Dinosaur footprints from the Lower Cretaceous, Batá Formation, Colombia (South
1414 America), the possible interchange of large ornithopods between southern Laurasia.,
1415 northern Gondwana. *The Geology of Colombia*, 2, pp.375-401.
- 1416 Novas, F.E., Pol, D., Canale, J.I., Porfiri, J.D., Calvo, J.O., 2009. A bizarre Cretaceous theropod
1417 dinosaur from Patagonia and the evolution of Gondwanan dromaeosaurids. *Proceedings of*
1418 *the Royal Society B: Biological Sciences*, 276(1659), pp.1101-1107.
- 1419 Paul, G.S., 2016. *The Princeton field guide to dinosaurs.*
- 1420 Paul, G.S., 2024. *The Princeton Field Guide to Dinosaurs (Princeton Field Guides).* Princeton
1421 University Press.
- 1422 Pearson, D.A., Schaefer, T., Johnson, K.R., Nichols, D.J., Hunter, J.P., 2002. Vertebrate
1423 biostratigraphy of the Hell Creek formation in southwestern North Dakota and northwestern
1424 South Dakota. *Geological society of America special paper*, 361(145), p.e167.
- 1425 Perle, A., 1999. A new maniraptoran theropod, *Achillobator giganticus* (Dromaeosauridae), from
1426 the Upper Cretaceous of Burkhan, Mongolia. *Ulan Bator: National University of Mongolia*,
1427 104 pp.
- 1428 Rolando, M.A., Cerroni, M.A., Marsà, J.A.G., Motta, M.J., Rozadilla, S., Eglí, F.B., Novas, F.E.,
1429 2021. A new medium-sized abelisaurid (Theropoda, Dinosauria) from the late cretaceous
1430 (Maastrichtian) Allen Formation of Northern Patagonia, Argentina. *Journal of South*
1431 *American Earth Sciences*, 105, p.102915.
- 1432 Romilio, A. 2020. *An Instructional Guide to Visualising Dinosaur Tracks.* Columbia, South
1433 Carolina, USA. Amazon; p. 36.
- 1434 Romilio, A., Tucker, R.T., Salisbury, S.W., 2013. Reevaluation of the Lark Quarry dinosaur
1435 Tracksite (late Albian–Cenomanian Winton Formation, central-western Queensland,
1436 Australia): no longer a stampede?. *Journal of Vertebrate Paleontology*, 33(1), pp.102-120.
- 1437 Sánchez-Fenollosa, S., Verdú, F.J., Cobos, A., 2023. The largest ornithopod (Dinosauria:
1438 Ornithischia) from the Upper Jurassic of Europe sheds light on the evolutionary history of

- 1439 basal ankylopollexians. *Zoological Journal of the Linnean Society*, 199(4), pp.1013-1033.
- 1440 Schroeder, K., Lyons, S.K., Smith, F.A., 2021. The influence of juvenile dinosaurs on
1441 community structure and diversity. *Science*, 371(6532), pp.941-944.
- 1442 Shu, L.S., Zhou, X.M., Deng, P., Wang, B., Jiang, S.Y., Yu, J.H., Zhao, X.X., 2009. Mesozoic
1443 tectonic evolution of the Southeast China Block: New insights from basin analysis. *Journal*
1444 *of Asian Earth Sciences*, 34(3), pp.376-391.
- 1445 Stevens, K.A., Ernst, S., Marty, D., 2016. Uncertainty and ambiguity in the interpretation of
1446 sauropod trackways (pp. 226-243). Bloomington: Indiana University Press.
- 1447 Stevens, K.A., Ernst, S., Marty, D., 2022. Coupling length: a generalized gleno-acetabular
1448 distance measurement for interpreting the size and gait of quadrupedal trackmakers. *Swiss*
1449 *Journal of Geosciences*, 115(1), p.18.
- 1450 Tanaka, I., 2021. Morphological variability of *Ciconia boyciana* (Aves: Ciconiidae) tracks in
1451 homogeneous sediment. *Palaios*, 36(4), pp.141-154.
- 1452 Tsuihiji, T. Watabe, M., Tsogtbaatar, K., Barsbold, R., Suzuki, S., 2012. A tyrannosauroid
1453 frontal from the Upper Cretaceous (Cenomanian-Santonian) of the Gobi Desert, Mongolia.
1454 *Vertebrata Palasiatica*. 50 (2), 102–110.
- 1455 Turner, M.L., Falkingham, P.L., Gatesy, S.M., 2020. It's in the loop: shared sub-surface foot
1456 kinematics in birds And other dinosaurs shed light on a new dimension of fossil track
1457 diversity. *Biology Letters*, 16(7), p.20200309.
- 1458 Van den Heever, A., Mhlongo, R., Benadie, K., Thomas, I., 2024. *Tracker Manual: A practical*
1459 *guide to animal tracking in southern Africa*. Penguin Random House South Africa.
- 1460 Vermeij, G.J., 2016. Gigantism and its implications for the history of life. *PLoS One*, 11(1),
1461 p.e0146092.
- 1462 Wan, X.Q., Chen, P.J., Wei, M.J. 2007. The cretaceous system in China. *Acta Geologica*
1463 *Sinica-English Edition*, 81(6), pp.957-983.
- 1464 Wang, J.Y., Li, X.H., Li, L.Q., Wang, Y.D., 2022. Cretaceous climate variations indicated by
1465 palynoflora in South China. *Palaeoworld*, 31(3), pp.507-520.
- 1466 Wang, M., Li, D., O'Connor, J.K., Zhou, Z., You, H., 2015. Second species of enantiornithine
1467 bird from the Lower Cretaceous Changma Basin, northwestern China with implications for
1468 the taxonomic diversity of the Changma avifauna. *Cretaceous Research*, 55, pp.56-65.
- 1469 Weems, R. E. 2006. Locomotor speeds and patterns of running behavior in non-maniraptoriform
1470 theropod dinosaurs. In J. D. Harris, S. G. Lucas, J. A. Spielmann, M. G. Lockley, A. R. C.
1471 Milner, & J. I. Kirkland (eds.), *The Triassic-Jurassic Terrestrial Transition*. New Mexico
1472 *Museum of Natural History and Science Bulletin* 37:379-389
- 1473 Wilson, J.A., Carrano, M.T., 1999. Titanosaurs., the origin of “wide-gauge” trackways: a
1474 biomechanical and systematic perspective on sauropod locomotion. *Paleobiology*, 25(2),
1475 pp.252-267.
- 1476 Wroblewski, A.F.J., Gulas-Wroblewski, B.E., 2021. Earliest evidence of marine habitat use by
1477 mammals. *Scientific Reports*, 11(1), p.8846.
- 1478 Wu, H., Jin, X., Du, T., Huang, M., Zheng, W., Sheng, Y., 2018. New findings and preliminary

- 1479 study of tetrapod track assemblages from Guanyintang Village, Yiwu City, Zhejiang
1480 Province. *Earth*, 8, 82-87.
- 1481 Wu, W., Godefroit, P., 2012. Anatomy, relationships of Bolong yixianensis, an Early Cretaceous
1482 iguanodontid dinosaur from western Liaoning, China. *Bernissart dinosaurs and Early*
1483 *Cretaceous terrestrial ecosystems*, 293, pp.293-333.
- 1484 Wyenberg-Henzler, T., Patterson, R.T., Mallon, J.C., 2022. Ontogenetic dietary shifts in North
1485 American hadrosaurids (Dinosauria: Ornithischia). *Cretaceous Research*, 135, p.105177.
- 1486 Xi, D., Wan, X., Li, G., Li, G., 2019. Cretaceous integrative stratigraphy and timescale of China.
1487 *Science China Earth Sciences*, 62, pp.256-286.
- 1488 Xing, L.D., Ba, J., Lockley, M.G., Klein, H., Yan, S.W., Romilio, A., Chou, C.Y., Persons,
1489 W.S.IV. 2018a. Late Triassic sauropodomorph and Middle Jurassic theropod tracks from
1490 the Xichang Basin, southwestern China: a first Chinese report for ichnogenus
1491 *Carmelopodus*. *Journal of Palaeogeography* 7(1): 1–13.
- 1492 Xing, L.D., Díaz-Martínez, I., Lallensack, J.N., Kim, K.S., Buckley, L.G., Romilio, A., Piñuela,
1493 L., Wang, D.H., Chen, Q.Y., Yang, Q., Chou, C.Y., Yin, H., Jin, Y.F. 2024a. Cretaceous
1494 vertebrate tracks. In: Lucas, S.G., Hunt, P.A., Klein, H. (Eds). *Vertebrate Ichnology: the*
1495 *Fossil Record of Prehistoric Behavior*. Elsevier. ISBN: 9780443138379
- 1496 Xing, L.D., Guo, Z.S., Wu, R., Du, C.L., Wang, D.H., Persons, W.S., 2023a. Cretaceous
1497 dinosaur and crocodylomorph egg records of the Sanshui Basin, Guangdong Province,
1498 southern China. *Journal of Palaeogeography*, 12(3), pp.401-418.
- 1499 Xing, L.D., Harris, J.D., Dong, Z.M., Lin, Y.L., Chen, W., Guo, S.B., Ji, Q., 2009. Ornithopod
1500 (Dinosauria: Ornithischia) Tracks from the Upper Cretaceous Zhutian Formation in
1501 Nanxiong Basin, China and General Observations on Large Chinese Ornithopod Footprints.
1502 *Geological Bulletin of China*. 28(7):829–843.
- 1503 Xing, L.D., Klein, H., Lockley, M.G., Wetzel, A., Li, Z.D., Li, J.J., Gierliński, G.D., Zhang, J.P.,
1504 Matsukawa, M., Divay, J.D., Zhou, L., 2014b. Changpeipus (theropod) tracks from the
1505 Middle Jurassic of the Turpan Basin, Xinjiang, Northwest China: review, new discoveries,
1506 ichnotaxonomy, preservation and paleoecology. *Vertebrata Palasiatica*. 52(2), 233–259
- 1507 Xing, L.D., Li, D., Harris, J.D., Bell, P.R., Azuma, Y., Fujita, M., Lee, Y.N., Currie, P.J., 2013.
1508 A new deinonychosaurian track from the Lower Cretaceous Hekou group, Gansu Province,
1509 China. *Acta Palaeontologica Polonica*, 58(4), pp.723-730.
- 1510 Xing, L.D., Liang, Z., Zhang, K., Wang, D., Zhang, X., Persons IV, W.S., Ren, Z., Liang, Z.,
1511 Xian, M., Zeng, Q., 2024c. Large theropod teeth from the Upper Cretaceous of Guangdong
1512 Province, Southern China. *Cretaceous Research*, 161, p.105914.
- 1513 Xing, L.D., Lockley, M.G., 2016. Early Cretaceous dinosaur and other tetrapod tracks of
1514 southwestern China. *Science Bulletin* 61(13): 1044–1051.
- 1515 Xing, L., Lockley, M.G., Jiang, Z., Klein, H., Persons IV, W.S., Zhang, P., Wan, X., 2021c.
1516 Variation in sauropod trackway pattern from the Tuchengzi Formation (Jurassic-Cretaceous
1517 boundary) in western Liaoning, China. *Cretaceous Research*, 118, p.104662.
- 1518 Xing, L.D., Lockley, M.G., Klein, H., Chou, C.Y., Wang, D.H., Persons, W.S., 2021b. A mid-

- 1519 Cretaceous dinosaur track assemblage from the Hengshan Formation in central Zhejiang,
1520 China. *Historical Biology*, 33(7), 973–980.
- 1521 Xing, L.D., Lockley, M.G., Klein, H., Peng, G.Z., Ye, Y., Jiang, S., Zhang, J.P., Persons,
1522 W.S.IV., Xu, T., 2016. A theropod track assemblage including large deinonychosaur tracks
1523 from the Lower Cretaceous of Asia. *Cretaceous Research* 65: 213–222.
- 1524 Xing, L.D., Lockley, M.G., Klein, H., Romilio, A., Persons, W.S.IV, Wan, X.Q. 2024b. First
1525 Grallator ichnospecies from the Tuchengzi Formation in North China: Review and new
1526 observations on grallatorid footprint in China. *New Mexico Museum of Natural History and
1527 Science Bulletin* 95: 403-433
- 1528 Xing, L.D., Lockley, M.G., Klein, H., Zhang, L.J., Romilio, A., Scott Persons, W., Peng, G.Z.,
1529 Ye, Y., Wang, M.Y., 2021d. The new ichnotaxon *Eubrontes nobitai* ichnosp. nov. and other
1530 saurischian tracks from the Lower Cretaceous of Sichuan Province and a review of Chinese
1531 *Eubrontes*-type tracks. *Journal of Palaeogeography*, 10, pp.1-19.
- 1532 Xing, L.D., Lockley, M.G., Li, D.L., Klein, H., Persons, W.S IV, Ye, Y., Zhang, J.P., Ran, H.,
1533 2017. Late Cretaceous Ornithopod-dominated, theropod, pterosaur track assemblages from
1534 the Nanxiong Basin, China: new discoveries, ichnotaxonomy, palaeoecology.
1535 *Palaeogeography, Palaeoclimatology, Palaeoecology*, 466: 303–313. DOI:
1536 10.1016/j.palaeo.2016.11.035
- 1537 Xing, L.D., Lockley, M.G., Marty, D., Zhang, J.P., Wang, Y., Klein, H., McCrea, R.T., Buckley,
1538 L.G., Belvedere, M., Mateus, O., Gierliński, G.D., Piñuela, L., Persons, W.S.IV, Wang, F.P.,
1539 Ran, H., Dai, H., Xie, X.M., 2015. An ornithopod-dominated tracksite from the Lower
1540 Cretaceous Jiaguan Formation (Barremian–Albian) of Qijiang, South-Central China: new
1541 discoveries, ichnotaxonomy, preservation and palaeoecology. *PLOS ONE* 10(10):
1542 e0141059
- 1543 Xing, L.D., Lockley, M.G., Mao, Z., Klein, H., Gu, Z., Bai, C., Qiu, L., Liu, Y., Romilio, A.,
1544 Persons IV, W.S., Wan, X., 2021a. A new dinosaur track site from the earliest Cretaceous
1545 (Berriasian) part of the Tuchengzi Formation, Hebei Province, China: Implications for
1546 morphology, ontogeny and paleocommunity structure. *Palaeogeography, Palaeoclimatology,
1547 Palaeoecology*, 580, p.110619.
- 1548 Xing, L.D., Lockley, M.G., Romilio, A., 2021e. An unusual dinosaur track assemblage from the
1549 Jurassic–Cretaceous boundary, Anning formation, Lufeng Basin, China. *Historical Biology*,
1550 33(4), pp.514-526.
- 1551 Xing, L.D., Lockley, M.G., Tang, Y., Romilio, A., Xu, T., Li, X., Tang, Y., Li, Y., 2018b.
1552 Tetrapod track assemblages from Lower Cretaceous desert facies in the Ordos Basin,
1553 Shaanxi Province, China and their implications for Mesozoic paleoecology.
1554 *Palaeogeography, Palaeoclimatology, Palaeoecology*, 507, pp.1-14.
- 1555 Xing, L.D., Lockley, M.G., Zhang, J.P., Klein, H., Persons, W.S.IV., Dai, H., 2014a. Diverse
1556 sauropod–, theropod–, ornithopod–track assemblages and a new ichnotaxon *Siamopodus*
1557 *xui* ichnosp. nov. from the Feitianshan Formation, Lower Cretaceous of Sichuan Province,
1558 southwest China. *Palaeogeography, Palaeoclimatology, Palaeoecology* 414: 79–97.

- 1559 Xing, L.D., Niu, K., Mallon, J., Miyashita, T., 2023b. A new armored dinosaur with double
1560 cheek horns from the early Late Cretaceous of southeastern China. *Vertebrate Anatomy*
1561 *Morphology Palaeontology*, 11.
- 1562 Xing, L.D., Niu, K.C., Lockley, M.G., Klein, H., Romilio, A., Persons, W.S.IV., Brusatte, S L.
1563 2019. A probable tyrannosaurid track from the Upper Cretaceous of Southern China.
1564 *Science Bulletin* 64(16): 1136–1139
- 1565 Xing, L.D., Niu, K.C., Wang, D.H., Prieto-Marquez, A. 2020. A partial articulated hadrosaurid
1566 skeleton from the Maastrichtian (Upper Cretaceous) of the Ganzhou area, Jiangxi Province,
1567 China. *Historical Biology* DOI: 10.1080/08912963.2020.1782397
- 1568 Xing, L.D., Peng, C., Lockley, M.G., Wang, Y., Li, D., Klein, H., Yang, J., Li, L., Persons, W.S.,
1569 Wang, M., 2021. A diversified tetrapod ichnite fauna from the Lower Cretaceous Hekou
1570 Group of Gansu Province, China. *Historical Biology*, 33(11), pp.3018-3030.
- 1571 Xu, X., Tan, Q., Gao, Y., Bao, Z., Yin, Z., Guo, B., Wang, J., Tan, L., Zhang, Y., Xing, H., 2018.
1572 A large-sized basal ankylopollexian from East Asia, shedding light on early biogeographic
1573 history of Iguanodontia. *Science Bulletin*, 63(9), pp.556-563.
- 1574 You, H., Ji, Q., Li, D., 2005. *Lanzhousaurus magnidens* gen. Et sp. Nov. From Gansu Province,
1575 China: the largest-toothed herbivorous dinosaur in the world. *Geological Bulletin of China*,
1576 24(9), 785-794.
- 1577 You, H., Luo, Z., Shubin, N.H., Witmer, L.M., Tang, Z., Tang, F., 2003. The earliest-known
1578 duck-billed dinosaur from deposits of late Early Cretaceous age in northwest China and
1579 hadrosaur evolution. *Cretaceous Research*, 24(3), pp.347-355.
- 1580 You, H., Morschhauser, E.M., Li, D., Dodson, P., 2018. Introducing the Mazongshan dinosaur
1581 fauna. *Journal of Vertebrate Paleontology*, 38(sup1), pp.1-11.
- 1582 Yu, F.M. 2013. *Dinosaurs in Zhejiang-The Investigation., Research of Dinosaur Fossils from*
1583 *Zhejiang Province*. Hangzhou: Zhejiang People’s Publishing House, 254 pp
- 1584 Zhang, J., Liu, Y., Flögel, S., Zhang, T., Wang, C., Fang, X., 2021. Altitude of the East Asian
1585 coastal mountains., their influence on Asian climate during early Late Cretaceous. *Journal*
1586 *of Geophysical Research: Atmospheres*, 126(22), p.e2020JD034413.
- 1587 Zheng, D., Wang, H., Li, S., Wang, B., Jarzembowski, E.A., Dong, C., Fang, Y., Teng, X., Yu,
1588 T., Yang, L., Li, Y., 2021. Synthesis of a chrono-and biostratigraphical framework for the
1589 Lower Cretaceous of Jiuquan, NW China: implications for major evolutionary events.
1590 *Earth-Science Reviews*, 213, p.103474.
- 1591 Zheng, F., Li, W.B., 1986. Cretaceous miospore assemblages of Fujian. *Acta Palaeontologica*
1592 *Sinica*, 25(2), pp.201-210.
- 1593 Zheng, W., Jin, X., Shibata, M., Azuma, Y., Yu, F., 2012. A new ornithischian dinosaur from the
1594 cretaceous Liangtoutang formation of Tiantai, Zhejiang Province, China. *Cretaceous*
1595 *Research*, 34, pp.208-219.
- 1596 Zhou, X., 2007. *Petrogenesis of the Late Mesozoic Granitoids in the Nanling Range and*
1597 *Geodynamic Evolution of Lithosphere*. Beijing: Science Press, pp. 691.
- 1598 Zhu, Z., Wu, J., You, Y., Jia, Y., Chen, C., Yao, X., Zheng, W., Xu, X., 2024. A new

1599 ankylosaurid dinosaur from the Upper Cretaceous of Jiangxi Province, southern
1600 China. *Historical Biology*, pp.1-17.

1601

1602

1603 **Supplementary Information**

1604 **Supplementary information 1.** The measurements (in cm and degrees) of all the newly
1605 discovered or re-described trackways and the relatively well-preserved isolated tracks from LXIs
1606 and LXIII tracksites.

1607 **Supplementary information 2.** The photographs and interpretive line drawings of the
1608 ornithopod trackways from LXIN without detailed descriptions.

1609 **Supplementary information 3.** The complete version of ichnofauna composition and their size
1610 distribution of the LXI tracksites. Both track length and width values in this table represent the
1611 mean value of the trackway or the sole isolated track from a certain type, which could could
1612 better represent the size of a single trackmaker.

1613

1614

Figure 1

Location of the Longxiang sites and the distribution of Longxiang tracksites (modified after from Niu and Xing, 2023).

The photograph of Longxiang tracksites distribution is modified basing on Google Earth satellite image (Nov 11, 2020) in Fujian Province, southwestern China.

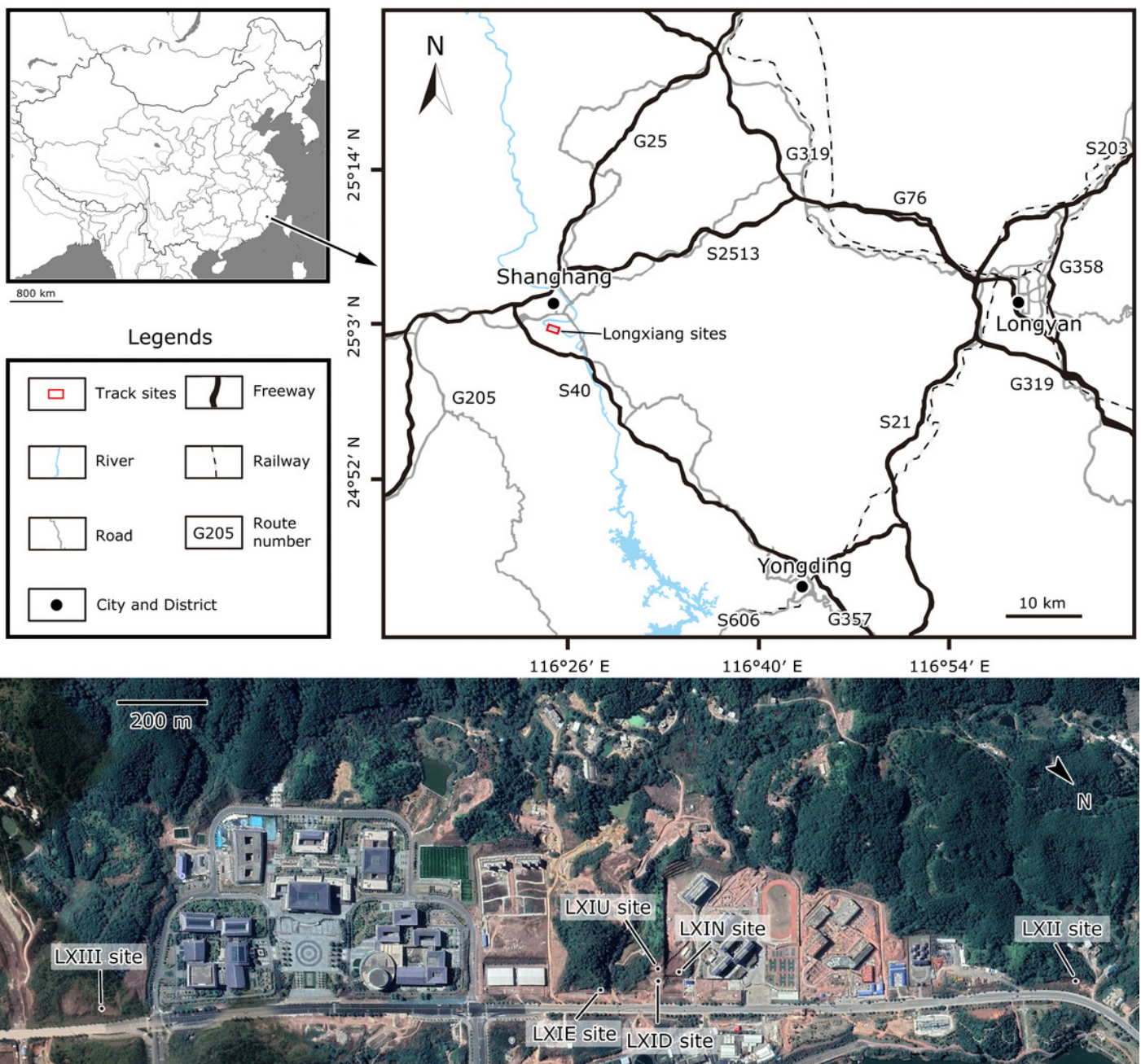


Figure 2

Stratigraphic section of the Cretaceous Shaxian Formation from Renhuai Basin with the position of the Longxiang tracklayers.

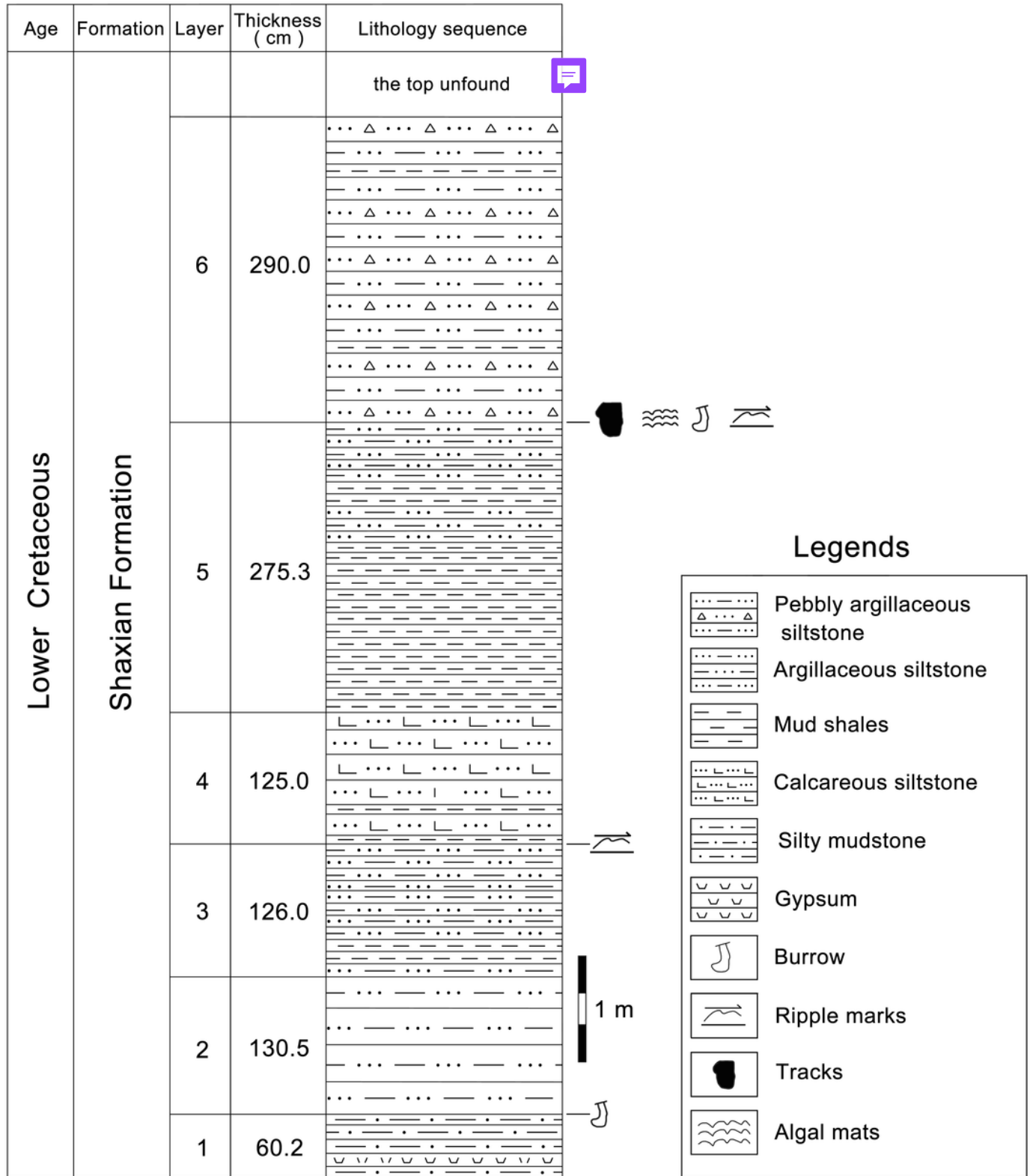


Figure 3

Interpretive line drawing and trackway orientation rose diagrams of the Longxiang IU (LXIU) site.

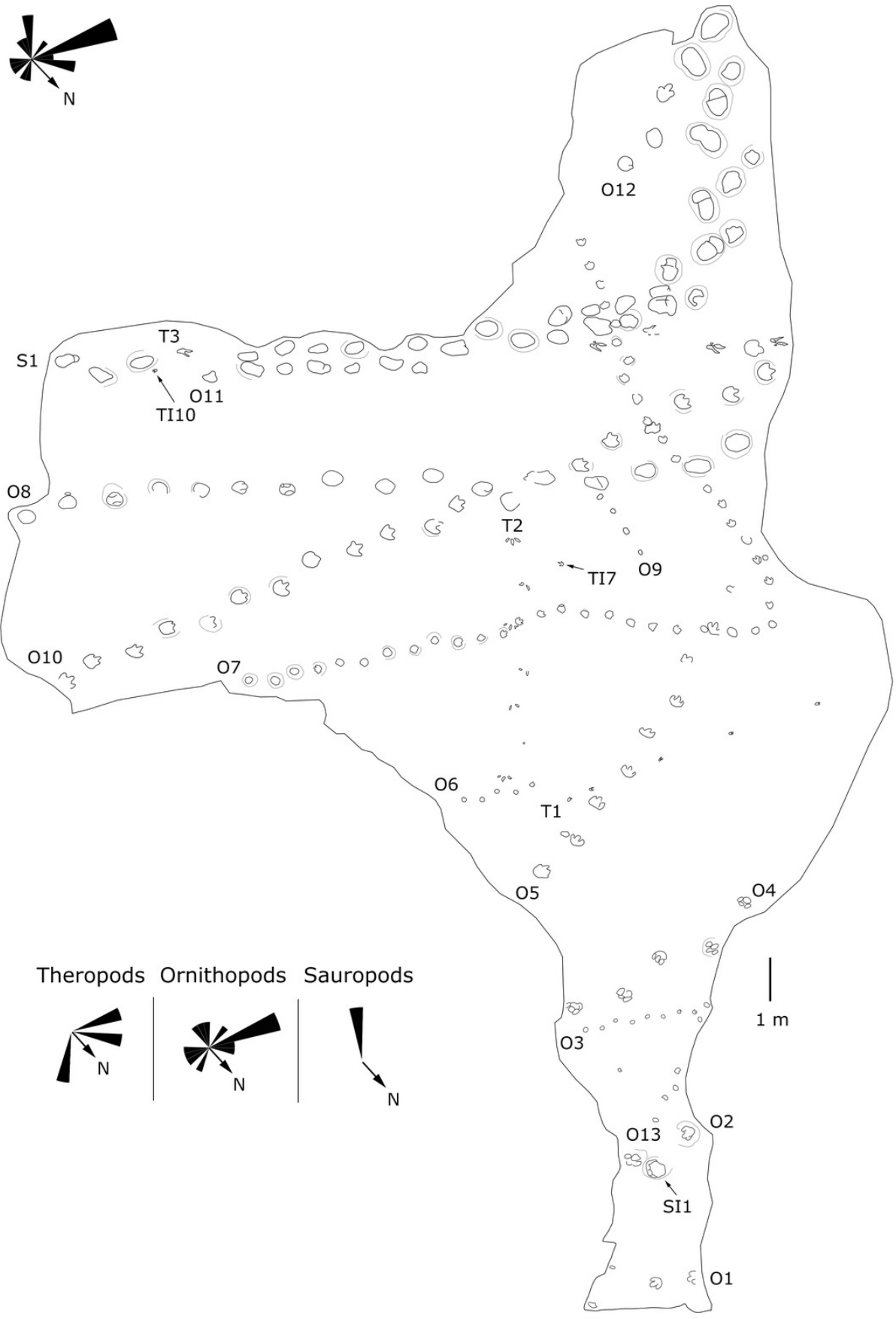


Figure 4

Interpretive line drawing and trackway orientation rose diagrams of the Longxiang ID (LXID) site.

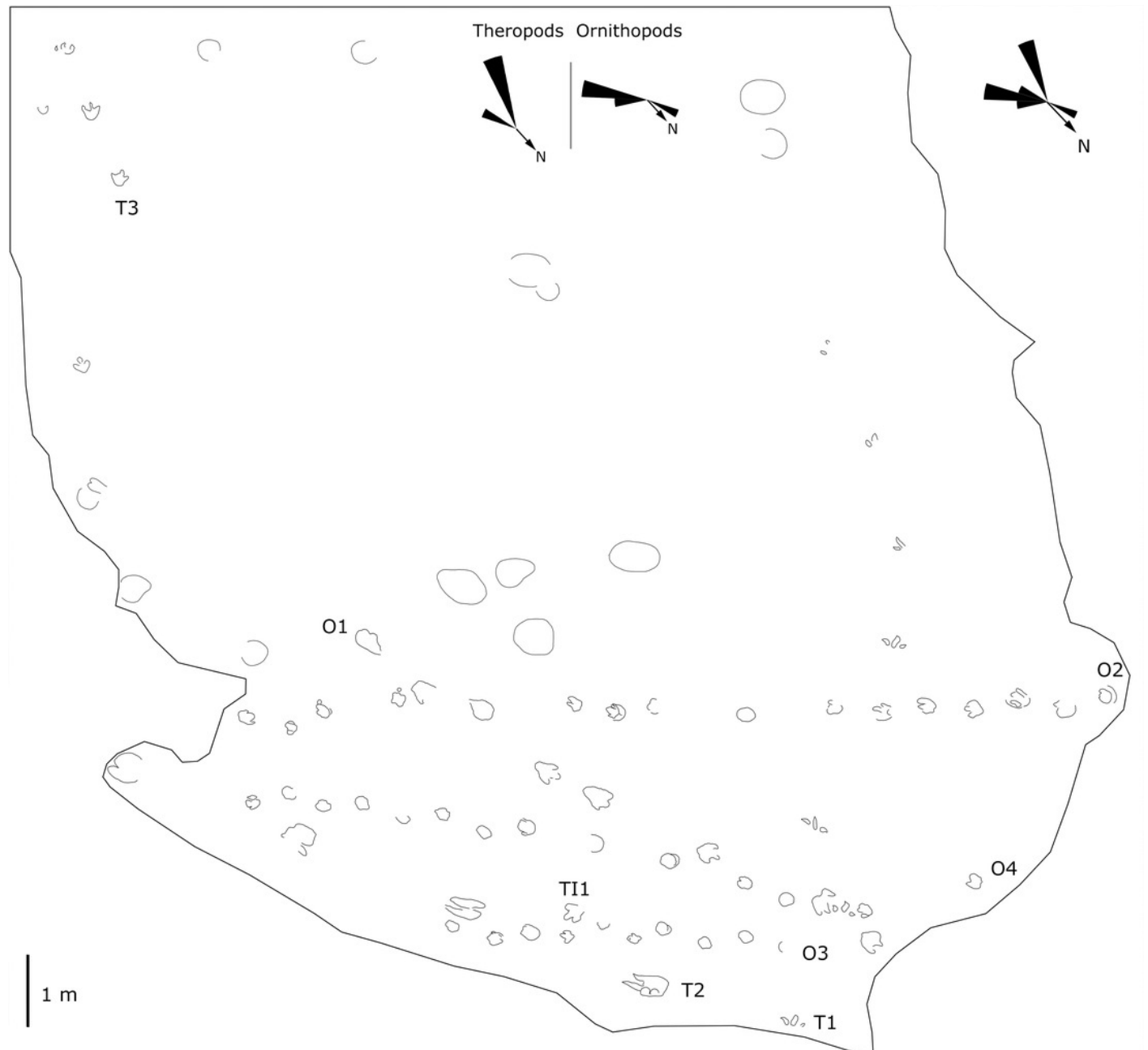


Figure 5

Interpretive line drawing and trackway orientation rose diagrams of the Longxiang IN (LXIN) site.



Figure 6

Photograph and interpretive line drawing of the slab (YLSNHM07318) from Longxiang IE (LXIE) site.

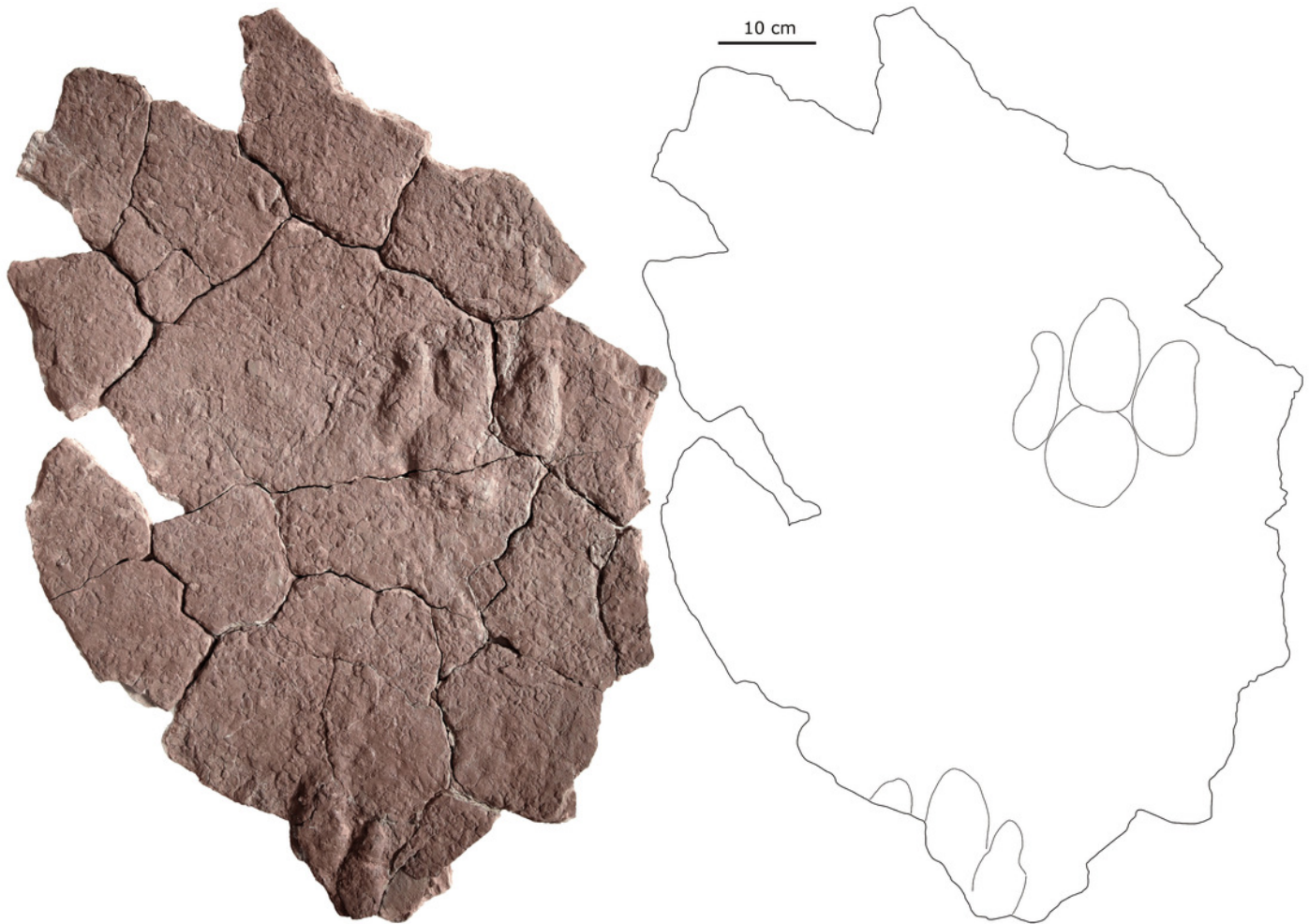


Figure 7

Photograph and interpretive line drawing of the dinosaur tracks from Longxiang II (LXII) site.

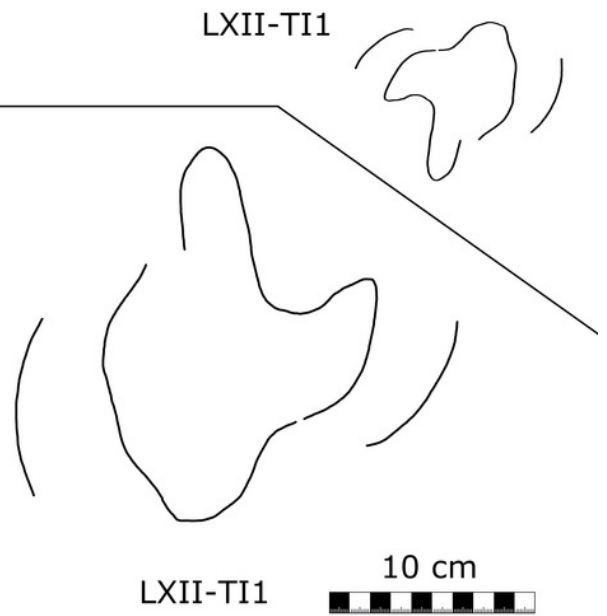
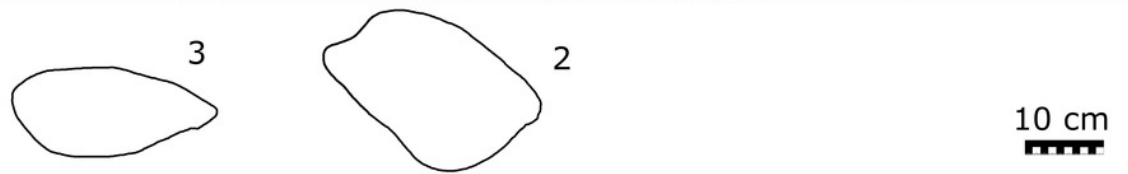


Figure 8

Interpretive line drawing of the Longxiang III (LXIII) site.



Figure 9

Photograph and interpretive line drawing of tracks from sauropod trackway LXIU-S1.

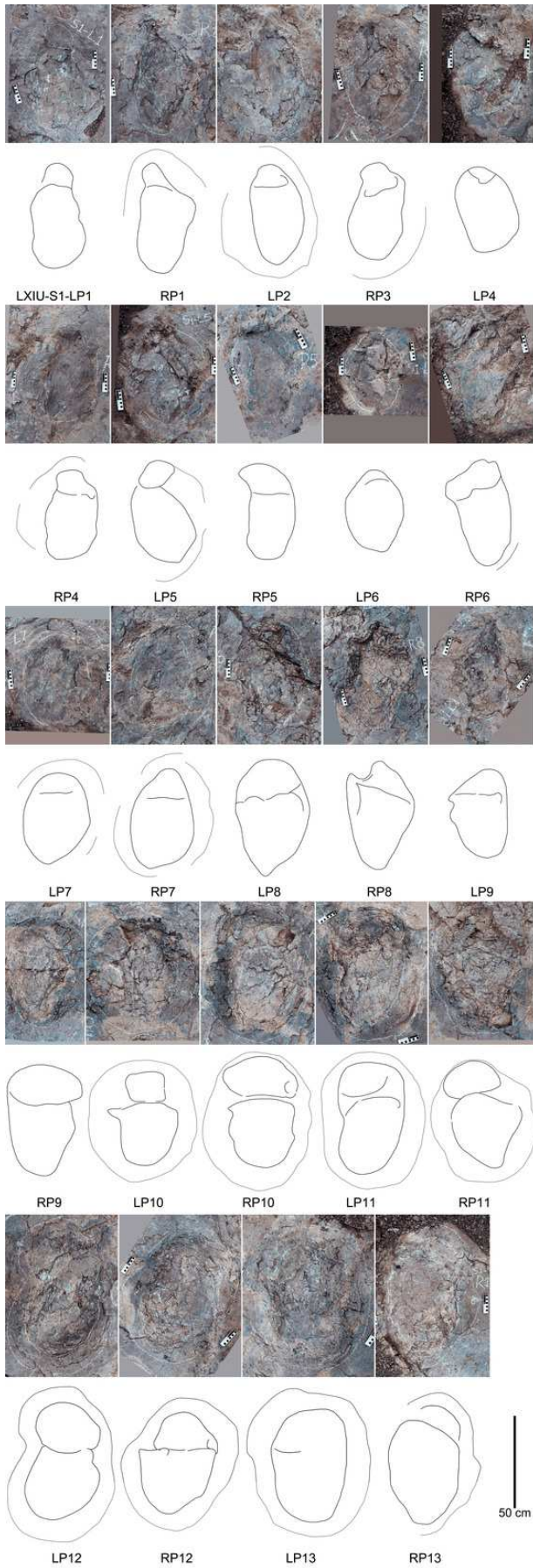
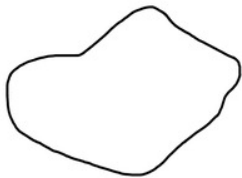
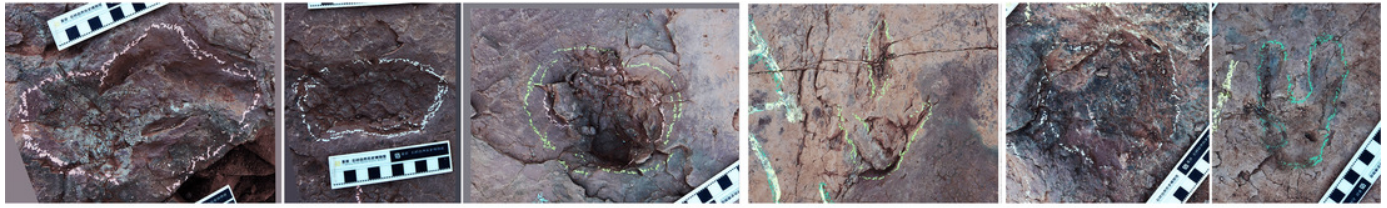


Figure 10

Photograph and interpretive line drawing of the isolated dinosaur tracks from LXIU site.



LXIU-TI0



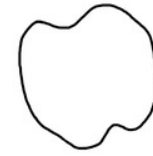
TI1



TI5



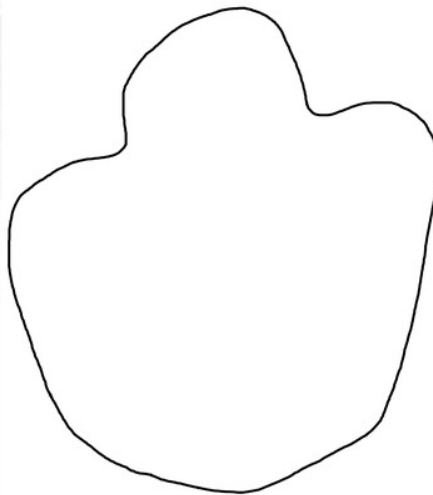
TI7



TI9

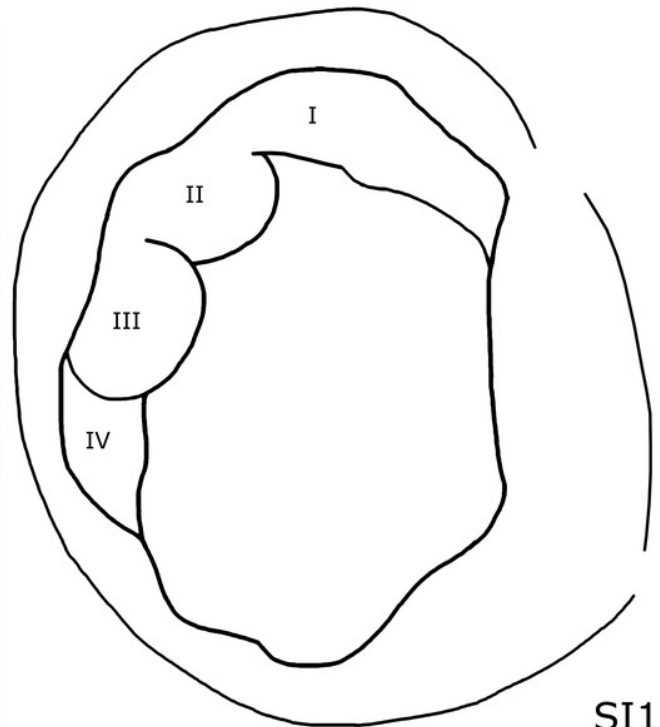
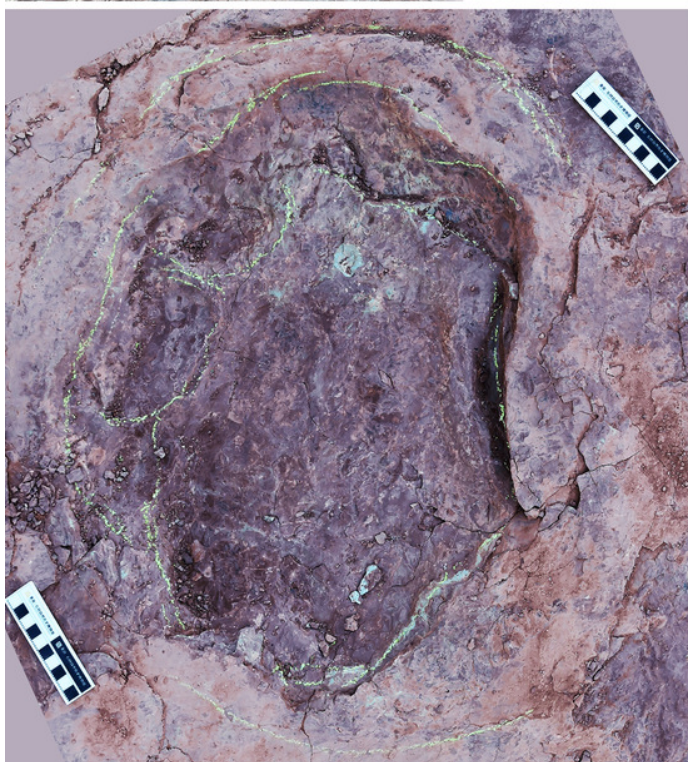


TI10



TI8

10 cm



SI1

Figure 11

Photograph and interpretive line drawing of sauropod trackway LXIN-S1.

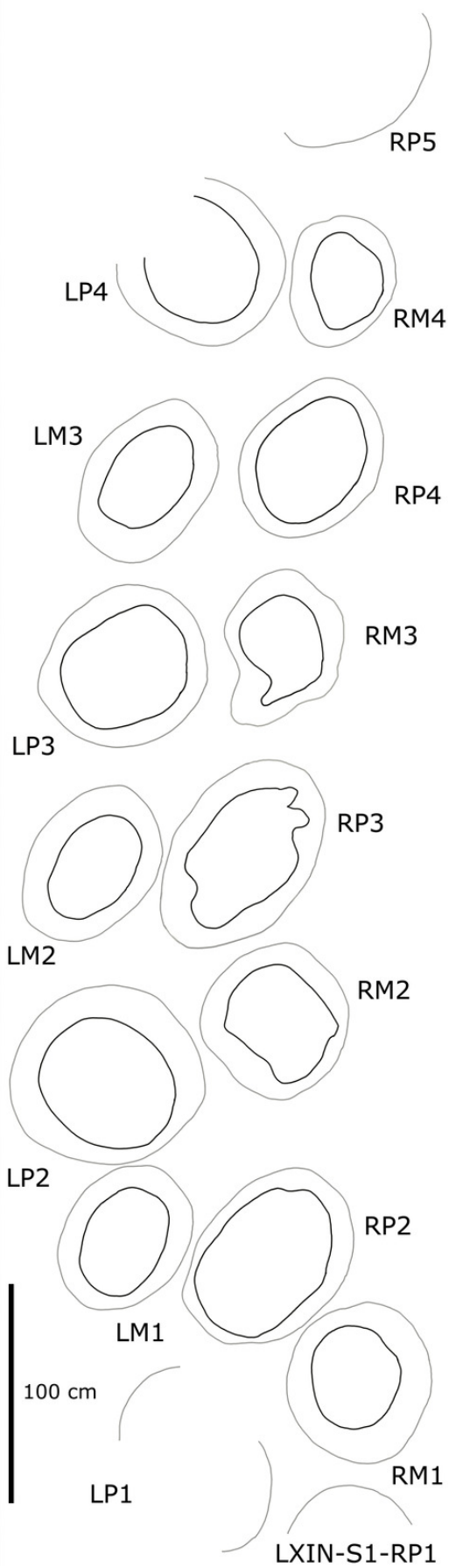
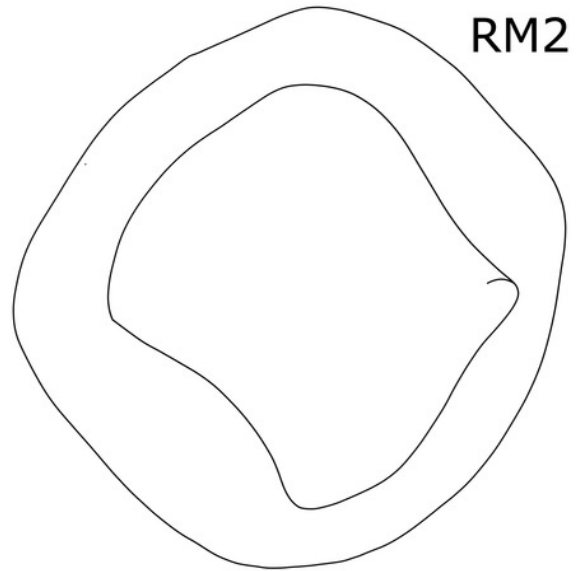


Figure 12

Close-in photographs and interpretive line drawings of sauropod tracks LXIN-S1-2.



RM2

LXIN-S1-RP2

50 cm

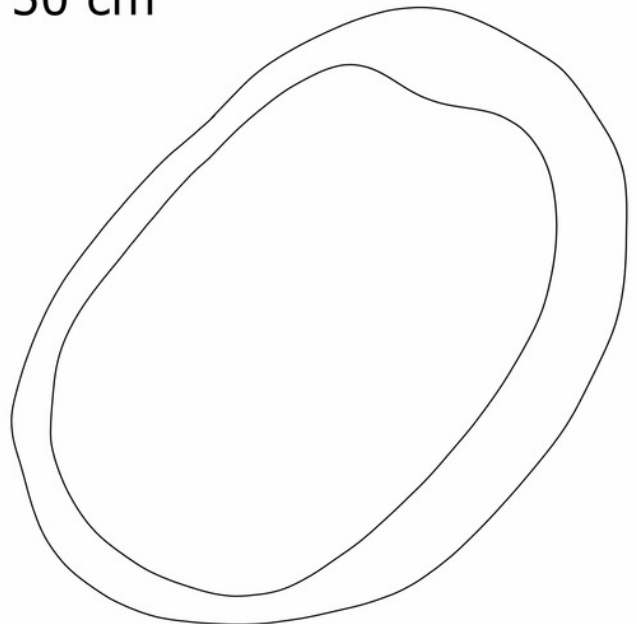


Figure 13

Photograph and interpretive line drawing of the isolated dinosaur tracks from LXIII.

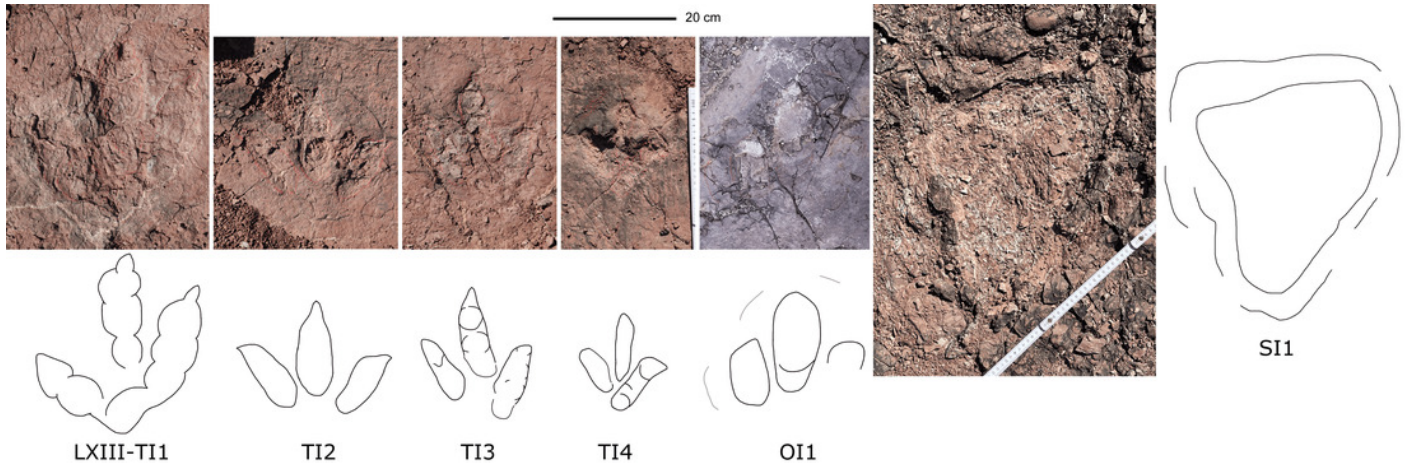


Figure 14

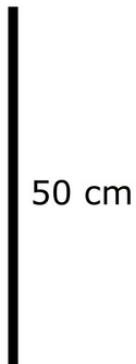
Photograph and interpretive line drawing of tridactyl theropod trackway LXIN-T1.



L2



R1



LXIN-T1-L1

Figure 15

Photograph and interpretive line drawing of tridactyl theropod trackway LXIN-T3.

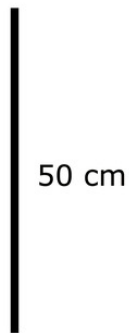


Figure 16

Photograph and interpretive line drawing of tridactyl theropod trackway LXIN-T5.

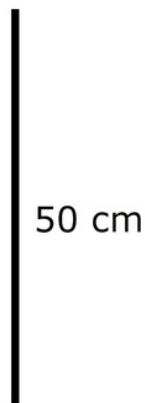
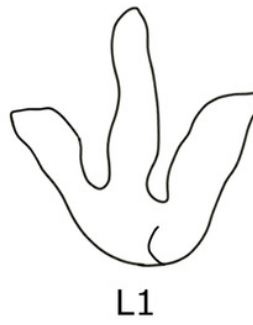
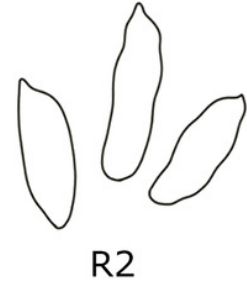


Figure 17

Close-in photographs and interpretive line drawings of tridactyl theropod tracks from LXIN site.

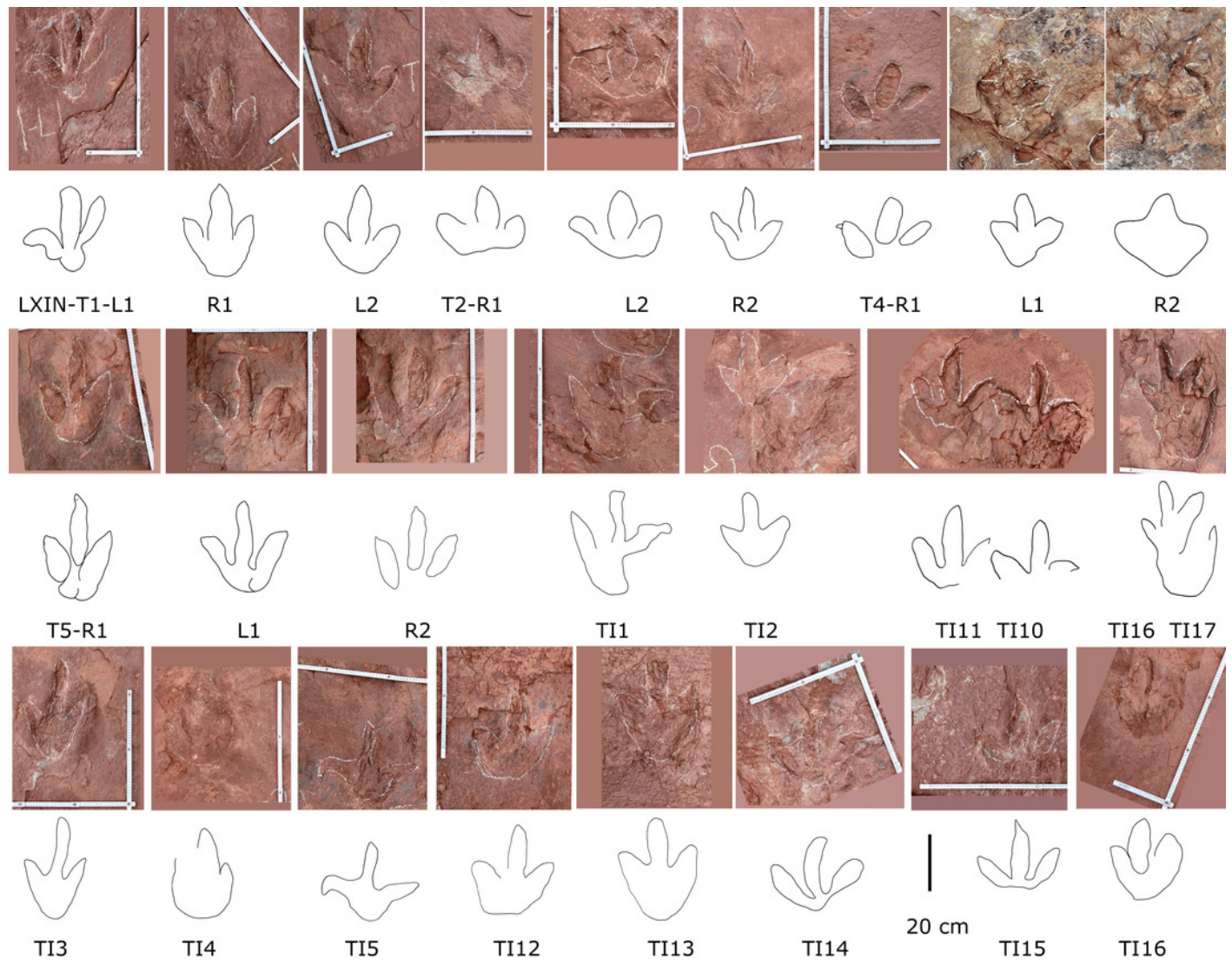


Figure 18

Photograph and interpretive line drawing of tridactyl theropod trackway LXIN-T2.





R2



L2



R1

50 cm



LXIN-T2-L1

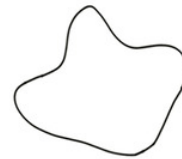
Figure 19

Photograph and interpretive line drawing of tridactyl theropod trackway LXIN-T4.

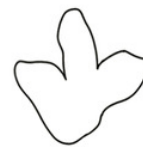




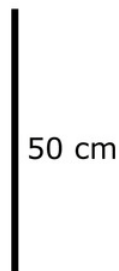
L2



R2



L1



LXIN-T4-R1

Figure 20

Close-in photographs and interpretive line drawings of tridactyl theropod tracks from LXID site.

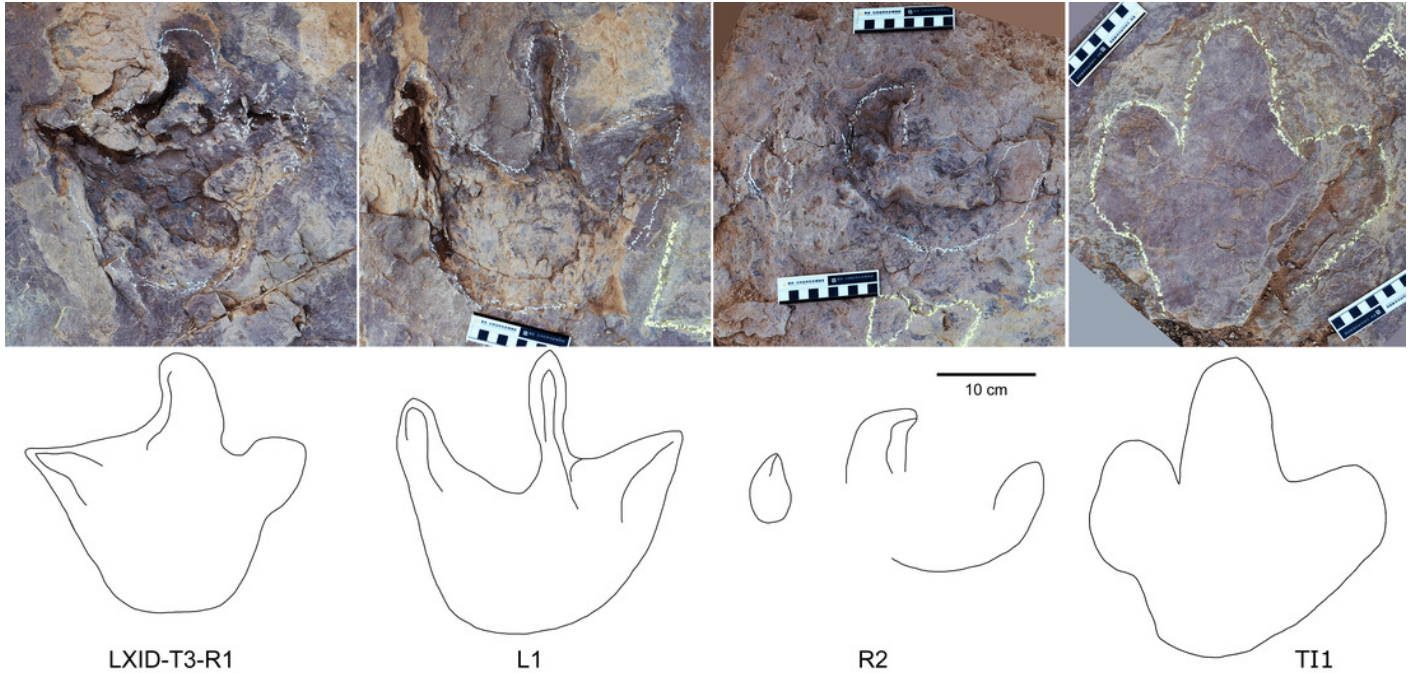


Figure 21

Close-in photographs and interpretive line drawings of tridactyl theropod tracks from trackway LXIU-T2.

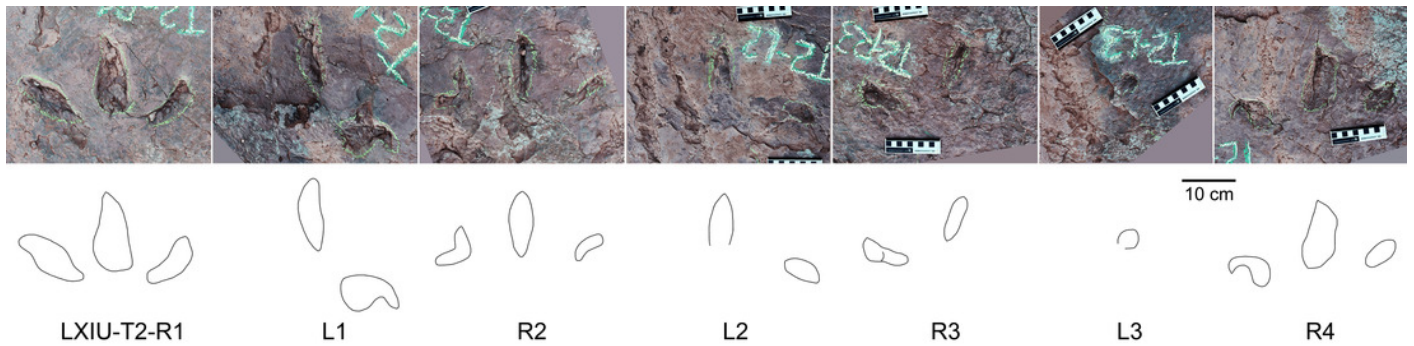


Figure 22

Close-in photographs and interpretive line drawings of tridactyl theropod tracks from trackway LXID-T1.

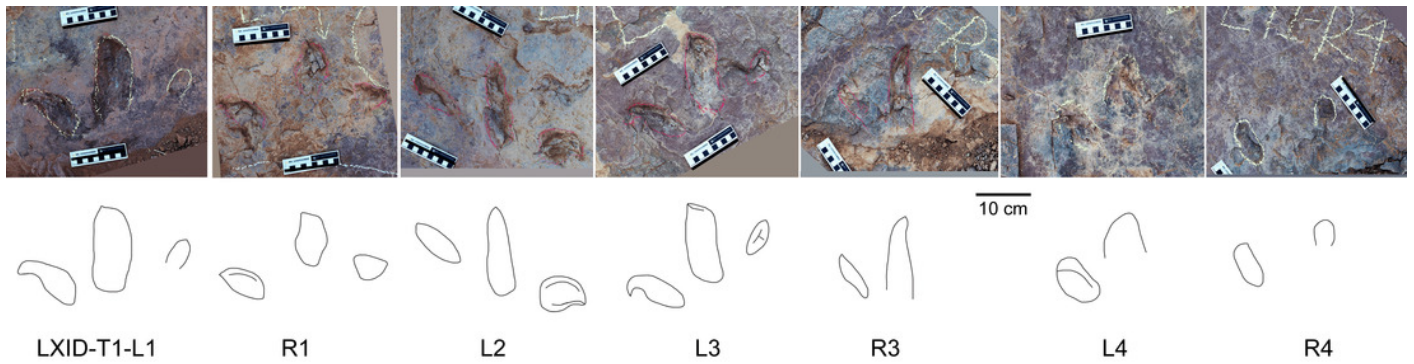


Figure 23

Close-in photographs, 3D models, 3D depth maps and interpretive line drawings of theropod and ornithopod tracks in trackways from LXIU site.

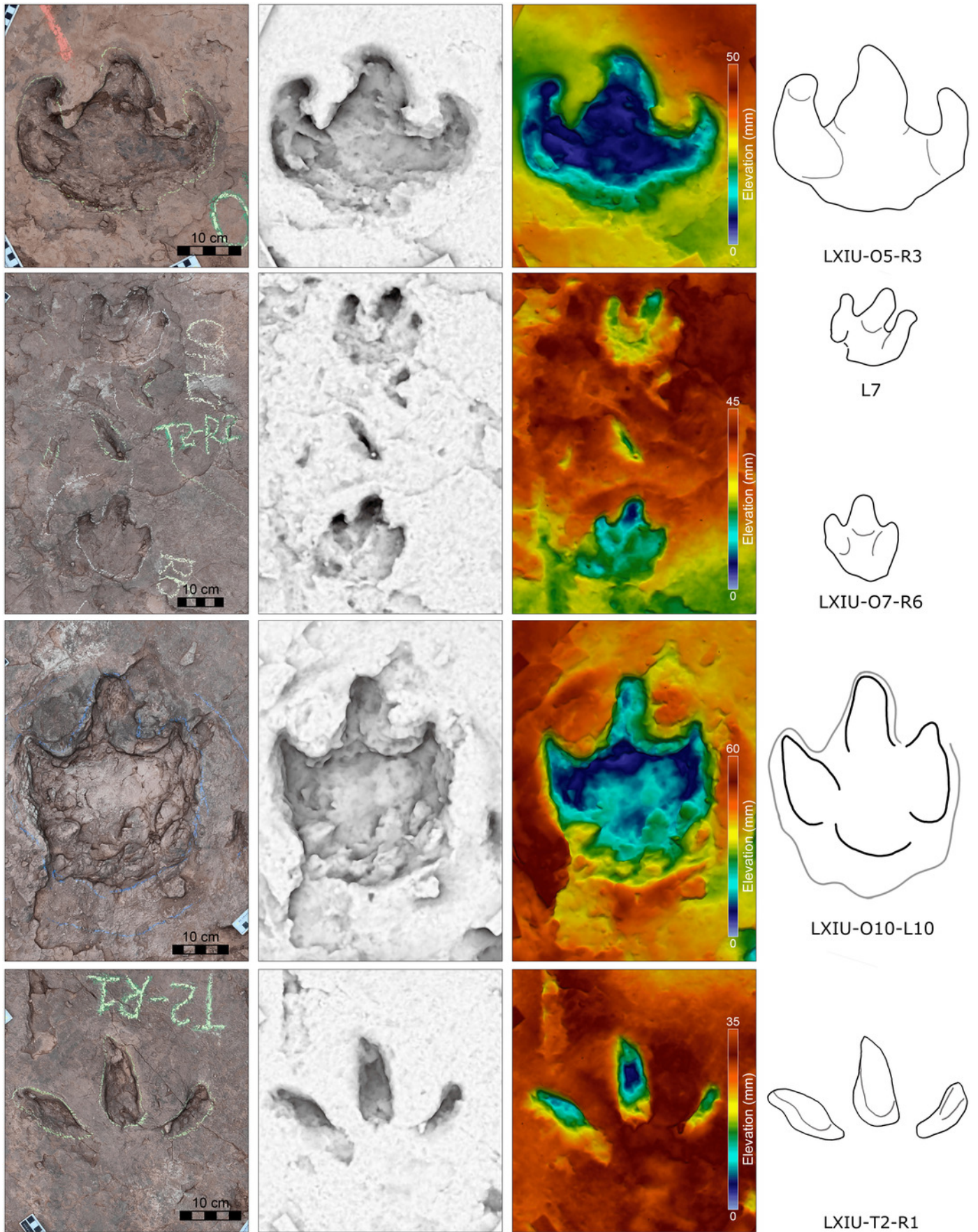


Figure 24

Close-in photographs and interpretive line drawings of *Velociraptorichnus* from trackway LXIU-T1.

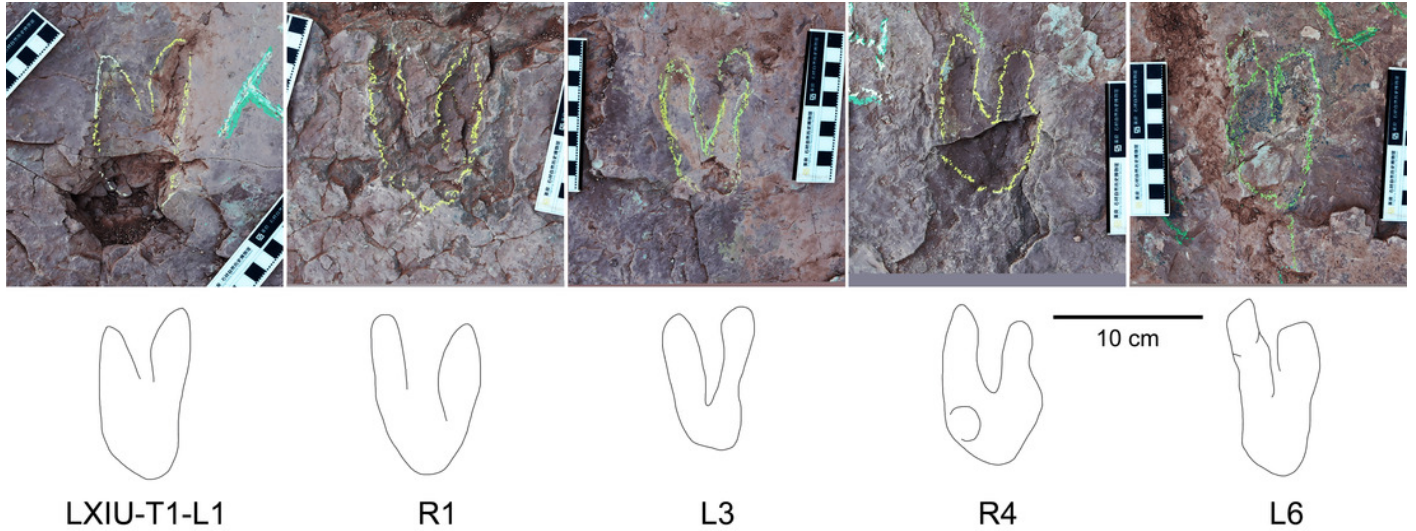


Figure 25

Close-in photographs and interpretive line drawings of *Fujianipus* from trackway LXIU-T3.

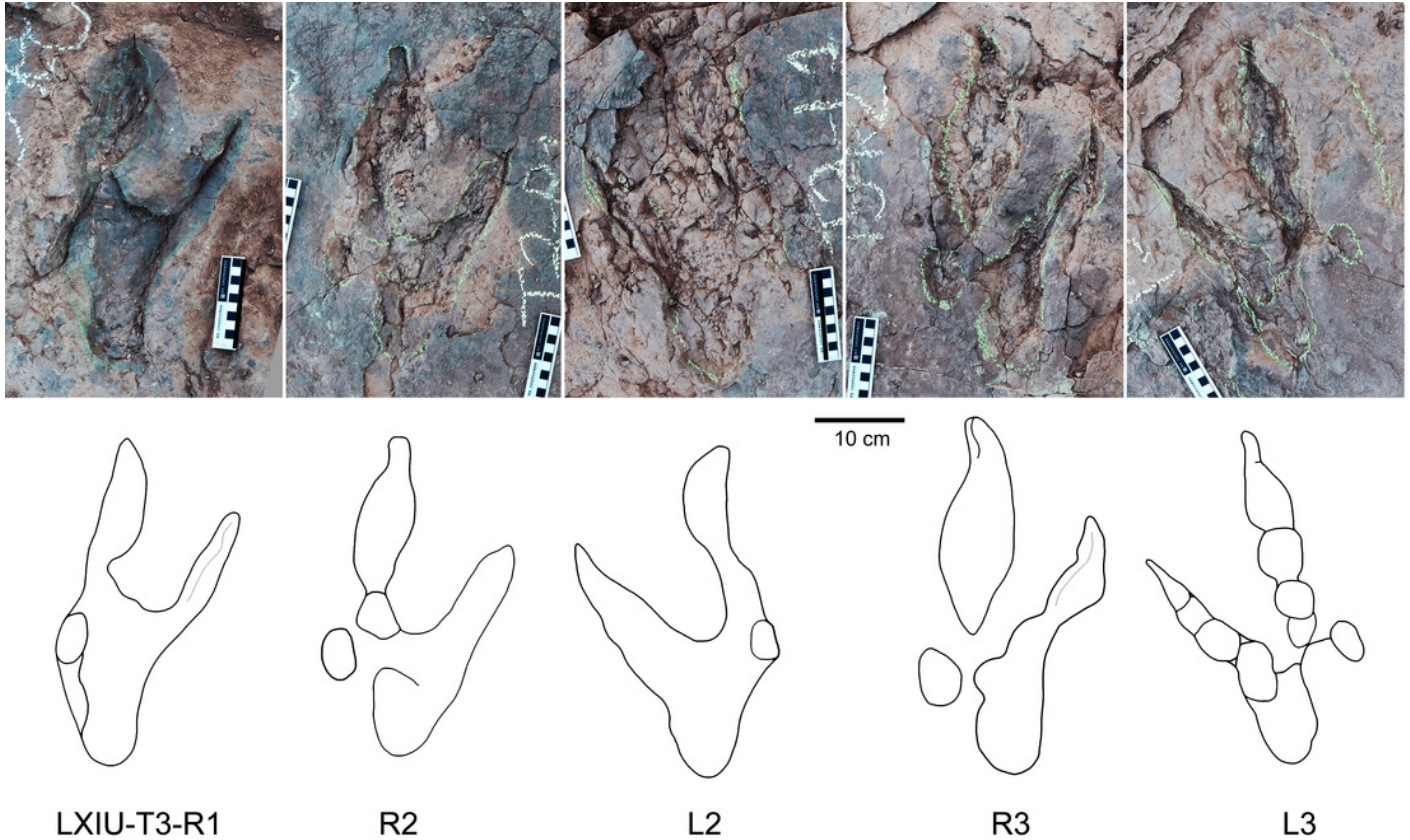


Figure 26

Close-in photographs and interpretive line drawings of possible didactyl theropod tracks from trackway LXID-T2.

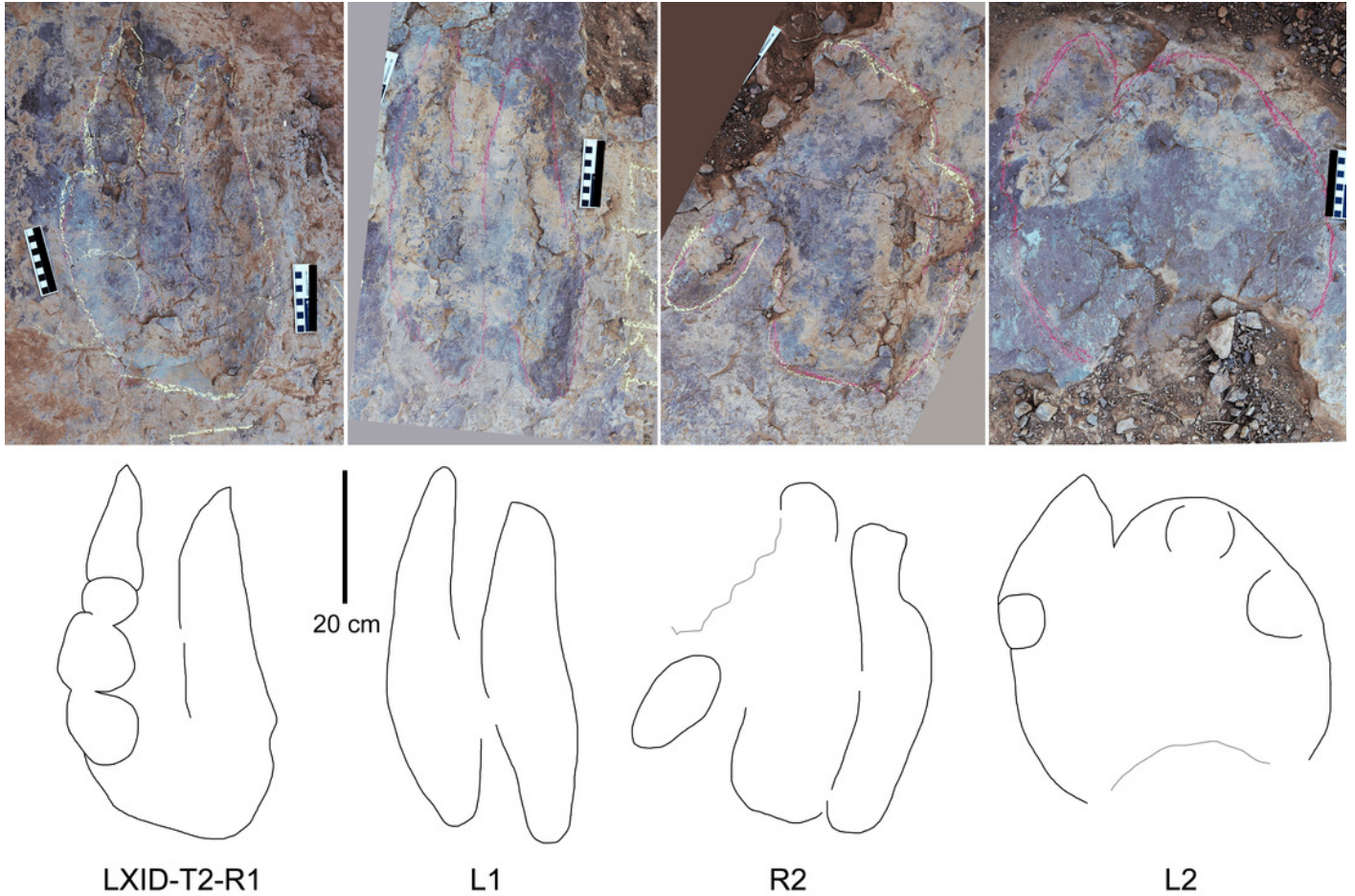


Figure 27

Box plot of ornithopod tracks size distribution from all the LXI tracksites.

The ornithopod track size is represented by the track length (in cm), for no anomalous length/width ratios are observed.

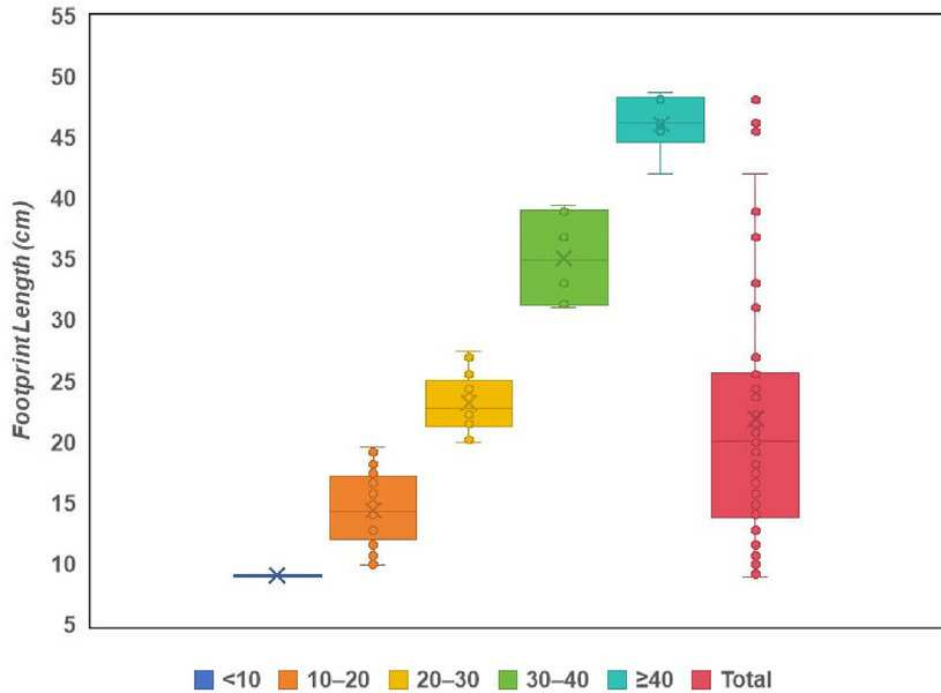


Figure 28

Close-in photographs and interpretive line drawings of ornithopod tracks from trackway LXID-O1.

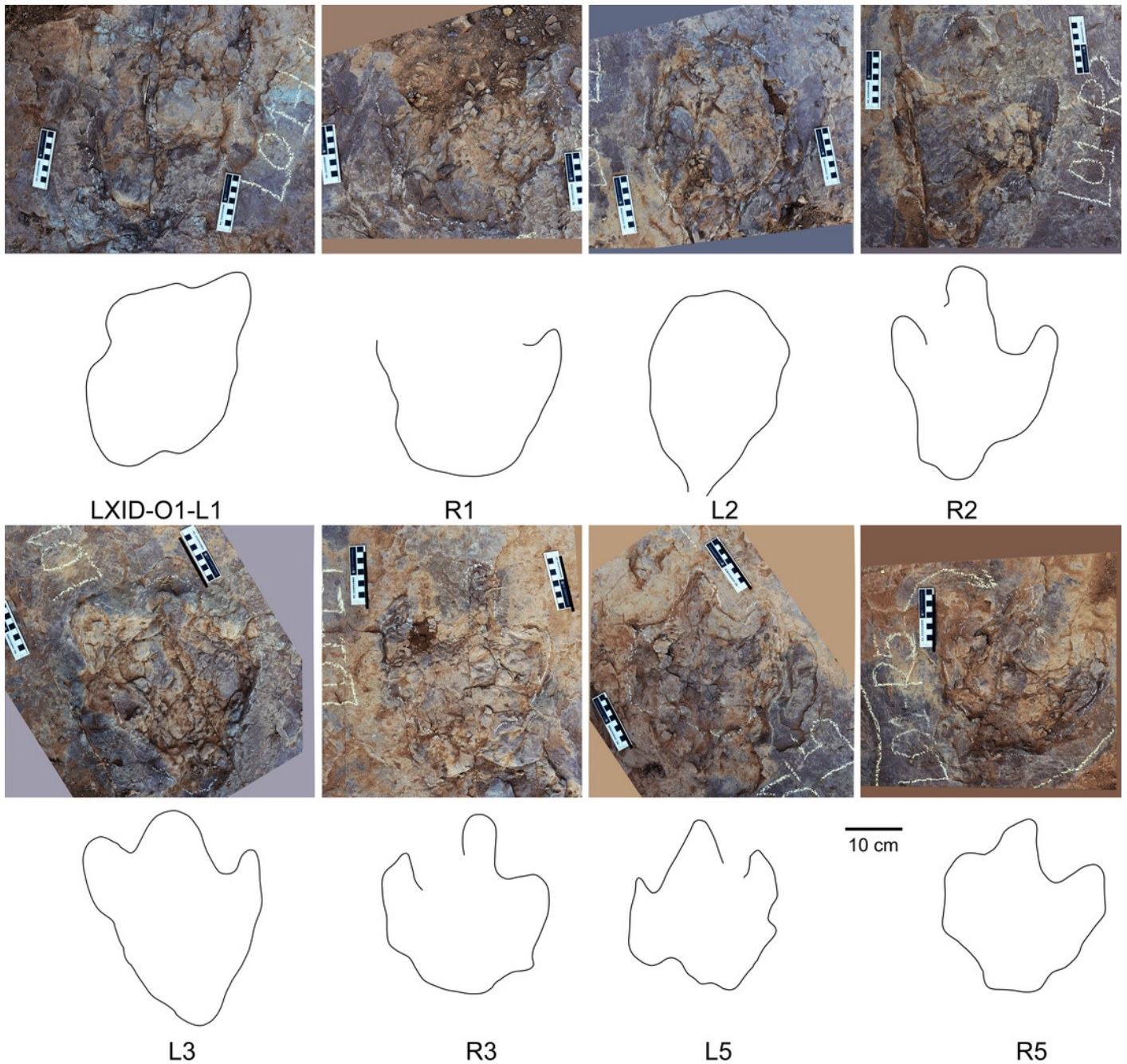


Figure 29

Close-in photographs and interpretive line drawings of ornithopod tracks from trackway LXID-02.

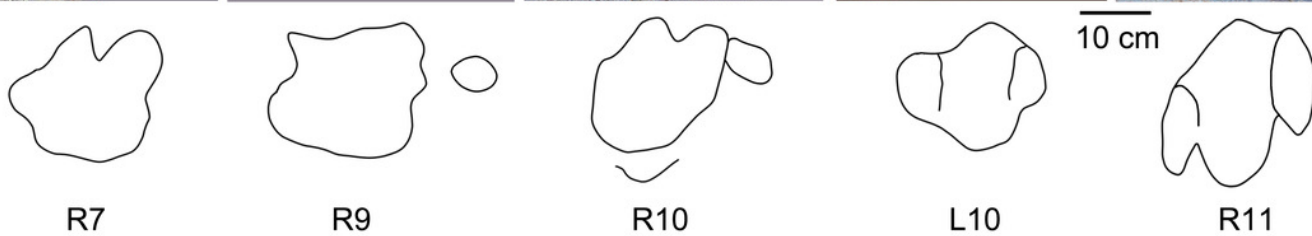
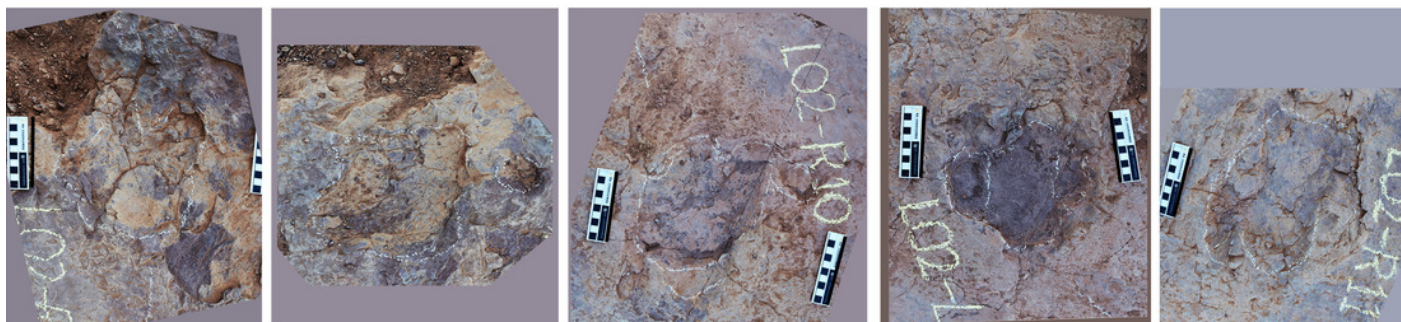
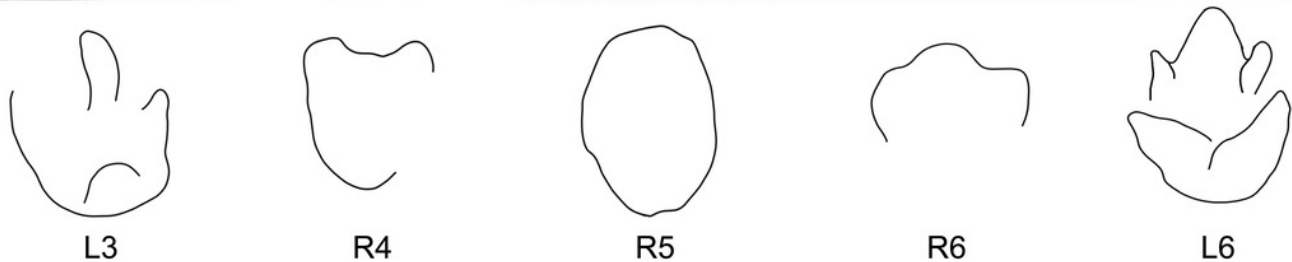
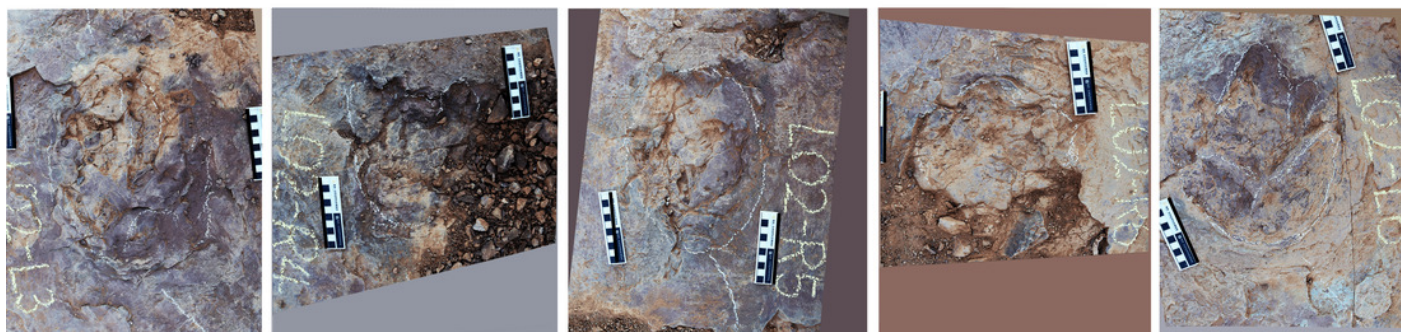
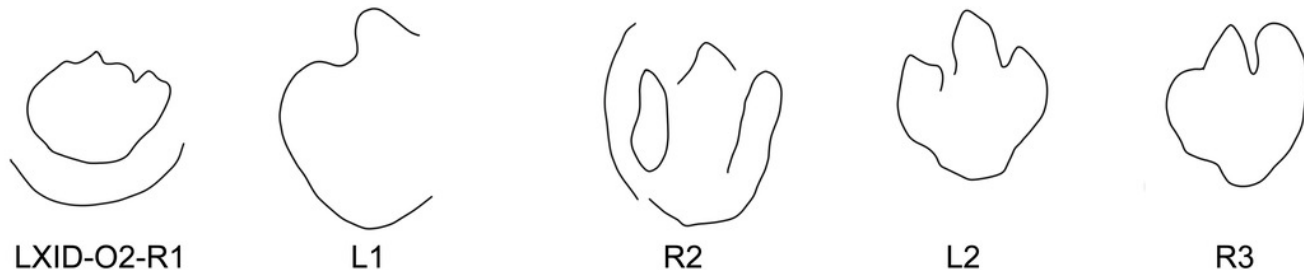
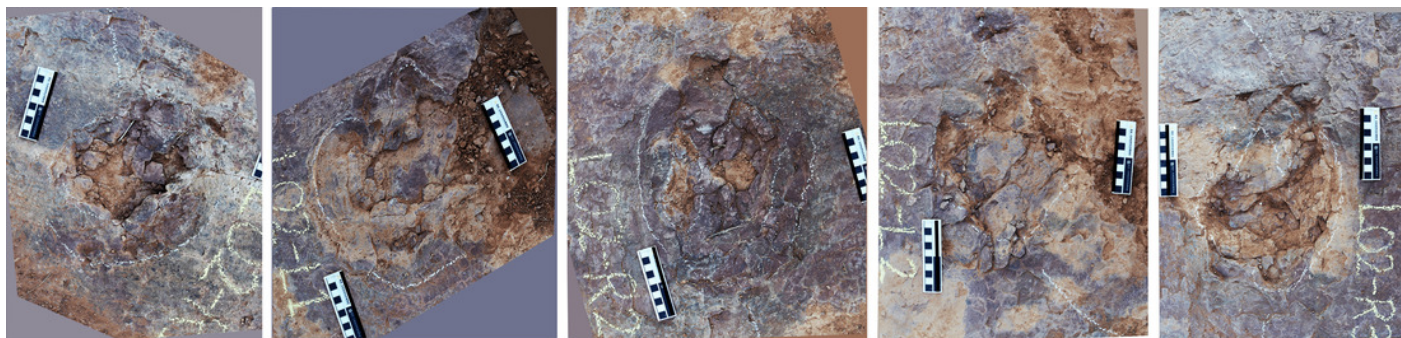


Figure 30

Close-in photographs and interpretive line drawings of ornithopod tracks from trackway LXID-O3.

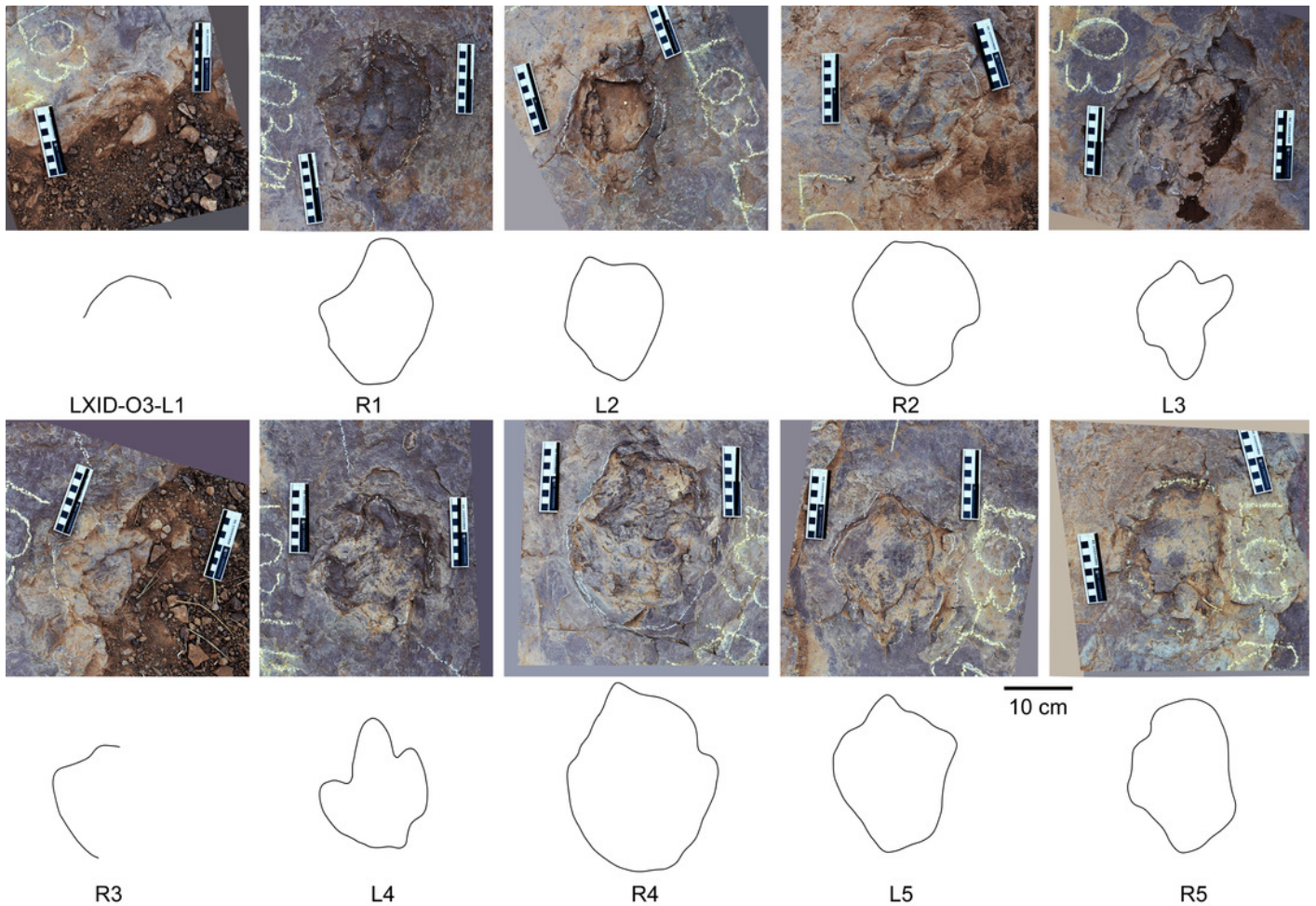


Figure 31

Close-in photographs and interpretive line drawings of ornithopod tracks from trackway LXID-O4.

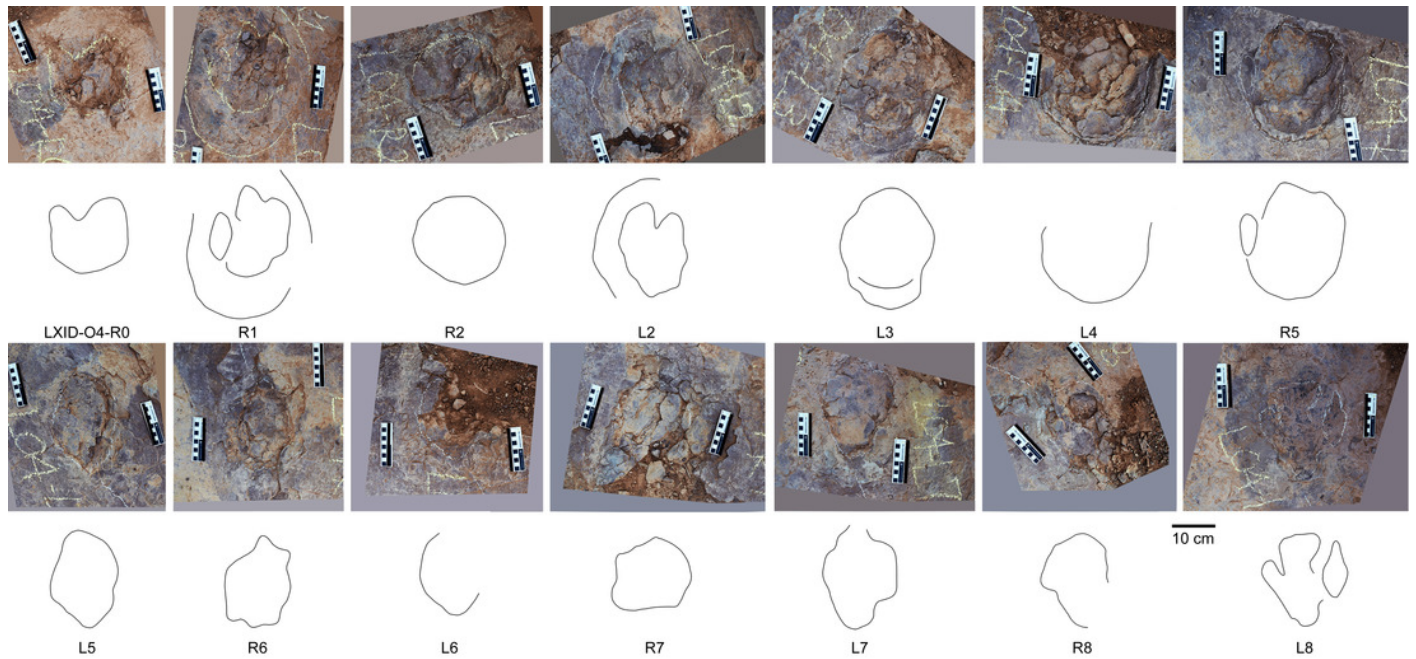


Figure 32

Close-in photographs and interpretive line drawings of ornithopod tracks from trackway LXIU-O3.

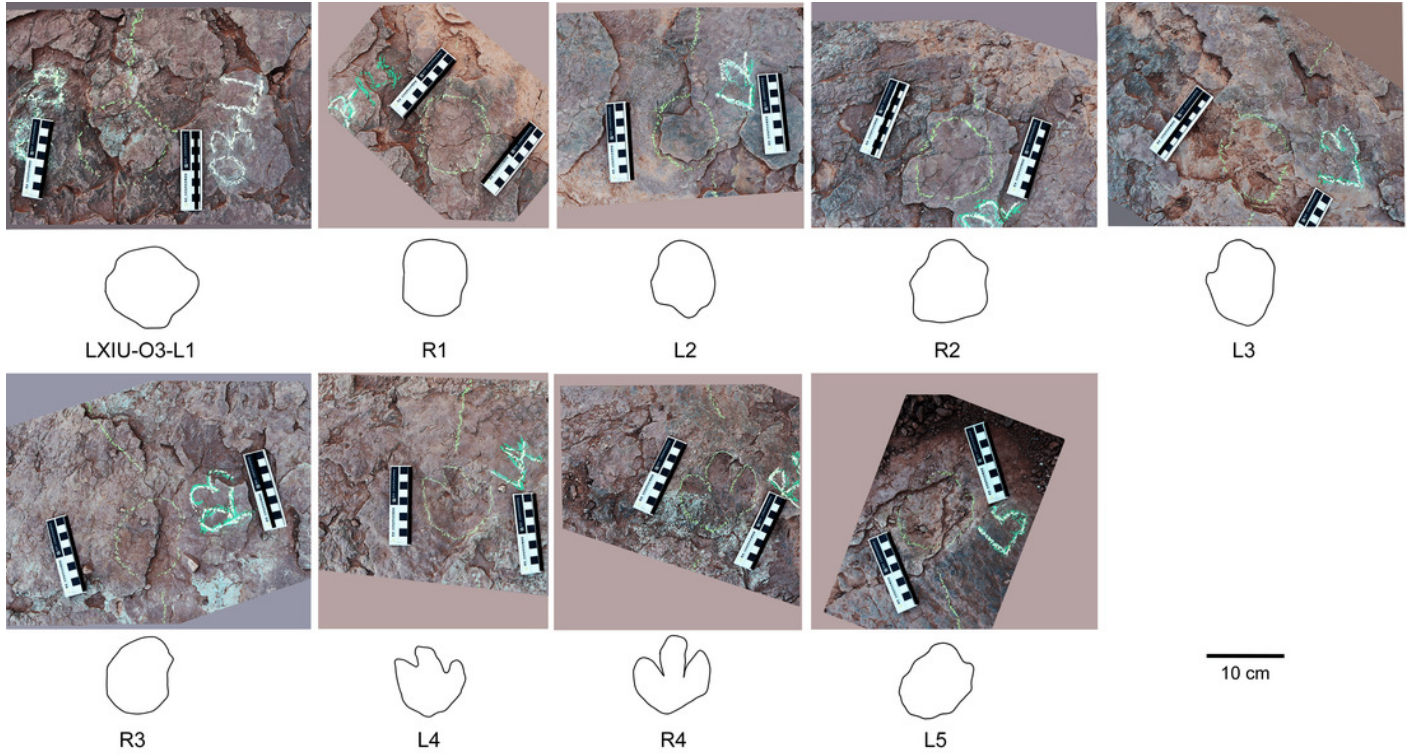


Figure 33

Close-in photographs and interpretive line drawings of ornithopod tracks from trackway LXIU-O6.

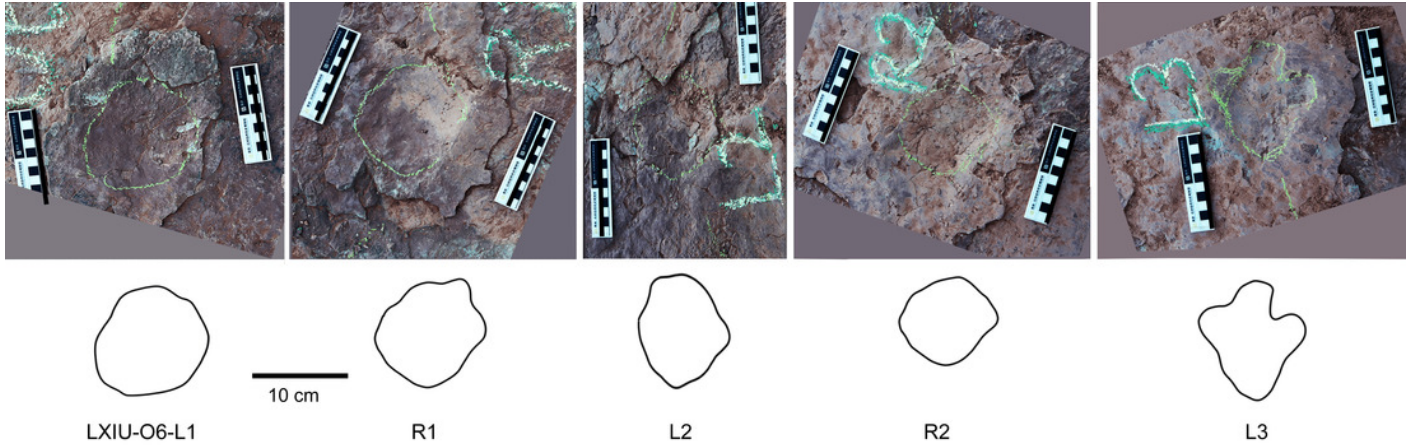


Figure 34

Close-in photographs and interpretive line drawings of ornithopod tracks from trackway LXIU-09.

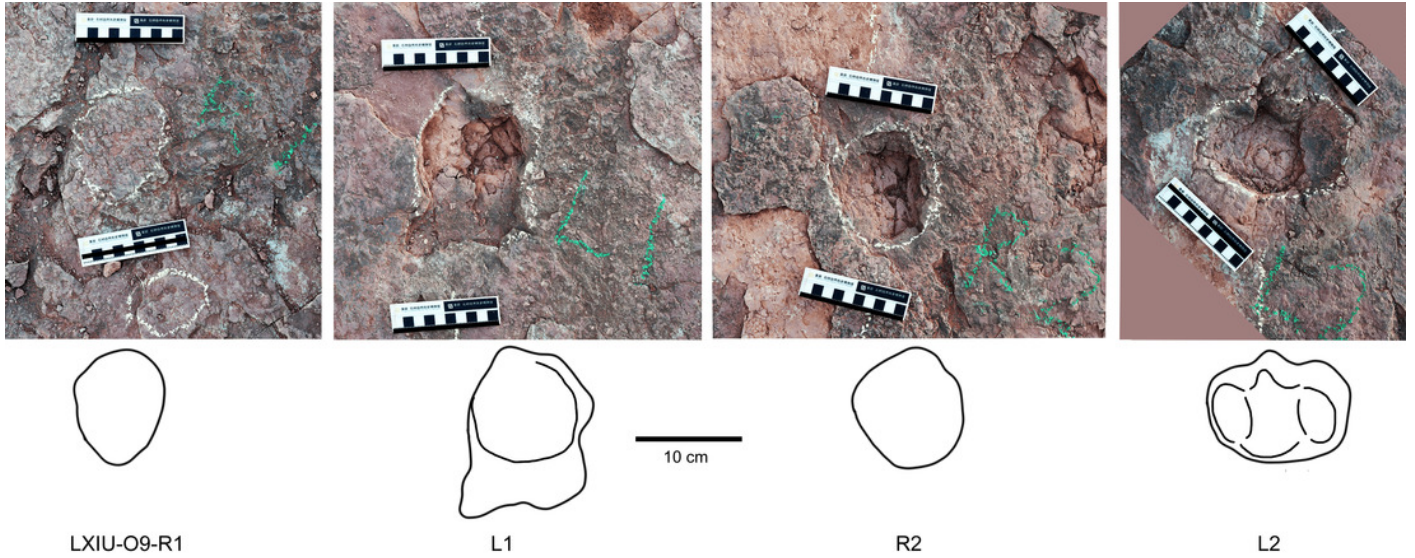


Figure 35

Close-in photographs and interpretive line drawings of ornithopod tracks from trackway LXIU-013.

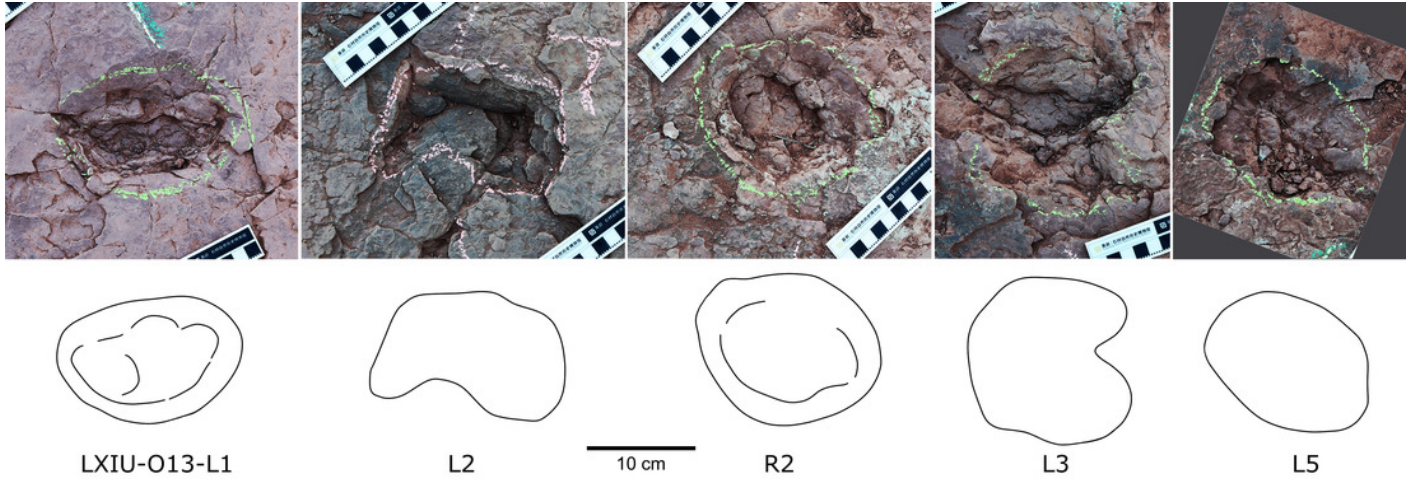


Figure 36

Close-in photographs and interpretive line drawings of ornithopod tracks from trackway LXIU-01.

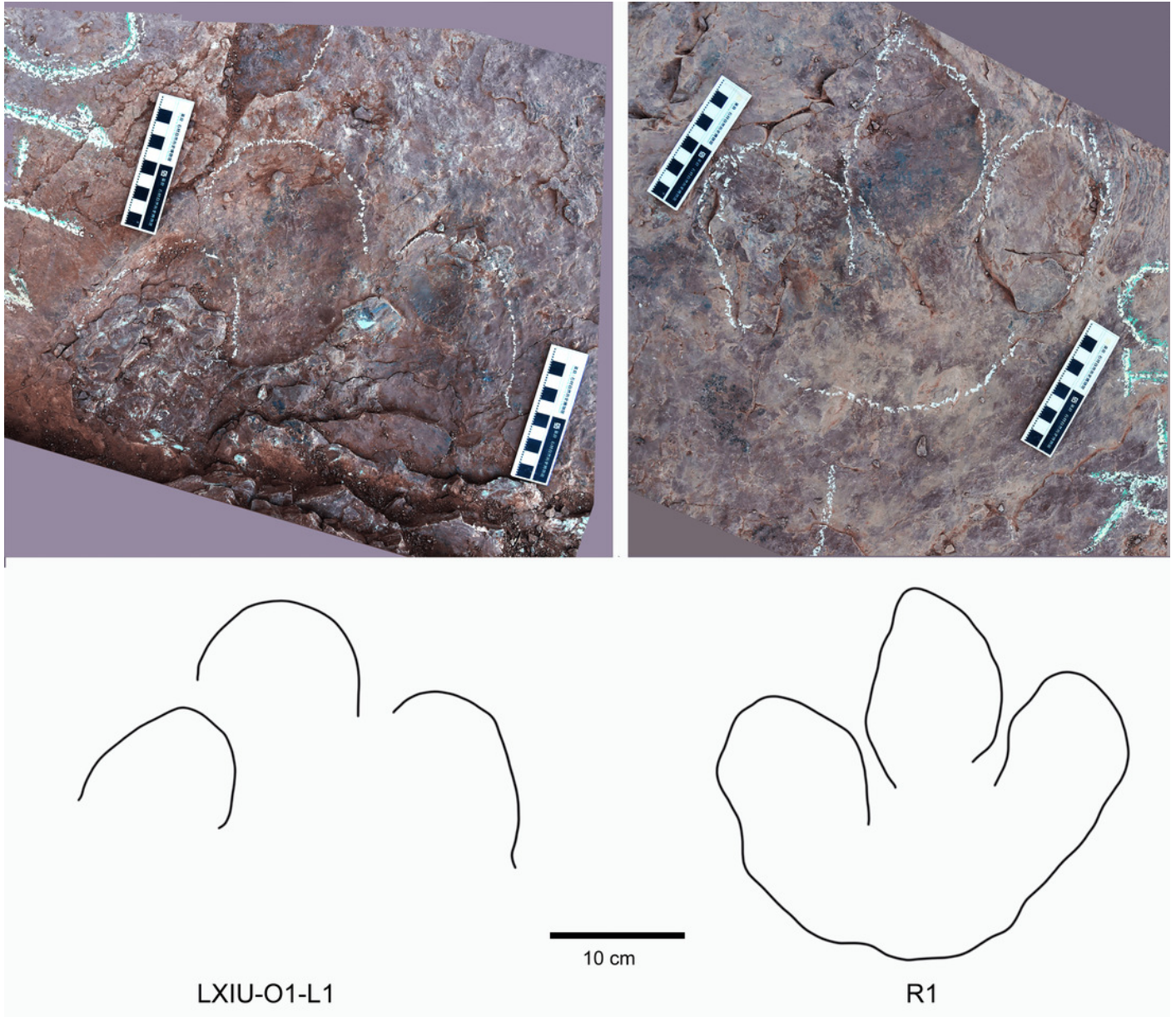


Figure 37

Close-in photographs and interpretive line drawings of ornithopod tracks from trackway LXIU-04.

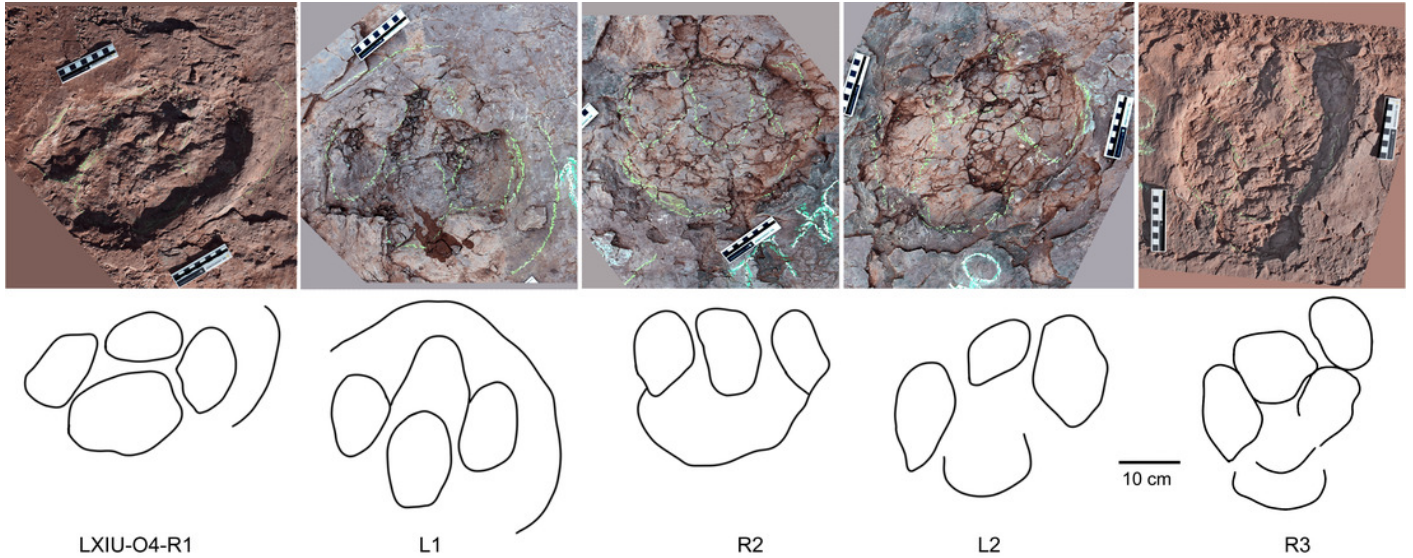


Figure 38

Close-in photographs and interpretive line drawings of ornithopod tracks from trackway LXIU-05.

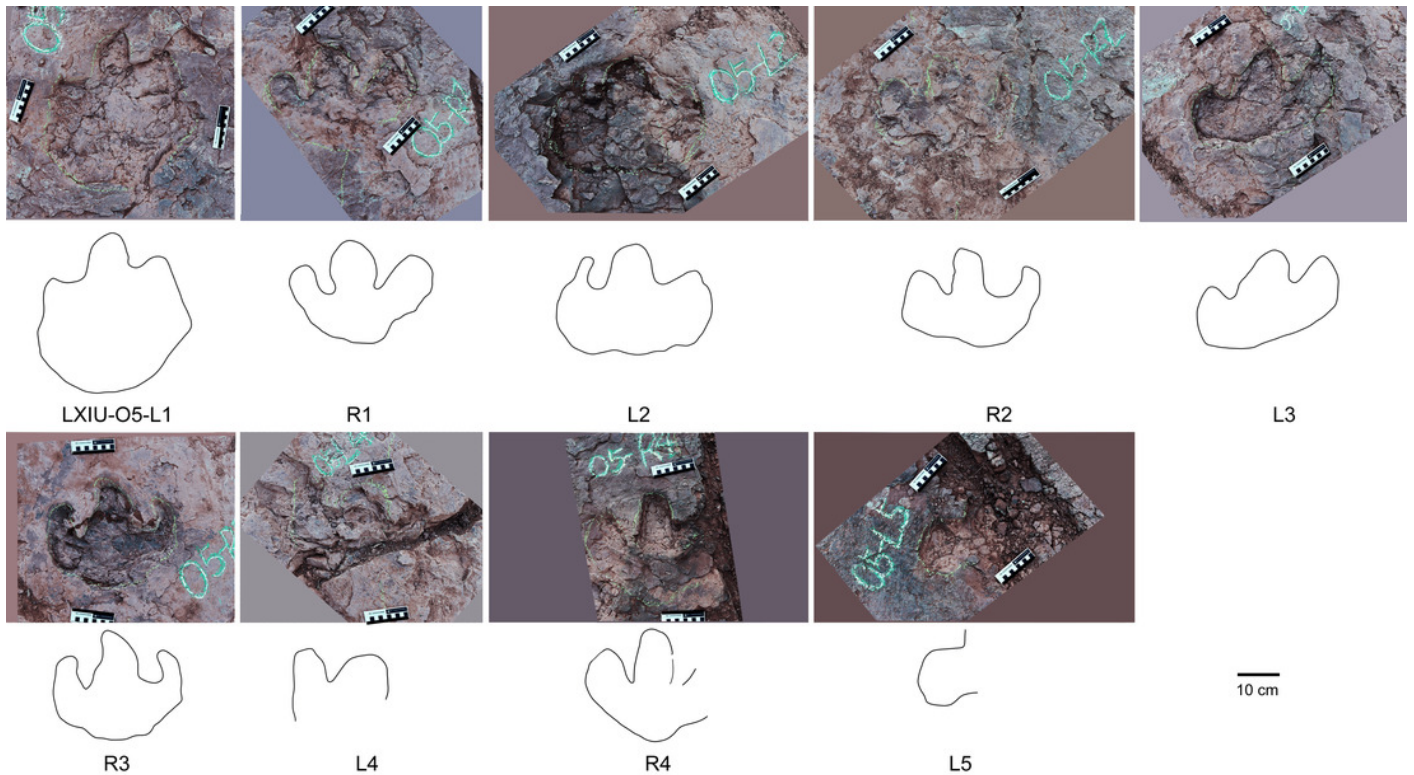


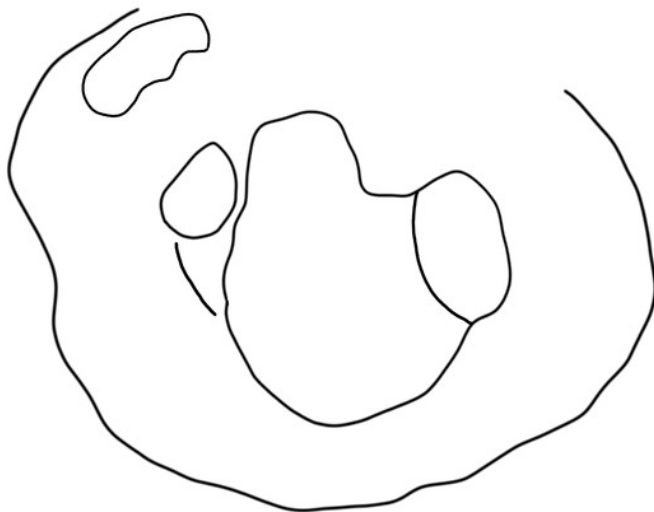
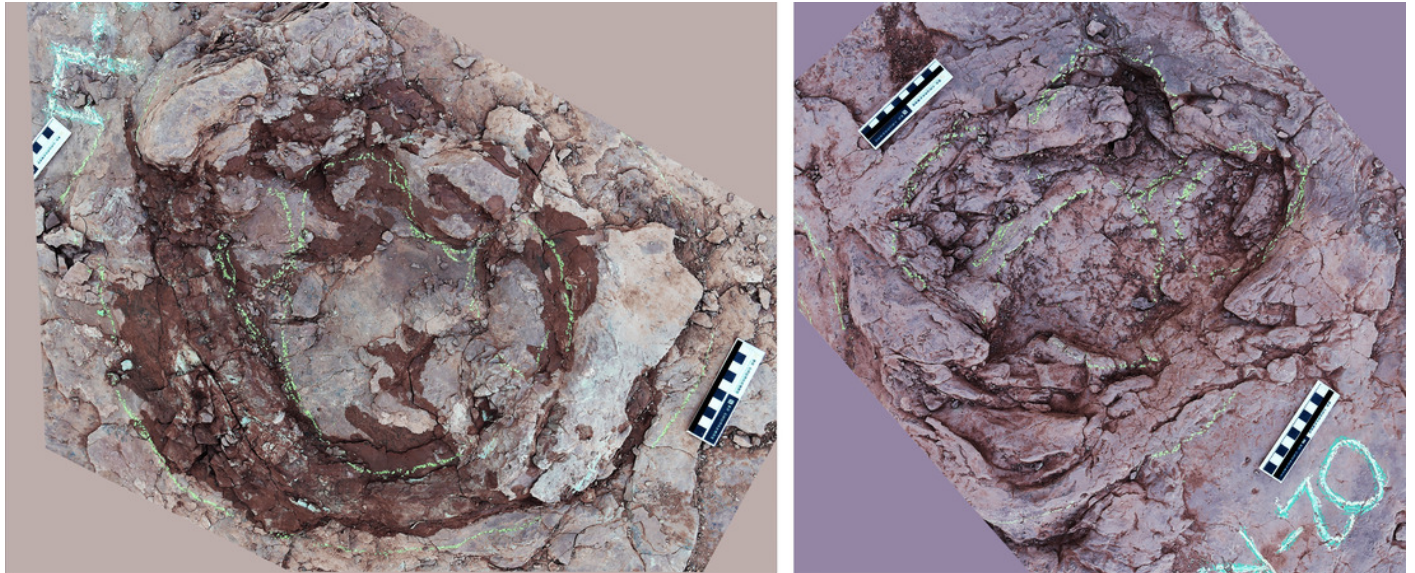
Figure 39

Close-in photographs and interpretive line drawings of ornithopod tracks from trackway LXIU-07.



Figure 40

Close-in photographs and interpretive line drawings of ornithopod tracks from trackway LXIU-O2.



LXIU-O2-L1



R1

10 cm

Figure 41

Close-in photographs and interpretive line drawings of ornithopod tracks from trackway LXIU-O8.

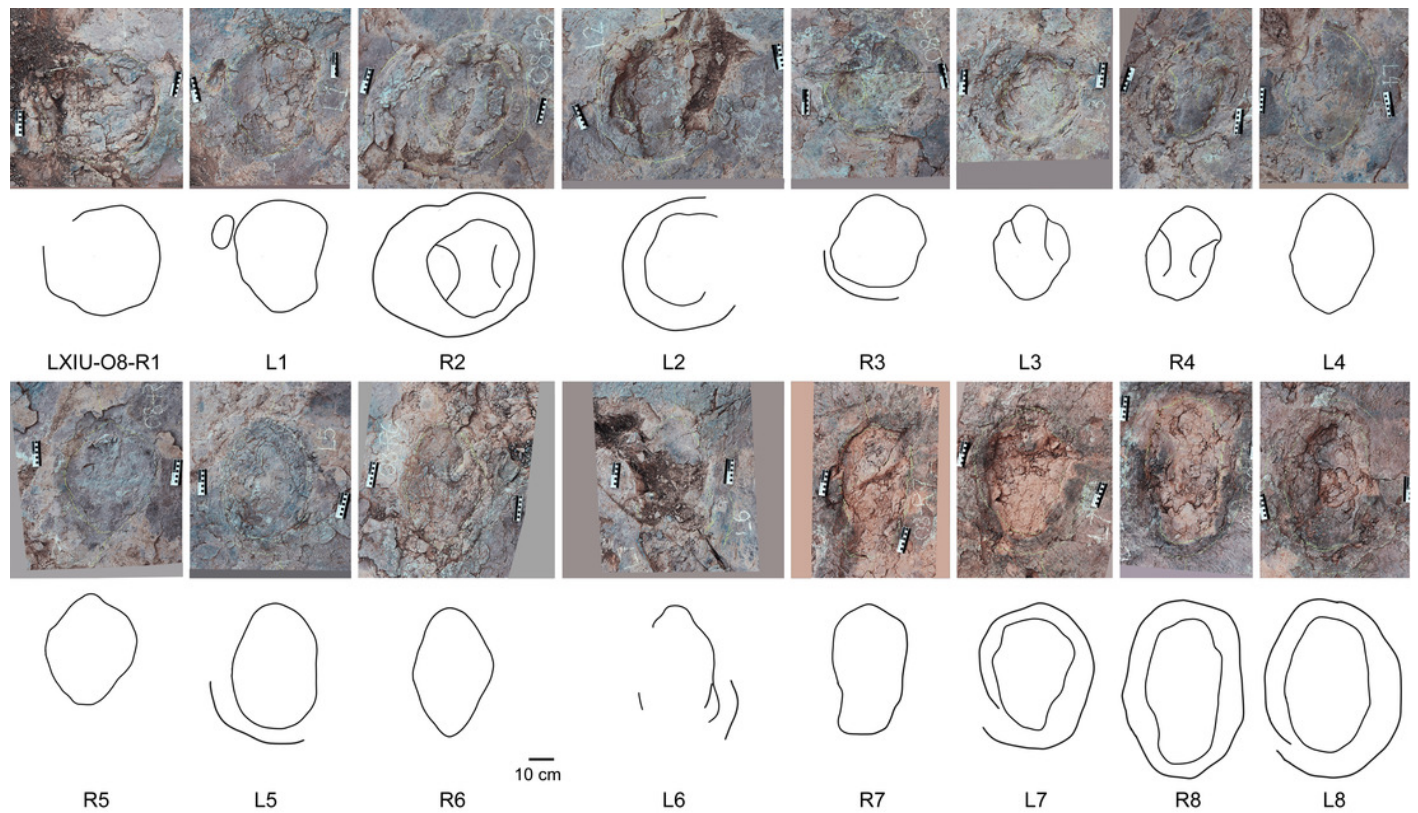


Figure 42

Close-in photographs and interpretive line drawings of ornithopod tracks from trackway LXIU-O10.

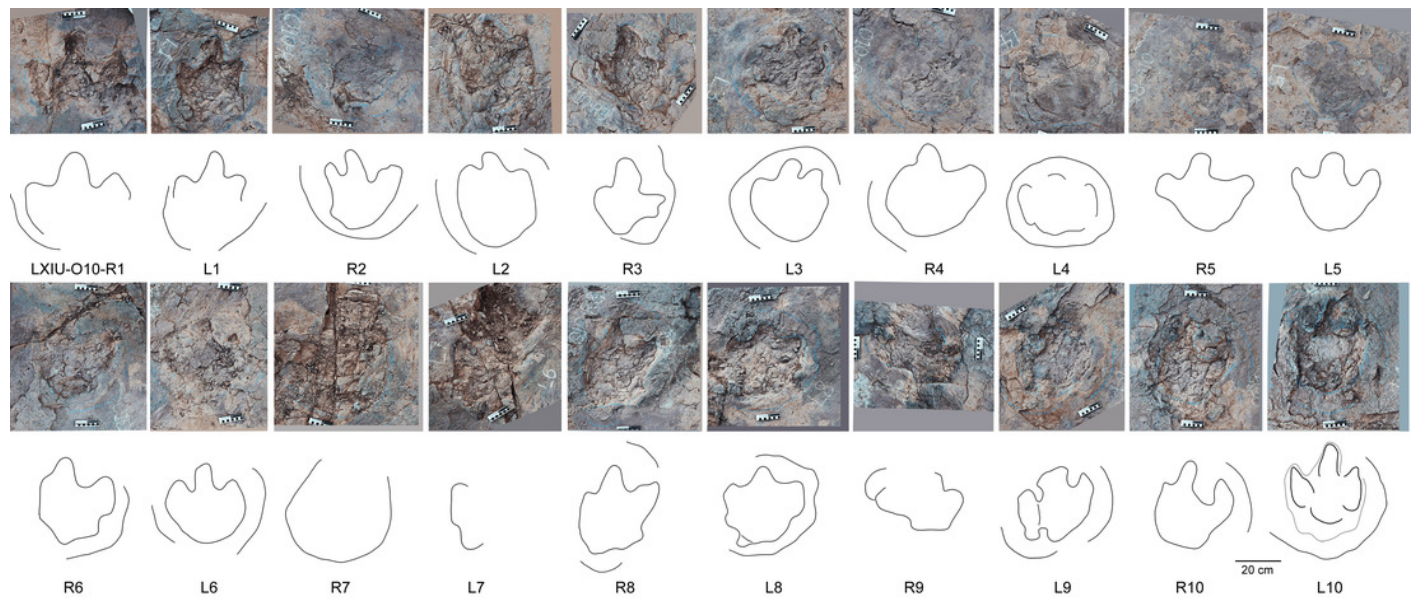


Figure 43

Close-in photographs and interpretive line drawings of ornithopod tracks from trackway LXIU-O11.

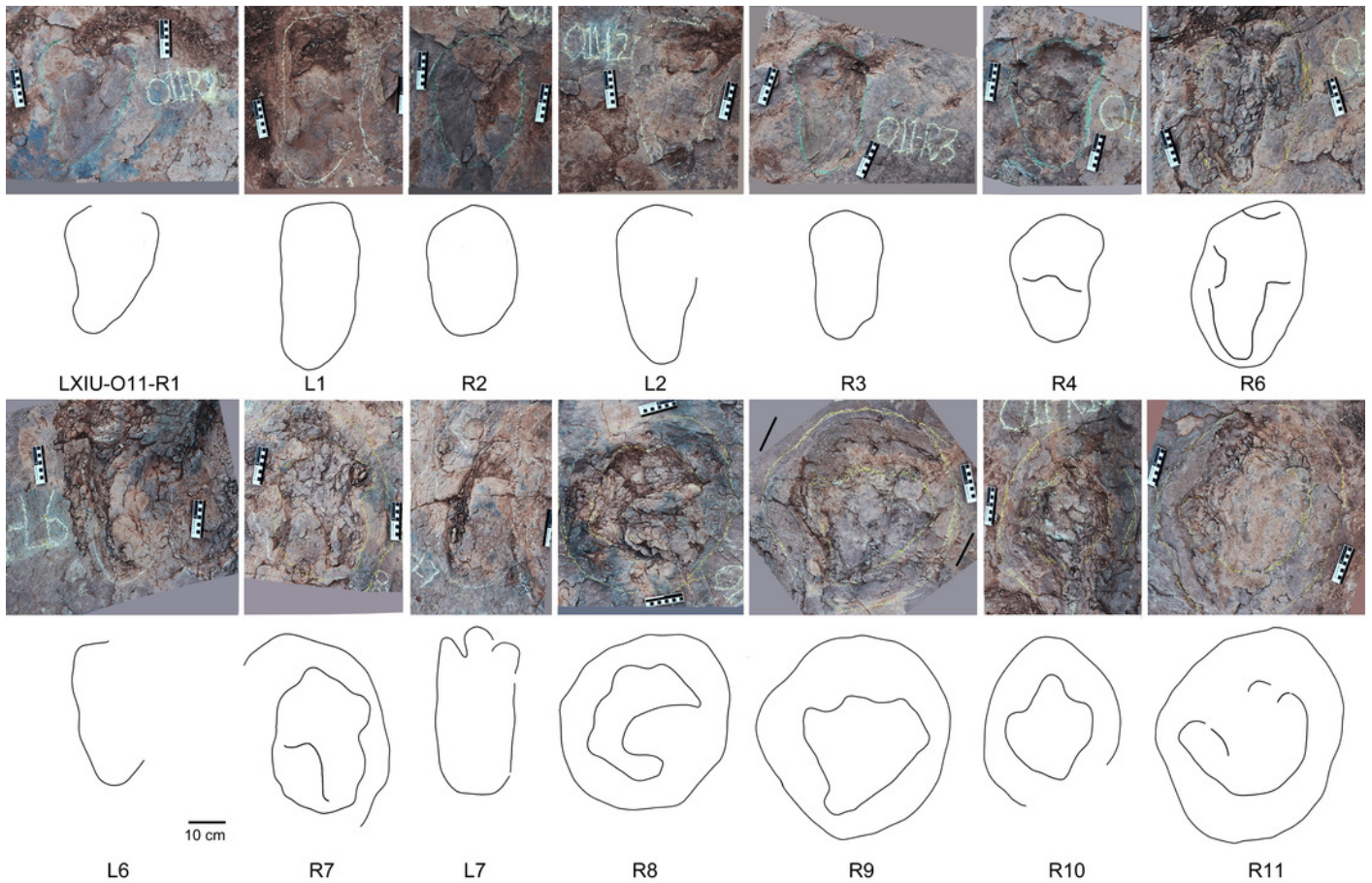
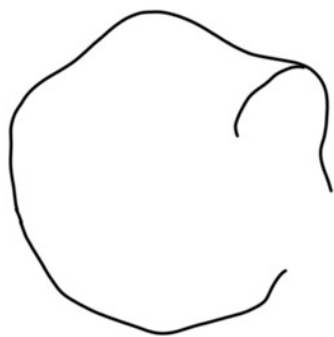
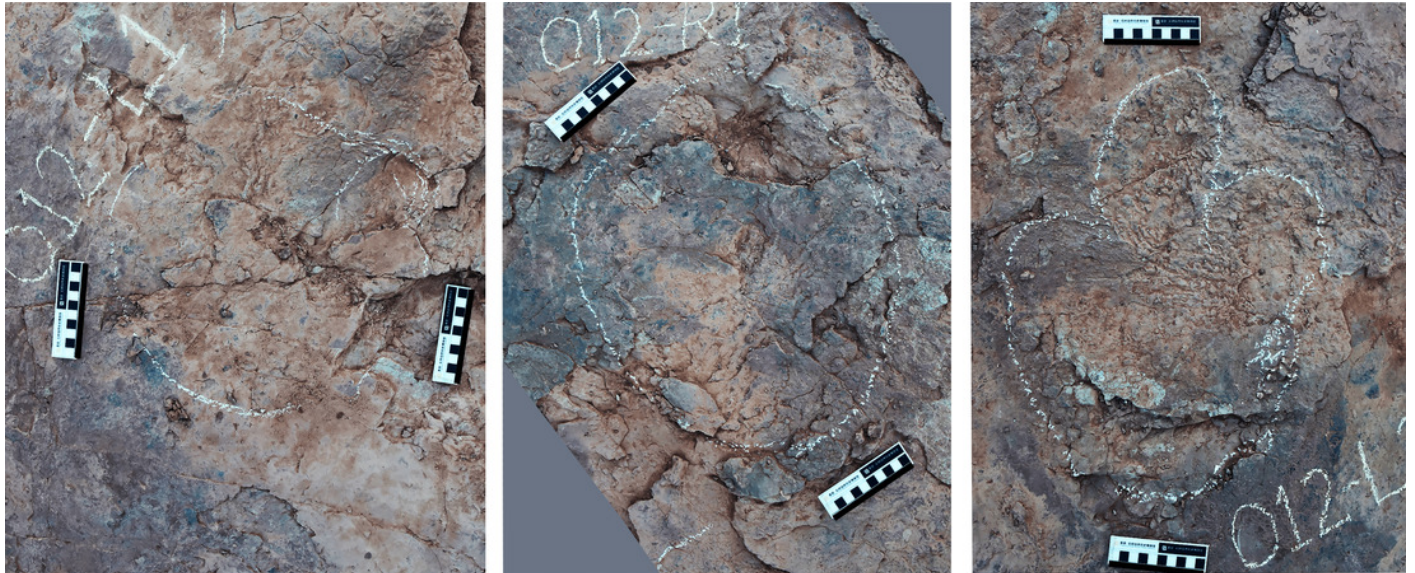
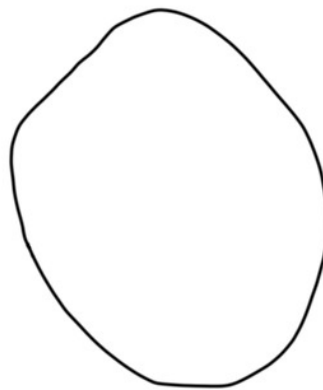


Figure 44

Close-in photographs and interpretive line drawings of ornithopod tracks from trackway LXIU-O12.



LXIU-O12-L1



R1

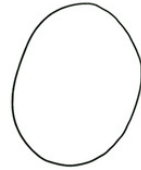


L2

10 cm

Figure 45

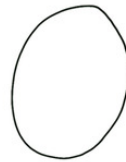
Photograph and interpretive line drawing of ornithopod trackway LXIN-01.



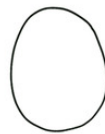
L3



R3



L2



R2



L1



LXIN-O1-R1

Figure 46

Photograph and interpretive line drawing of ornithopod trackway LXIN-01.

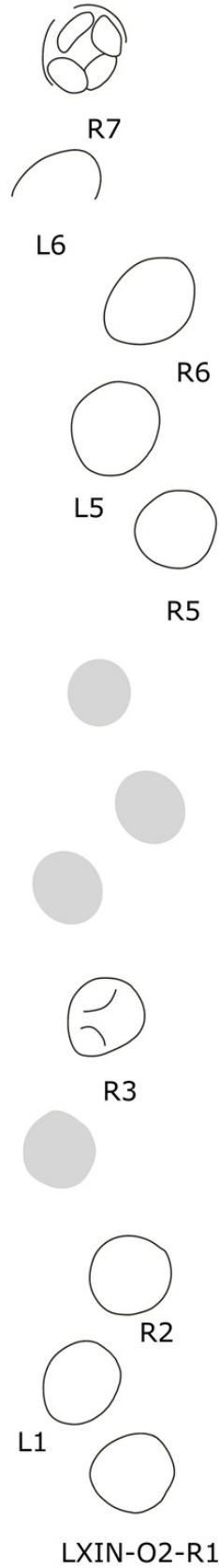
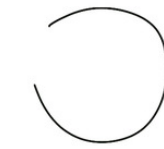


Figure 47

Photograph and interpretive line drawing of ornithopod trackway LXIN-O11 and O48.



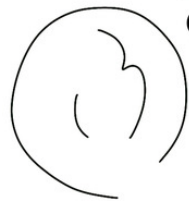
O11-R3



O11-L2



O48-L2



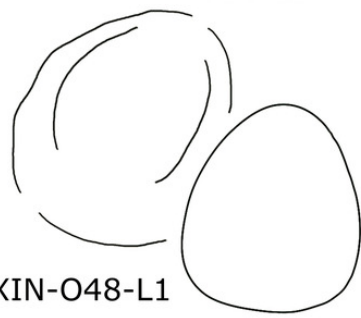
O11-R2



O48-R1



O11-L1



LXIN-O48-L1

LXIN-O11-R1

50 cm

Figure 48

Photograph and interpretive line drawing of ornithopod trackway LXIN-012.

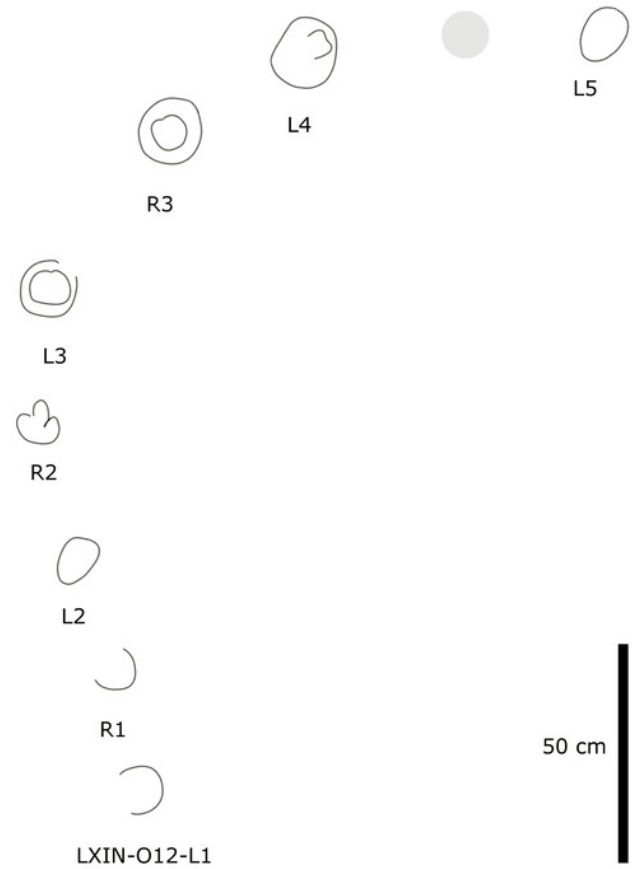
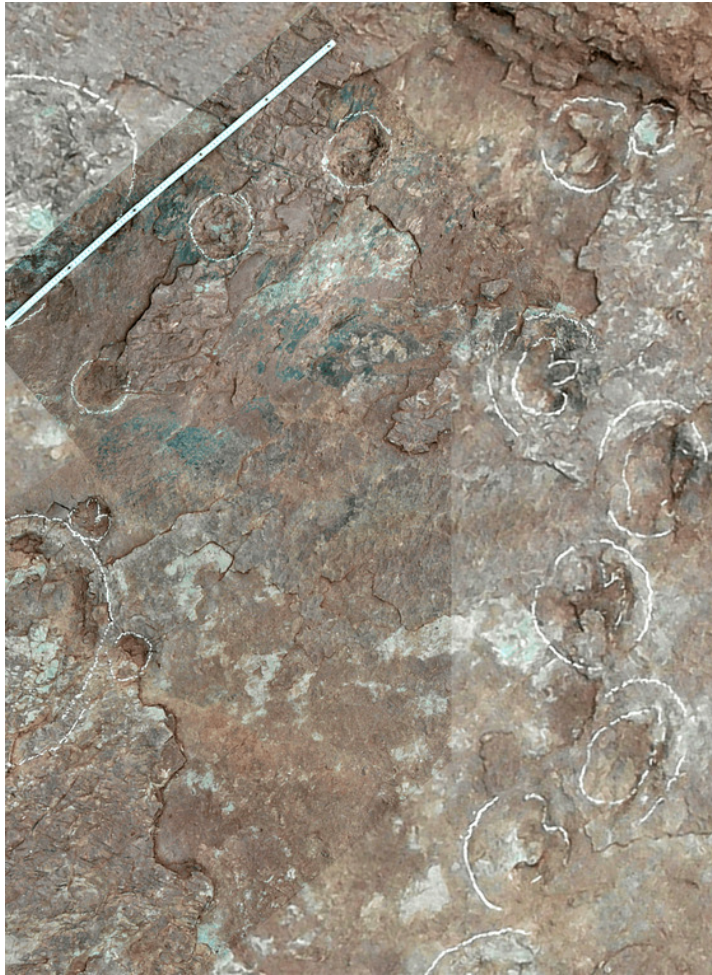


Figure 49

Photograph and interpretive line drawing of ornithopod trackway LXIN-028.



L4



R3



L3

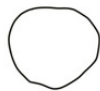


R2



R1

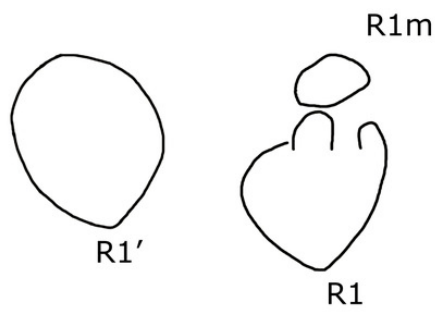
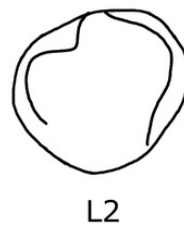
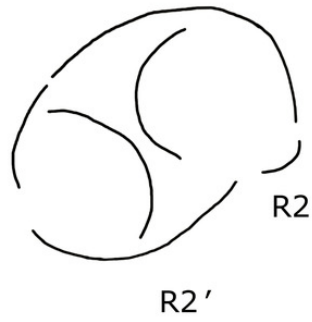
50 cm



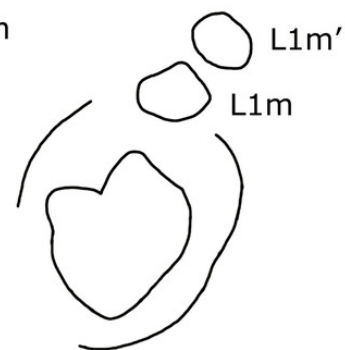
LXIN-O28-L1

Figure 50

Photograph and interpretive line drawing of ornithopod trackway LXIN-041.



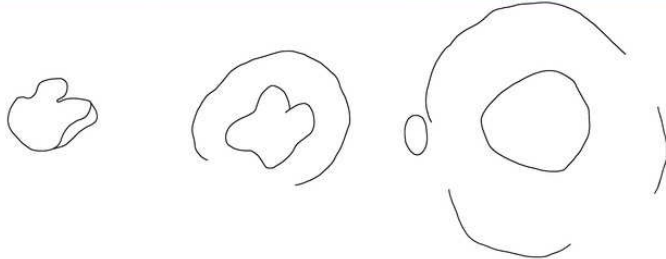
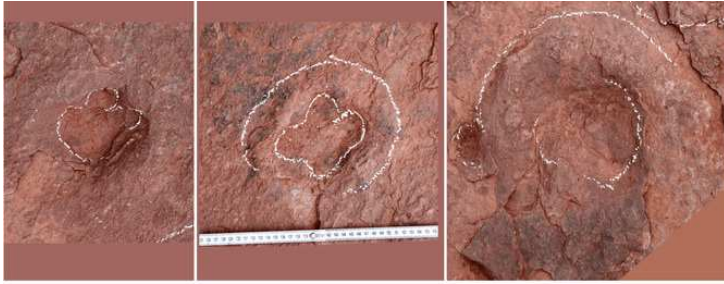
50 cm



LXIN-O41-L1

Figure 51

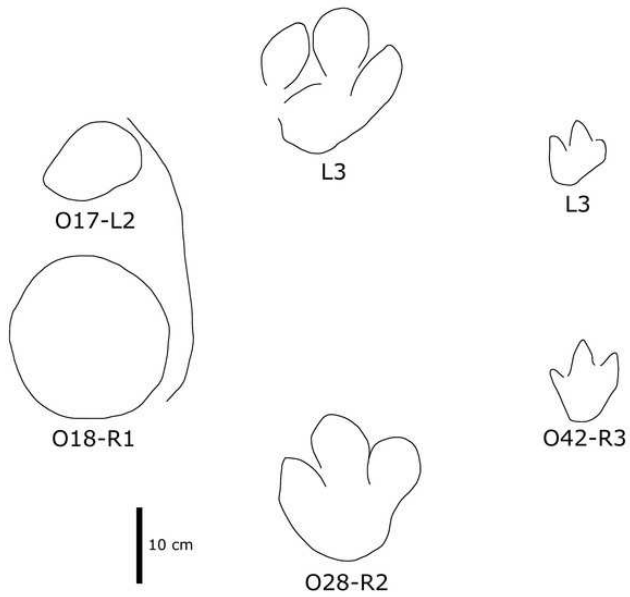
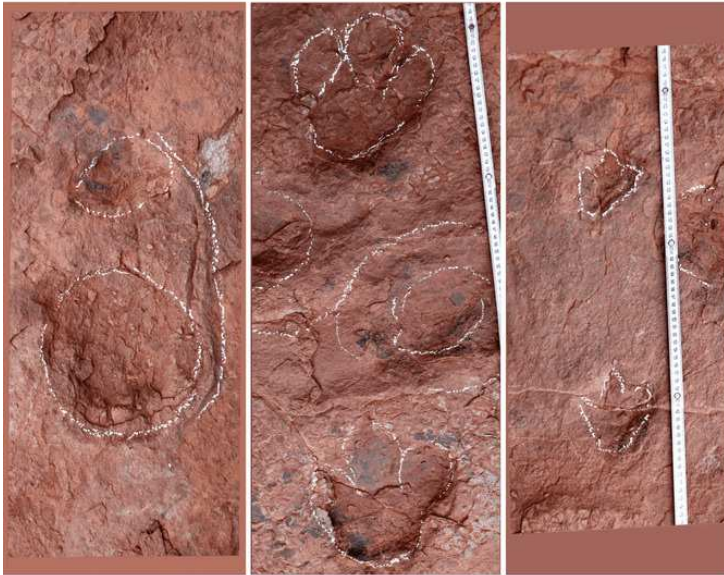
Close-in photographs and interpretive line drawings of ornithopod tracks from trackway in LXIN site.



O22-L1

O23-R8

LXIN-O33-R2



O17-L2

L3

L3

O18-R1

O42-R3

10 cm

O28-R2

Table 1 (on next page)

The ichnofauna composition of the Longxiang I (LXI) tracksites.

The frequency of each trackmaker type is represented by the number of trackways, and it should be noted that the sole isolated track from the *Grallator* morphotype is the only trackway counted as such due to its uniqueness. The interval of large ornithopod includes all the trackways with a mean track length of ≥ 25 cm.

1 **Table 1.** The ichnofauna composition of the LXI tracksites. The frequency of each trackmaker
 2 type is represented by the number of trackways, and it should be noted that the sole isolated track
 3 from the *Grallator* morphotype is the only trackway counted as such due to its uniqueness. The
 4 interval of large ornithopod includes all the trackways with a mean track length of ≥ 25 cm.
 5

	Frequency	Probability	large/total, ornithopod
Total (LXIs included)			
Total	79		
Ornithopods	66	0.84	0.27
Sauropods	2	0.03	
Theropods	11	0.14	
LXIN			
Total	54		
Ornithopods	48	0.89	0.19
Sauropods	1	0.02	
Theropods	5	0.09	
LXID			
Total	7		
Ornithopods	4	0.57	0.25
Sauropods	0	0	
Theropods	3	0.43	
LXIU			
Total	17		
Ornithopods	13	0.76	0.62
Sauropods	1	0.06	
Theropods	3	0.18	
LXIE			
Total	1		
Ornithopods	1	1	0
Sauropods	0	0	
Theropods	0	0	

6

7